AN ABSTRACT OF THE DISSERTATION OF

Kelly E. Gleason for the degree of Doctor of Philosophy in Geography presented on May 6, 2015.

Title: Forest Fire Effects on Radiative and Turbulent Fluxes over Snow: Implications for Snow Hydrology

Abstract approved:

_____

Anne W. Nolin

As a result of a warming climate, subsequent declining snowpack, and a century of fire suppression, forest fires are increasing across the western United States. However, we still do not fully understand how forest fire effects snowpack energy balance, nor the volume and availability of snow melt and associated water resources. This dissertation investigated the radiative and turbulent energy fluxes over snow in a burned and unburned forest site using a suite of experimental, modeling, and remote sensing methods to determine the overall impact of forest fire disturbance to snowpack energy balance and snow hydrology.

For three years following the Shadow Lake Fire, which occurred in September 2011 at the crest of the Oregon Cascades, a suite of field experiments were maintained, including snow water equivalent and snow spectral albedo measurement transects, snow surface sampling, snow depth and basic micro-meteorological monitoring and eddy covariance measurements of turbulent heat fluxes. These data were used to empirically characterize forest fire effects to the radiative and turbulent

fluxes over snow, to parameterize key drivers of snowpack energy balance and to model forest fire effects to snow hydrology using a physically-based spatially distributed snowpack energy and mass balance model for both the burned and unburned forest sites. This resulted in three papers summarizing forest fire effects to snowpack energy balance and implications for snow hydrology.

This dissertation documented forest fire effects to the radiative and turbulent fluxes over snow and evaluated implications for snow hydrology. These results showed a 40% reduction in snow albedo in the burned forest during the ablation period in the first year following fire, while 60% more solar radiation reached the snow surface, driving a 200% increase in net shortwave radiation. This dissertation documented that both sensible and latent heat fluxes were double the magnitude and variability in the burned forest compared to the nearby unburned forest. These results showed that the turbulent fluxes over snow can be periodically large and substantial over time. The contribution of sensible heat flux and loss of energy by the latent heat flux is responsible for a loss of snow mass of approximately 2% that measured snowmelt in the burned forest site during the clear-sky snowmelt period. Overall, the radiative fluxes dominate the overall snowpack energy balance in burned and unburned forests. An empirically-based parameterization was developed to represent the temporal and spatial variability of snow albedo relative to days-since-snowfall in the burned and unburned forests, which was employed in a physically based spatially distributed snowpack energy and mass balance model. Using this variable snow albedo parameterization improved model performance in both burned and unburned forest sites, and better captured the temporal and spatial variability of snow albedo

and snow water equivalent than a fixed albedo parameterization. Overall this evaluation demonstrated that even though more snow may accumulate in burned areas than unburned forests, the combined effect of the increased postfire radiative forcing to snow and increased turbulent fluxes over snow accelerates snow melt, shortens the duration of snow cover, and advances the date of snow disappearance across the extent of the burned forest.

Although this research focused on a relatively small burned area in the western Oregon Cascades, it has broad applications from regional to global scales particularly in forested maritime snow-dominated watersheds. Eighty percent of forest fires in the western United States occur in the seasonal snow zone, and those fires are 4.4 times larger than outside the seasonal snow zone. As forest fires increase and snowpacks decrease across forested montane headwater regions of the western US and beyond, it is critical that we incorporate forest fire disturbance effects to snow hydrology in our hydrologic modeling applications and our natural resource management decisions.

Forest Fire Effects on Radiative and Turbulent Fluxes over Snow: Implications for Snow Hydrology

by
Kelly E. Gleason

A DISSERTATION
Submitted to
Oregon State University

in partial fulfillment of
the requirements for the
degree of

Doctor of Philosophy

Presented May 6, 2015
Commencement June 2015

Doctor of Philosophy dissertation of Kelly E. Gleason presented on

May 6, 2015

APPROVED:

Major Professor, representing Geography

Dean of the College of Earth, Ocean, and Atmospheric Sciences

Dean of the Graduate School

I understand that my dissertation will become part of the permanent collection of Oregon State University libraries. My signature below authorizes release of my dissertation to any reader upon request.

Kelly E. Gleason, Author

ACKNOWLEDGEMENTS

This dissertation would not have been possible without funding from a National Science Foundation Hydrologic Sciences Rapid Grant entitled, Impacts of Forest Fire on Snow Accumulation and Melt (#1213612), and a National Science Foundation Water Sustainability and Climate Award entitled, WW2100: Anticipating water scarcity and informing integrative water system response in the Pacific Northwest (#1039192).

I would like to express my sincere thanks to my advisor, Dr. Anne Nolin, who has been an excellent mentor. She has always supported my scientific questions and research strategies, provided sound guidance, and set high expectations to support me in achieving my goals. I would like to thank my committee, Dr. John Bailey, Dr. Julia Jones, and Dr. Christoph Thomas, for adding breadth and depth to my dissertation research. I would like to thank Dr. Christoph Thomas and Dr. Chad Higgins for lending me with your field equipment, without your trust and expertise this research would not have been nearly as interesting. I would like to I would like to acknowledge my Graduate Council Representative, Dr. Dennis Albert for his time and efforts. Also, I would like to thank the administrative staff for Geosciences for generally making my graduate experience so much easier.

This dissertation required an immense amount of field work, including over 2000 person hours spent in the field, and over 200 man hours spent in the lab. I would like to thank all the interns and helpers that worked long hard hours to collect these data. I would thank the OSU Geomatics Group for conducting the TLS surveys. I would like to thank Glen Liston for helping me troubleshoot programming

SnowModel. I would like to thank Noah Molotch for providing me with the wind redistribution code for use in the BRT paper. My fellow graduate students and friends have been a tremendous help in accomplishing this work.

Finally I would like to thank my family. Thank you Dad for always encouraging me to ask questions and chase my dreams. Thank you Mom for supporting my strength and determination. Thank you Fiona for giving me perspective and inspiration. Thank you Nathaniel for believing in me, and in us; you are my dream come true.

CONTRIBUTION OF AUTHORS

In Chapter 3, Dr. Chris Thomas was the primary developer of the eddy covariance flux processing code.

In Chapter 4, Dr. Glen Liston was the primary developer of SnowModel. Glen also helped troubleshoot recoding the model to incorporate forest fire effects to snow albedo.

In Chapter 6, Travis Roth was the snow technician who collected field data in the ForEST (Forest Elevation Snow Transect) snow monitoring network. Also in this chapter, Noah Molotch provided the wind redistribution code.

TABLE OF CONTENTS

Page

TABLE OF CONTENTS (Continued)

Page

TABLE OF CONTENTS (Continued)

Page

LIST OF FIGURES

LIST OF FIGURES (Continued)

LIST OF FIGURES (Continued)

LIST OF FIGURES (Continued)

LIST OF FIGURES (Continued)

LIST OF FIGURES (Continued)

LIST OF TABLES

LIST OF EQUATIONS

DEDICATION

To my daughter Fiona, the big trees, and the polar bears who inspire me.
May you have a diverse, bountiful, and lasting world to inspire you.

1 Forest Fires Effects on Radiative and Turbulent Fluxes over Snow: Implications for Snow Hydrology

1.1 Introduction

Mountain snowpack serves as an important natural reservoir of water, recharging aquifers, sustaining streams, and providing important ecosystem services [*Buytaert et al.*, 2011; *Campbell et al.*, 2011; *Knowles et al.*, 2012; *Tague and Grant*, 2009; *Troy et al.*, 2012]. In the montane western United States, most annual precipitation falls as snow [*Serreze et al.*, 1999], yet rising temperatures have reduced snowpacks in the western US and beyond [*Abatzoglou*, 2011; *Brown and Mote*, 2009; *Dettinger et al.*, 2004; *Knowles et al.*, 2006; *Mote et al.*, 2005; *Pederson et al.*, 2013].

A key consequence of increased temperatures and declining snowpack has been an increase in wildfire frequency, extent, intensity, and duration across the western US [*Dennison et al.*, 2014; *Westerling et al.*, 2006], boreal Alaska [*Kasischke et al.*, 2010] and Russia [*Shvidenko and Schepaschenko*, 2013]. Total burned area in the western US is likely to continue to increase as air temperature continues to rise [*Littell et al.*, 2009; *Moritz et al.*, 2012; *Semmens and Ramage*, 2012; *Westerling et al.*, 2011]. Although we have limited understanding of how this increasing forest fire disturbance regime will affect snow-water resources in headwater forested ecosystems.

1.2 Background

Snow and ecosystems are intricately connected, with snow serving as a key moisture source for forests, while forests fundamentally affect snow accumulation and ablation processes. Snow hydrology (storage vs runoff) is dependent on snowpack energy balance, especially during the spring snowmelt season [*Marks and Dozier*, 1992]. The net snowpack energy balance (Q*) is equivalent to the sum of the radiative, turbulent, conductive, and advective fluxes (Figure 1.1). Specifically, these include the net shortwave (Q_K), longwave (Q_L), sensible (Q_H), and latent (Q_E) heat fluxes, conduction from the underlying ground surface (Q_G), and advected energy from rainfall and melt (Q_M) (Equation 1.1).

$$Q^* = Q_K + Q_L + Q_H + Q_E + Q_G + Q_M \quad \text{(Equation 1.1)}$$

Net shortwave radiation (Q_K), includes the incident solar spectral irradiance minus the spectral exitance integrated over the visible and near-IR wavelengths (0.35-0.8). Incident spectral irradiance is a function of latitude, land cover, and physiography. Spectral exitance is dependent on the reflectivity of the snow surface, which is based on the snow grain radius, solar zenith angle, and concentration of light absorbing impurities [*Warren and Wiscombe*, 1980; *Wiscombe and Warren*, 1980]. Forest canopies alter the intensity and spectral composition of incident spectral irradiance as a function of forest transmissivity and Beer's Law [*Hardy et al.*, 2004; *Pomeroy and Dion*, 1996] as well as the reflectivity of the snow surface as a result of the deposition and concentration of organic debris [*Melloh et al.*, 2002].

Net longwave radiation (Q_L), includes the incident thermal irradiance minus the thermal exitance integrated over the IR wavelengths. Incident thermal irradiance is a function of atmospheric conditions and land cover characteristics. Thermal exitance is dependent on the emissivity of the snow surface, which is fairly constant at 0.98 as snow is a near blackbody radiator. Forest canopies alter the intensity of incident thermal irradiance as a function of forest structure, canopy and trunk temperature, and Stephan's Law [*Lawler and Link*, 2011].

Net turbulent fluxes are partitioned into the sensible (Q_H), and latent (Q_E), heat fluxes, and are second only to radiation in relative contribution to snowpack energy balance during spring. These fluxes are carried to and from the snow surface as a result of turbulent eddies in the surface boundary layer [*Morris*, 1989]. These fluxes are formally the covariance of vertical wind velocity, and fluctuations of temperature for sensible heat, or water vapor for latent heat. Forest canopies alter the sensible and latent heat fluxes by reducing wind speeds and turbulence, particularly under stable conditions. Also, forest canopies intercept falling snow, and retain it above the snowpack, where wind speeds are greater, and a large proportion of snowfall may be lost to the atmosphere through sublimation [*Molotch et al.*, 2007]. Although in maritime snow climates such as the Pacific Northwest, sublimation from the forest canopy may be relatively small, and less important to the overall snowpack mass balance [*Storck et al.*, 2002].

Net ground heat flux (Q_G), generally represents a very minor source of snowpack energy unless snow depths are shallow enough to transmit solar energy to the soil surface. During the early winter season, conduction from the soil can slowly melt snowpack basal layers and form an ice lens beneath the snowpack. However this contribution gradually diminishes in spring. Advected energy (Q_M) from rainfall and melt can introduce conductive heat energy as relatively warm rain percolates into the snowpack, and as it freezes it releases the energy associated with the latent heat of fusion into the surrounding snowpack. Because forest canopies are relatively dark, they absorb incoming solar radiation and reemit it as longwave radiation. This energy melts intercepted snow in the forest canopy which falls as throughfall and either refreezes in the snowpack or moves through the snowpack in flow channels.

Before snow melt can occur from within the snowpack, energy inputs contribute to fulfilling the cold content of the snowpack. The entire snowpack must warm until it is isothermal at 0° C, before liquid water is yielded from the base of the snowpack. This requires considerable energy during the winter when snowpack energy budget components are relatively small. However, once snowmelt begins in spring, the cold content becomes relatively insignificant. The cold content of the snowpack is a function of its density, depth, the specific heat of ice, and the temperature gradient.

Forest fires fundamentally alter forest canopy effects to the snowpack energy balance by reducing canopy interception, increasing transmission of shortwave

radiation, modulating longwave radiation, and increasing turbulent fluxes [*Burles and Boon*, 2011; *Liu et al.*, 2005; *Winkler et al.*, 2010; *Winkler*, 2011]. The sloughing of charred debris from standing dead trees onto the snowpack has been suggested as an additional important forcing of earlier melt (S. Boon, personal communication). Anecdotal evidence suggests that snowpack in burned areas melt out earlier than clean snow outside the burned area (R. Julander, National Resource Conservation Service, Snow Survey Supervisor; personal communication). There have only been few studies evaluating forest fire effects to snowpack energy balance and resulting snowmelt hydrology. None of these have investigated how both post-fire structural changes to the forest canopy, and lowering of the snow surface albedo due to the deposition of charred debris together alter snowpack energy balance and snow melt.

As forest fire frequency, extent, intensity and duration continue to increase across the seasonal snow zone, the effects of these disturbances to the snowpack energy balance and snow ablation are of serious importance, particularly in the western United States. The timing and volume of snowmelt is a critical parameter in operational and research hydrology, but we do not understand the temporal or spatial variability of forest fire effects to the snowpack energy balance or subsequent volume and availability of snow-water resources.

The overarching question motivating this dissertation is:

How does forest fire disturbance effect the snowpack energy balance and the volume and availability of snow-water resources?

1.3 A Field Laboratory: Disturbance and Opportunity

A lightning strike sparked the Shadow Lake Forest Fire on August 28, 2011, in the sub-alpine forest near the highest elevations of the McKenzie River Basin (3,300 km^2), in the heart of the western Oregon High Cascades. The Shadow Lake Fire burned approximately 42 km^2 of dense fir and hemlock forests in the Mt Washington Wilderness on the north and west flanks of Mt. Washington near Santiam Pass (Figure 2.2). The Shadow Lake Fire burned forests near and adjacent to already scorched areas from the 365 km^2 B & B Fire Complex (ca. 2003) and the 50 km^2 George Washington Fire (ca. 2006). This area is prone to frequent wildfires and deep snowpacks, with over 3 m of snow water equivalent in a typical winter [*Taylor and Hannan*, 1999]. High elevation snowpack is the primary source of groundwater recharge for the McKenzie River Basin, which contributes over 90% of flow in the McKenzie River [*Tague and Grant*, 2004; 2009], and 25% of low flows during the late summer and early fall in the greater Willamette River Basin [*Jefferson et al.*, 2008]. In a high-severity burned area of the Shadow Lake Fire, and in a nearby unburned forest, paired study sites were selected based on forest characteristics, burn severity, and USFS permit restrictions. In 2011, the first winter following fire, a broad experimental field campaign was employed to evaluate forest fire effects to snow accumulation, snowpack energy balance, and subsequent snow ablation. This work was continued for three years following fire until summer 2014.

1.4 Objectives

In order to address this overarching research question we focused on four primary objectives that evaluate the immediate and enduring forest fire effects to the snowpack energy balance and volume and duration of snow-water resources. This research used multiple methods including a suite of field-based monitoring and experimental approaches coupled with statistical methods, and physically based modeling of snowpack energy balance. Specifically, the objectives of this research were:

Objective 1: Characterize forest fire effects to snow accumulation and ablation.

1a. Quantify forest structure using hemispherical photography and terrestrial laser scanner to determine forest metrics in the burned and unburned forests.

1b. Quantify snow accumulation and ablation using snowcourses, snowpits, and snow pingers to determine snow volume and snow duration in the burned and unburned forests.

Objective 2: Characterize forest fire effects to shortwave radiative fluxes over snow.

2a. Quantify snowpack surface debris concentrations using sampling of snowpack surface in the burned and unburned forests.

2b. Quantify broadband and spectral snow albedo using micro-meteorological stations and spectrometer surveys in the burned and unburned forests.

Objective 3: Characterize forest fire effects to turbulent fluxes over snow.

3a. Quantify temperature and humidity gradient over snow, and calculate sensible and latent heat fluxes using bulk-transfer calculations.

3b. Quantify sensible and latent heat fluxes directly using eddy covariance measurements, corrections, and calculations.

Objective 4: Evaluate the temporal and spatial variability of forest fire effects to the volume and duration of snow-water resources.

4a. Parameterize key mechanisms driving forest fire effects to snow accumulation and ablation.

4c. Model forest fire effects to snow albedo, and the volume and duration of snow water equivalent across the burned area using SnowModel, with the incorporated parameterization.

4d. Validate forest fire effects to snow albedo, and the duration of snow water equivalent across the burned area using remote sensing data.

4d. Evaluate extent of forest fire disturbance in the seasonal snow zone across the western United States.

1.5 Organization of the Dissertation

This dissertation is organized into three chapters that address the stated objectives followed by a concluding chapter. Each chapter builds on the previous section and further advances our understanding of forest fire effects to snowpack energy balance and the volume and availability of snow-water resources. The goal of this research is to develop an understanding of forest fire disturbance effects to snowpack storage, and provide a tool for hydrologic modelers to quantify these disturbance effects in the snow-dominated forested headwaters of the western US.

Chapter 2, "Charred forests increase snowmelt: effects of burned woody debris and incoming solar radiation on snow ablation", documents snow albedo was 40% lower in the burned forest during ablation, while 60% more solar radiation reached the snow surface, driving a 200% increase in net shortwave radiation.

Chapter 3, "Charred forests magnify turbulent fluxes over snow: an experimental evaluation using eddy covariance and bulk-transfer methods in a burned and unburned forest in the Oregon High Cascades", evaluates probability distribution functions of the sensible and latent heat fluxes over snow using a direct and indirect sampling method in a burned and unburned forest.

Chapter 4, "Charred forests accelerate snow albedo decay: A new parameterization of the post-fire radiative forcing on snow", documents temporal variability of snow albedo relative to days-since-snowfall in burned and unburned

forests, and employs an empirically-derived parameterization of forest fire effects to snow albedo decay in a snowpack energy and mass balance model.

Chapter 5, Conclusion, provides a synthesis of the dissertation, and summarizes key findings, suggests research that builds on chapters 2 through 4, and discusses potential management implications of forest fire effects to snow-water resources.

Appendix A, "Classifying the spatial distribution of snow water equivalent to develop a representative snow monitoring network in a forested mountain watershed", is an additional contribution to the dissertation, which uses a non-parametric approach to classify the variability of snow water equivalent relative to landscape physiography to distribute a snow monitoring network.

The research presented in this dissertation provides a mechanistic understanding of widespread forest fire disturbance effects to snow-water resources. This research provides the first characterization of forest fire effects to snow-water resources using a physically-based energy balance perspective that quantifies mechanistic interactions between ecological disturbance processes, optics, and snow hydrology. The research provides the first parameterization of post-fire radiative forcing on snow to incorporate forest fire effects to snowpack energy balance within a physically-based spatially distributed hydrology model. This research provides the first experimental evaluation of snowpack turbulent fluxes in a burned forest using both direct and indirect methods. This research provides a quality dataset of an

important ecosystem interaction with currently scant data resources, as well as a tool for hydrologic modelers to evaluate forest fire disturbance effects to snow-water resources.

1.6 References

Abatzoglou, J. T. (2011), Influence of the PNA on declining mountain snowpack in the Western United States, *International Journal of Climatology*, *31*(8), 1135-1142.

Brown, R. D., and P. W. Mote (2009), The response of northern hemisphere snow cover to a changing climate, *Journal of Climate*, *22*(8), 2124-2145.

Burles, K., and S. Boon (2011), Snowmelt energy balance in a burned forest plot, Crowsnest Pass, Alberta, Canada, *Hydrological Processes*, *25*(19), 3012-3029.

Buytaert, W., F. Cuesta-Camacho, and C. Tobon (2011), Potential impacts of climate change on the environmental services of humid tropical alpine regions, *Global Ecology and Biogeography*, *20*(1), 19-33.

Campbell, J. L., S. V. Ollinger, G. N. Flerchinger, H. Wicklein, K. Hayhoe, and A. S. Bailey (2011), Past and projected future changes in snowpack and soil frost at the Hubbard Brook Experimental Forest, New Hampshire, USA, *Hydrological Processes*, *24*(17), 2465-2480.

Dennison, P. E., S. C. Brewer, J. D. Arnold, and M. A. Moritz (2014), Large wildfire trends in the western United States, 1984-2011, *Geophysical Research Letters*, *41*(8), 2928-2933.

Dettinger, M. D., D. R. Cayan, M. Meyer, and A. E. Jeton (2004), Simulated hydrologic responses to climate variations and change in the Merced, Carson, and American River basins, Sierra Nevada, California, 1900-2099, *Climatic Change*, *62*(1-3), 283-317.

Hardy, J. P., R. Melloh, G. Koenig, D. Marks, A. Winstral, J. W. Pomeroy, and T. Link (2004), Solar radiation transmission through conifer canopies, *Agricultural and Forest Meteorology*, *126*(3-4), 257-270.

Jefferson, A., A. Nolin, S. Lewis, and C. Tague (2008), Hydrogeologic controls on streamflow sensitivity to climate variation, *Hydrological Processes*, *22*(22), 4371-4385.

Kasischke, E. S., D. L. Verbyla, T. S. Rupp, A. D. McGuire, K. A. Murphy, R. Jandt, J. L. Barnes, E. E. Hoy, P. A. Duffy, and M. Calef (2010), Alaskas changing fire regime implications for the vulnerability of its boreal forests, *Canadian Journal of Forest Research*, *40*(7), 1313-1324.

References (continued)

Knowles, J. F., P. D. Blanken, M. W. Williams, and K. M. Chowanski (2012), Energy and surface moisture seasonally limit evaporation and sublimation from snow-free alpine tundra, *Agricultural and Forest Meteorology*, *157*, 106-115.

Knowles, N., M. D. Dettinger, and D. R. Cayan (2006), Trends in snowfall versus rainfall in the Western United States, *Journal of Climate*, *19*(18), 4545-4559.

Lawler, R. R., and T. E. Link (2011), Quantification of incoming all-wave radiation in discontinuous forest canopies with application to snowmelt prediction, *Hydrological Processes*, *25*(21), 3322-3331.

Littell, J. S., D. McKenzie, D. L. Peterson, and A. L. Westerling (2009), Climate and wildfire area burned in western U. S. ecoprovinces, 1916-2003, *Ecological Applications*, *19*(4), 1003-1021.

Liu, H. P., J. T. Randerson, J. Lindfors, and F. S. Chapin (2005), Changes in the surface energy budget after fire in boreal ecosystems of interior Alaska: An annual perspective, *Journal of Geophysical Research - Atmospheres*, *110*(D13).

Marks, D., and J. Dozier (1992), Climate and energy exchange at the snow surface in the alpine region of the Sierra Nevada, 2, Snow cover energy balance, *Water Resources Research*, *28*(11), 3043-3054.

Melloh, R. A., J. P. Hardy, R. N. Bailey, and T. J. Hall (2002), An efficient snow albedo model for the open and sub canopy, *Hydrological Processes*, *16*(18), 3571-3584.

Molotch, N. P., P. D. Blanken, M. W. Williams, A. A. Turnipseed, R. K. Monson, and S. A. Margulis (2007), Estimating sublimation of intercepted and sub-canopy snow using eddy covariance systems, *Hydrological Processes*, *21*(12), 1567-1575.

Moritz, M. A., M.-A. Parisien, E. Batllori, M. A. Krawchuk, J. Van Dorn, D. J. Ganz, and K. Hayhoe (2012), Climate change and disruptions to global fire activity, *Ecosphere*, *3*(6), art49.

Morris, E. (1989), Turbulent transfer over snow and ice, *Journal of Hydrology*, *105*(3), 205-223.

References (continued)

Mote, P. W., A. F. Hamlet, M. P. Clark, and D. P. Lettenmaier (2005), Declining mountain snowpack in western north America, *Bulletin of the American Meteorological Society*, *86*(1), 39.

Pederson, G. T., J. L. Betancourt, and G. J. McCabe (2013), Regional patterns and proximal causes of the recent snowpack decline in the Rocky Mountains, US, *Geophysical Research Letters*, 1-6.

Pomeroy, J. W., and K. Dion (1996), Winter radiation extinction and reflection in a boreal pine canopy: Measurements and modelling, *Hydrological Processes*, *10*(12), 1591-1608.

Semmens, K. A., and J. Ramage (2012), Investigating correlations between snowmelt and forest fires in a high latitude snowmelt dominated drainage basin, *Hydrological Processes*, *26*(17), 2608-2617.

Serreze, M. C., M. P. Clark, R. L. Armstrong, D. A. McGinnis, and R. S. Pulwarty (1999), Characteristics of the western United States snowpack from snowpack telemetry (SNOTEL) data, *Water Resources Research*, *35*(7), 2145-2160.

Shvidenko, A. Z., and D. G. Schepaschenko (2013), Climate change and wildfires in Russia, *Contemporary Problems of Ecology*, *6*(7), 683-692.

Storck, P., D. P. Lettenmaier, and S. M. Bolton (2002), Measurement of snow interception and canopy effects on snow accumulation and melt in a mountainous maritime climate, Oregon, United States, *Water Resources Research*, *38*(11).

Tague, C., and G. E. Grant (2004), A geological framework for interpreting the low-flow regimes of Cascade streams, Willamette River Basin, Oregon, *Water Resources Research*, *40*(4).

Tague, C., and G. E. Grant (2009), Groundwater dynamics mediate low-flow response to global warming in snow-dominated alpine regions, *Water Resources Research*, *45*.

Taylor, G., and C. Hannan (1999), *The climate of Oregon: From rain forest to desert*, 211 pp., Oregon State University Press, Corvallis, Oregon.

References (continued)

Troy, T. J., J. Sheffield, and E. F. Wood (2012), The role of winter precipitation and temperature on northern Eurasian streamflow trends, *Journal of Geophysical Research - Atmospheres*, *117*.

Warren, S. G., and W. J. Wiscombe (1980), A model for the spectral albedo of snow, 2. Snow containing atmospheric aerosols, *Journal of the Atmospheric Sciences*, *37*(12), 2734-2745.

Westerling, A. L., H. G. Hidalgo, D. R. Cayan, and T. W. Swetnam (2006), Warming and earlier spring increase western US forest wildfire activity, *Science*, *313*(5789), 940.

Westerling, A. L., B. P. Bryant, H. K. Preisler, T. P. Holmes, H. G. Hidalgo, T. Das, and S. R. Shrestha (2011), Climate change and growth scenarios for California wildfire, *Climatic Change*, *109*, 445-463.

Wigmosta, M. S., L. W. Vail, and D. P. Lettenmaier (1994), A distributed hydrology-vegetation model for complex terrain, *Water Resources Research*, *30*(6), 1665-1680.

Winkler, R., S. Boon, B. Zimonick, and K. Baleshta (2010), Assessing the effects of post-pine beetle forest litter on snow albedo, *Hydrological Processes*, *24*(6), 803-812.

Winkler, R. D. (2011), Changes in snow accumulation and ablation after a fire in south-central British Columbia, *Streamline Watershed Management Bulletin*, *14*(2), 1-7.

Wiscombe, W. J., and S. G. Warren (1980), A model for the spectral albedo of snow. I: Pure snow, *Journal of the Atmospheric Sciences*, *37*(12), 2712-2733.

1.7 Figures

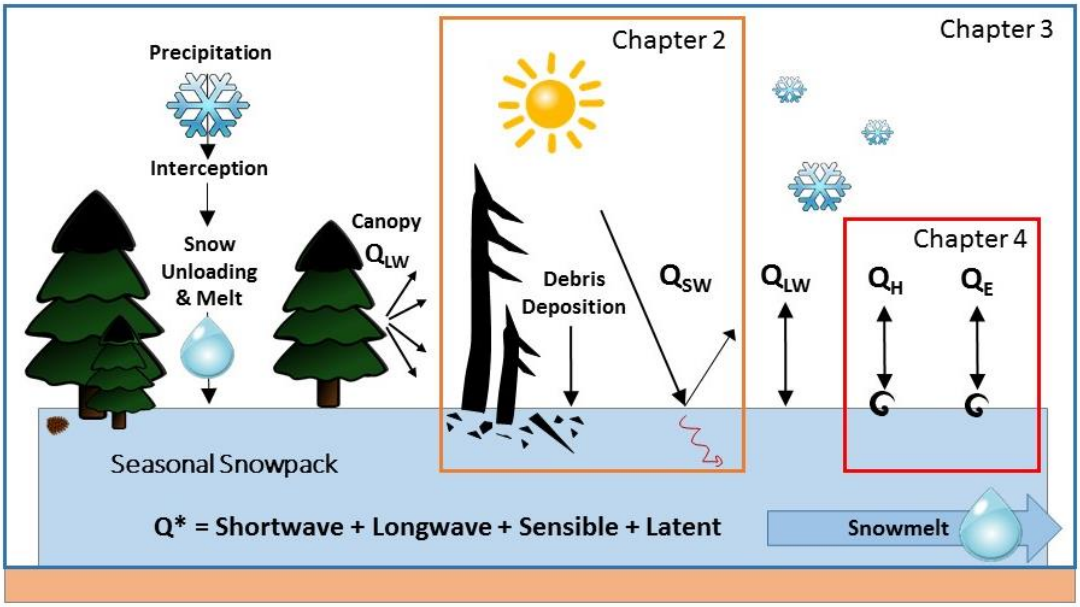

Figure 1.1. Forest effects to snowpack energy balance; adapted from *Marks and Dozier* [1992], and *Wigmosta et al.* [1994], and drawn to demonstrate the contribution of Chapters 2 - 4 (orange, red, and blue boxes) to improving the understanding of forest fire effects to the snowpack energy balance.

2 Charred Forests Increase Snowmelt: Effects of Burned Woody Debris and Incoming Solar Radiation on Snow Ablation

Charred Forests Increase Snowmelt: Effects of Burned Woody Debris and Incoming Solar Radiation on Snow Ablation

Kelly E. Gleason, Anne W. Nolin, and Travis R. Roth

Geophysical Research Letters
Volume 40, Pages 4654-4661.
Published September 2013

2.1 Abstract

We document effects of post-fire forest conditions on snow accumulation, albedo, and ablation in the Oregon Cascades. We measured snow water equivalent, solar radiation, snow albedo, and snowpack surface debris at a pair of burned and unburned forest plots. Snow accumulation was greater in the burned forest; however the snowpack disappeared 23 days earlier and had twice the ablation rate than in the unburned forest. Snow albedo was 40% lower in the burned forest during ablation, while approximately 60% more solar radiation reached the snow surface, driving a 200% increase in net shortwave radiation. Significant amounts of pyrogenic carbon particles and larger burned woody debris shed from standing charred trees accumulated on the snowpack and darkened its surface. Spatial analysis showed that across the Western US, 80% of all forest fires occurred in the seasonal snow zone, and were 4.4 times larger than fires outside the seasonal snow zone.

2.2 Introduction

In the montane western United States, most annual precipitation falls as snow [*Serreze et al.*, 1999], yet rising temperatures have reduced snowpacks [*Abatzoglou*, 2011; *Brown and Mote*, 2009; *Knowles et al.*, 2006; *Mote et al.*, 2005; *Pederson et al.*, 2013]. Key consequences of this have been increases in wildfire frequency, size, intensity, and duration across the western United States [*Westerling et al.*, 2006]. Total burned area in the western US is anticipated to increase [*Littell et al.*, 2009; *Moritz et al.*, 2012; *Westerling et al.*, 2011] as a result of climate change and fire suppression [*Marlon et al.*, 2012].

Forest fire affects patterns of snow accumulation and ablation by reducing canopy interception, increasing light transmission, and modifying the surface energy balance [*Burles and Boon*, 2011; *Harpold et al.*, 2013; *Winkler*, 2011]. Previous work showed that snow ablation rates are accelerated as much as 57% and snow disappeared 4-15 days earlier in a burned forest [*Burles and Boon*, 2011; *Skidmore et al.*, 1994; *Winkler*, 2011] but these studies omitted measurements of burned debris and its effect on snow spectral albedo. The objective of this paper is to demonstrate how charred forests decrease snow albedo through debris deposition, and how when combined with increased solar radiation, this leads to earlier snow disappearance.

Because snow is highly reflective in the visible wavelengths (400-700 nm), even a small decrease in visible albedo will dramatically increase net shortwave radiation [*Dozier et al.*, 2009]. Previous work has shown that light absorbing

impurities in snow, such as dust and soot, can lead to substantial radiative heating and faster snow melt rates [*Flanner et al.*, 2009; *Painter et al.*, 2012; *Painter et al.*, 2007; *Skiles et al.*, 2012]. Compared with mineral dust, carbon soot is an order of magnitude more effective at absorbing solar energy in the visible wavelengths [*Warren and Wiscombe*, 1980]. Although far more coarse than dust and soot, debris from the forest canopy accumulates on the snowpack and reduces albedo [*Hardy et al.*, 2000; *Melloh et al.*, 2001]. For decades after a fire, burned woody debris (BWD) including pyrogenic carbon [*Preston and Schmidt*, 2006], charcoal, charred woody detritus, and partially charred needles, cones, and bark are shed from standing burned trees onto the snowpack [*Dunn and Bailey*, 2012]. While it is visibly apparent that BWD darkens the snow surface (Figure 2.1), the effects on snow spectral albedo and snowpack ablation have not been quantified. This investigation provides the first measurements of snow spectral albedo and snow surface BWD in a burned forest, and provides evidence for the impacts of wildfire on snow accumulation and ablation.

2.3 Site Description

The study area is located in the Oregon High Cascades at an elevation of 1750 m, in the headwaters of the McKenzie River Basin, a major tributary to the Willamette River. This area receives approximately 3000 mm of precipitation a year, most of which falls as snow from November to April [*Taylor and Hannan,* 1999]. In late summer 2011, the Shadow Lake Fire burned 42 km^2 of High Cascades mixed conifer forest [*Franklin and Dyrness,* 1973] in the Willamette and Deschutes National Forests (Figure 2.2). About 50% of the area burned with moderate-to-high burn severity, with near total loss of forest canopy (Figure 2.3). This location serves as an ideal field laboratory for our paired study of snowpack dynamics and snow albedo in a severely burned forest (BF) plot and in an adjacent, unburned forest (UF) plot.

2.4 Research Methods

2.4.1 Measuring post-fire snow spectral albedo and net radiation

Snow spectral albedo was measured every 20 m along a 200 m transect in the burned and unburned study sites using an Analytical Spectral Devices Full-Range Portable Field Spectrometer™ (ASD-FR) equipped with a cosine receptor, mounted on a 110-cm long horizontally leveled rod. The ASD-FR has a spectral resolution of 10 nm over a spectral range of 350-2500 nm. Measurements were made on 25 March 2013 (accumulation period) and 04 May 2012 and 01 May 2013 (ablation period). All spectral measurements were made within one hour of solar noon under clear sky conditions.

Solar radiation was measured from upward- and downward-facing LI-COR™ 200-s pyranometers installed at 5 m above ground on a tower located at the transect center in each plot. The pyranometers have a spectral range of 400–1100 nm and a 180º field-of-view. Power supply issues at both sites restricted the coincident radiation data to two periods: 04 - 27 February (accumulation period) and 8 May - 01 July (ablation period). Hourly mean incoming and outgoing solar radiation values were calculated using all snow-free data for solar elevation angle > 30°. Hourly mean broadband snow albedo was calculated, when snow depth was greater than 30 cm, as the ratio of outgoing to incoming solar radiation.

We quantified changes in net shortwave radiation using pyranometer-measured broadband albedo and ASD-FR-measured snow spectral albedo. For

comparison with the pyranometer data, we convolved the ASD-FR measurements over the spectral range of the pyranometer.

2.4.2 Snow debris concentration and spectral reflectance characterization

At spectral albedo measurement locations we collected a snow surface sample (0.5 m^2 area × 0.03 m depth) for subsequent filtration. Snow samples were melted in a 30°C oven and filtered using pre-weighed Whatman™ glass fiber filters (55 mm & 0.7 µm pore size) with vacuum filtration. Sampled filtrate and oven-dried debris were weighed to determine the mass of debris per unit mass of snow water equivalent. Filters were retained for measurement of spectral reflectance of the debris. Spectral reflectance factors of filtered debris samples were measured relative to a calibrated Spectralon® target using the ASD-FR equipped with an 8° foreoptic on 07 September 2012. Debris consisted of a thick (>5 mm) layer completely covering the filter.

2.4.3 Snow surveys and forest structure measurements

We measured snow depth and snow water equivalent (SWE) along 0.5 km transects in both plots. Monthly measurements were made from December 2011 to April 2012, and bi-weekly measurements were made from 15 April 2012 until snow disappearance. Snow depth was measured every 10 m, and SWE was measured every 100 m. At each SWE measurement location, snow surface samples were collected for debris filtration as described above.

Forest structure within each plot was characterized using a Riegl VZ400™ terrestrial laser scanner (TLS). TLS metrics including tree height, crown radius, forest

density; and aerial visualizations were produced within a 250-m radius using Cyclone™ and ArcGIS™ (Figure 3). We also quantified canopy closure every 50 m along each transect using hemispherical digital photos (Nikon Coolpix 995 w/leveled fish-eye lens) and Gap Light Analyzer 2.0 [*Frazer et al.*, 1999].

2.4.4 Geospatial analysis

To provide a broader spatial context for our field study, we mapped coincident areas of wildfire, seasonal snow, and forest cover over the western US using ArcGIS. We used data from the Moderate Resolution Imaging Spectroradiometer (MODIS) including MOD10A2 500-m 8-day maximum snow covered area product [*Hall*, 2006] and the MOD44B 250-m vegetation continuous fields (VCF) product [*DiMiceli*, 2011] for years 2000-2012. Based on Robinson and Frei [2000], we selected January 15th to represent the maximum winter snow cover extent for the western US, and for each year used the MOD10A2 image nearest that date. Snow cover frequency in each MODIS pixel was calculated as the ratio of the number of years when snow was observed relative to the number of years in the data record. The seasonal snow zone was defined by pixels with snow cover frequency of at least 25%. Forest cover pixels were identified using the MODIS VCF product that we aggregated to 500 m to match the snow product resolution. Forests were defined by pixels with forest cover of at least 20%. Burned area was determined using fire perimeter spatial data from the Geospatial Multi-Agency Coordination Group (GEOMAC) data distribution site [*Walters et al.*, 2008] for 2000-2012.

2.5 Results and Discussion

2.5.1 Post-fire snow spectral albedo and net radiation

During the accumulation period, the burned and unburned forests showed no difference in albedo (as measured with ASD-FR and pyranometers; Figures 2.4 & 2.5). Because of frequent snowfall events, the effect of BWD on albedo was negligible during this period. However, during the ablation period, BWD concentrated on the snowpack surface, decreasing snow albedo by 40%. Previous research has shown that particulates larger than 5 μm in diameter are typically not flushed downward through the snowpack with meltwater [*Conway et al.*, 1996], and thus concentrate on the snowpack surface during ablation [*Painter et al.*, 2012]. Throughout the accumulation (acc.) and ablation (abl.) periods, spectral albedo in the unburned forest maintained uniform spatial variability (acc. 0.74 ±0.02, abl. 0.58±0.02), while the temporal variability of broadband albedo increased during ablation (acc. 0.67±0.13, abl. 0.38 ±0.18). Spectral albedo in the burned forest maintained uniform spatial variability (acc. 0.75±0.04, abl. 0.42±0.05), while the temporal variability of broadband albedo decreased (acc. 0.68±0.08, abl. 0.28±0.03) during ablation.

Mean solar radiation incident on the snow surface was approximately 60% greater in the burned forest than in the unburned forest (Figure 2.5). Particularly in the unburned forest, the downward-facing pyranometers may have had trees in a portion of their field-of-view, thereby underestimating snow albedo. Also in the

unburned forest, snow albedo was lower than for pristine snow due to deposition of forest litter. Our measurements were comparable with reported values [*Burles and Boon*, 2011; *Melloh et al.*, 2002].

In the burned forest, lower snow albedo combined with increased canopy transmissivity resulted in greater net shortwave radiation compared with the unburned forest (Table 2.1). During the accumulation period, net shortwave radiation was 60% greater in the burned forest. While during ablation, net shortwave radiation was over 200% greater in the burned forest. Spatial (Figure 2.4) and temporal (Figure 2.5) within-site variability in snow albedo, incoming solar radiation, and BWD concentrations, combined with fine-scale heterogeneity in snow dynamics [c.f. *Jost et al.*, 2007 and references therein], introduces uncertainty in the results, but is outweighed by large overall increases in net shortwave radiation.

2.5.2 Snow debris concentration and spectral reflectance characterization

Filtered snow samples collected in both plots during the accumulation period showed no significant differences in their respective debris concentrations (grams of debris per kilogram of snow). However, samples from the ablation period showed that the burned forest had more than double the mean debris concentration (UF: 2.4±2.4 g/kg; BF: 7.1±11.8 g/kg). Spectral reflectance factor measurements of filtered debris showed that the BWD samples had 25% lower reflectance than debris from the unburned forest snowpack (Figure 2.4). The greater concentration of darker debris in the burned forest suggests it had a greater radiative impact on snowmelt.

Although we did not explicitly quantify debris concentrations in proximity to trees we noted that debris concentrations were highest near tree trunks. Our sampling strategy captured the range of spatial variability of spectral albedo and debris concentrations.

2.5.3 Forest structure and post-fire snow dynamics

In the burned forest, TLS data showed a 500% reduction in stem density (UF: 1 tree per 6.7 m^2; BF: 1 tree per 34.0 m^2). Hemispherical image analysis showed a 300% reduction in mean canopy density compared with the unburned forest (UF: 66±5%; BF: 22±4%). Snow survey results showed that the loss of overstory decreased canopy snow interception, thereby increasing snow accumulation on the ground. Maximum SWE was 11% greater in the burned forest (UF: 90±21 cm; BF: 101±29 cm), but it disappeared 23 days earlier than in the unburned forest (Figure 2.6). After the date of peak SWE, average snow ablation rate in the burned forest was almost twice as fast as in the unburned forest (UF: 1.2 cm d^{-1}; BF: 2.3 cm d^{-1}). The snowpack in the unburned forest disappeared 75 days after the date of peak SWE, whereas the snowpack in the burned forest disappeared in 47 days, over 60% faster.

2.5.4 Fire in the seasonal snow zone in the western United States

Our spatial analysis demonstrated that from 2000-2012, over 80% of forest fires in the western US burned in the seasonal snow zone (Figure 2.7). These forest fires in the seasonal snow zone were 4.4 times larger than those outside the seasonal snow zone. Since 2000, over 44,000 km^2 of forests in the seasonal snow zone have

burned. These snow-dominated headwater catchments in the western US are likely being influenced by the post-fire snow albedo/canopy transmissivity effect. The relative importance of this effect will vary across scales with snow climate [*Sturm et al.*, 1995], forest type, and burn severity. From a large watershed perspective, we note that in the western US nearly half (48%) of all forest fires in the seasonal snow zone lie within the Columbia River Basin of the Pacific Northwest.

2.6 Conclusions

While the competing effects of increased snow accumulation and increased snow ablation rate have been previously documented in fire-affected watersheds [*Burles and Boon*, 2011; *Harpold et al.*, 2013; *Pomeroy et al.*, 2012; *Skidmore et al.*, 1994; *Winkler*, 2011], this study was the first to address the additional forcing of earlier melt due to the effects of BWD on snow albedo. The snowpack surface darkened with the concentrated BWD, was primed to absorb more than double the incoming solar radiation.

While this study addressed first year post-fire effects on snow albedo and incoming solar radiation, the longer-term effects remain unclear. Studies have shown that burned forests remain standing for decades after fire disturbance depending on forest composition, forest structure, and burn severity [*Acker et al.*, 2013; *Bigler and Veblen*, 2011; *Dunn and Bailey*, 2012]. Previous work estimated a half-life of standing burned fine-fuels ($\leq$ 23 cm) to be approximately 10 years [*Dunn and Bailey*, 2012]. As long as charred trees remain standing, they can contribute BWD to the snowpack surface. Six years after a fire, Burles and Boon [2011] measured higher snow albedo values in a burned forest than in a control forest. Eventually, snow in burned forests will have less debris and therefore higher albedo compared with unburned forests, thereby reducing net solar radiation at the snowpack surface. Until forest regeneration, their radiation balance may resemble that of an alpine snowpack

above treeline. Such conjecture invites further investigation such as longer-term studies in burned forest stands of different post-fire ages.

Paradoxically, by removing the dark forest canopy and exposing the underlying snowcover, wildfire increases the overall winter/spring albedo of the land surface, creating a negative atmospheric radiative forcing [*Chambers et al.*, 2005; *Chapin et al.*, 2000; *O'Halloran et al.*, 2012]. However, from the perspective of the snowpack, the albedo is decreased following a wildfire, and subsequent radiative heating and accelerated melt may have ecohydrological implications for forested snow-dominated headwater catchments [*Kelly and Goulden*, 2008].

As climate continues to change, fire extent and severity are likely to increase across catchments of the mountain West [*Moritz et al.*, 2012]. The "new normal" of increasingly large high-severity forest fires will have implications for changes in the amount and timing of snowmelt runoff in the western US.

2.7 References

Abatzoglou, J. T. (2011), Influence of the PNA on declining mountain snowpack in the Western United States, *International Journal of Climatology*, *31*(8), 1135-1142.

Acker, S. A., J. Kertis, H. Bruner, K. O'Connell, and J. Sexton (2013), Dynamics of coarse woody debris following wildfire in a mountain hemlock (*Tsuga mertensiana*) forest, *Forest Ecology and Management*, *302*, 231-239.

Bigler, C., and T. T. Veblen (2011), Changes in litter and dead wood loads following tree death beneath subalpine conifer species in northern Colorado, *Canadian Journal of Forest Research-Revue Canadienne De Recherche Forestiere*, *41*(2), 331-340.

Brown, R. D., and P. W. Mote (2009), The Response of Northern Hemisphere Snow Cover to a Changing Climate, *Journal of Climate*, *22*(8), 2124-2145.

Burles, K., and S. Boon (2011), Snowmelt energy balance in a burned forest plot, Crowsnest Pass, Alberta, Canada, *Hydrological Processes*, *25*(19), 3012-3029.

Chambers, S. D., J. Beringer, J. T. Randerson, and F. S. Chapin (2005), Fire effects on net radiation and energy partitioning: Contrasting responses of tundra and boreal forest ecosystems, *Journal of Geophysical Research - Atmospheres*, *110*(D9).

Chapin, F. S., et al. (2000), Arctic and boreal ecosystems of western North America as components of the climate system, *Global Change Biology*, *6*, 211-223.

Conway, H., A. Gades, and C. Raymond (1996), Albedo of dirty snow during conditions of melt, *Water Resources Research*, *32*(6), 1713-1718.

DiMiceli, C. M., M.L. Carroll, R.A. Sohlberg, C. Huang, M.C. Hansen, and J.R.G. Townshend (2011), Vegetation Continuous Fields MOD44B, edited by U. o. Maryland, College Park, Maryland.

Dozier, J., R. O. Green, A. W. Nolin, and T. H. Painter (2009), Interpretation of snow properties from imaging spectrometry, *Remote Sensing of Environment*, *113*, S25-S37.

Dunn, C. J., and J. D. Bailey (2012), Temporal dynamics and decay of coarse wood in early seral habitats of dry-mixed conifer forests in Oregon's Eastern Cascades, *Forest Ecology and Management*, *276*, 71-81.

References (continued)

Flanner, M. G., C. S. Zender, P. G. Hess, N. M. Mahowald, T. H. Painter, V. Ramanathan, and P. J. Rasch (2009), Springtime warming and reduced snow cover from carbonaceous particles, *Atmospheric Chemistry and Physics*, *9*(7), 2481-2497.

Franklin, J. F., and C. Dyrness (1973), *Natural vegetation of Oregon and Washington*, US Government Printing Office Washington.

Frazer, G., C. Canham, and K. Lertzman (1999), Gap Light Analyzer (GLA): Imaging software to extract canopy structure and gap light transmission indices from true-colour fisheye photographs, user's manual and program documentation, *Simon Fraser University, Burnaby, BC.[doi: 10.1016/S0168-1923 (01) 00274-X]*.

Hall, D. K., George A. Riggs, and Vincent V. Salomonson (2006), MODIS/Terra Snow Cover 8-day L3 Global 500m Grid V005, edited by N. S. a. I. D. Center, Boulder, Colorado.

Hardy, J., R. Melloh, P. Robinson, and R. Jordan (2000), Incorporating effects of forest litter in a snow process model, *Hydrological Processes*, *14*(18), 3227-3237.

Harpold, A. A., J. A. Biederman, K. Condon, M. Merino, Y. Korgaonkar, T. Nan, L. L. Sloat, M. Ross, and P. D. Brooks (2014), Changes in snow accumulation and ablation following the Las Conchas Forest Fire, New Mexico, USA, *Ecohydrology*, *7*(2), 440-452.

Kelly, A. E., and M. L. Goulden (2008), Rapid shifts in plant distribution with recent climate change, *Proceedings of the National Academy of Sciences of the United States of America*, *105*(33), 11823-11826.

Knowles, N., M. D. Dettinger, and D. R. Cayan (2006), Trends in snowfall versus rainfall in the Western United States, *Journal of Climate*, *19*(18), 4545-4559.

Littell, J. S., D. McKenzie, D. L. Peterson, and A. L. Westerling (2009), Climate and wildfire area burned in western U. S. ecoprovinces, 1916-2003, *Ecological Applications*, *19*(4), 1003-1021.

Marlon, J. R., et al. (2012), Long-term perspective on wildfires in the western USA, *Proceedings of the National Academy of Sciences of the United States of America*, *109*(9), E535-E543.

References (continued)

Melloh, R. A., J. P. Hardy, R. E. Davis, and P. B. Robinson (2001), Spectral albedo/reflectance of littered forest snow during the melt season, *Hydrological Processes*, *15*(18), 3409-3422.

Melloh, R. A., J. P. Hardy, R. N. Bailey, and T. J. Hall (2002), An efficient snow albedo model for the open and sub canopy, *Hydrological Processes*, *16*(18), 3571-3584.

Moritz, M. A., M.-A. Parisien, E. Batllori, M. A. Krawchuk, J. Van Dorn, D. J. Ganz, and K. Hayhoe (2012), Climate change and disruptions to global fire activity, *Ecosphere*, *3*(6), art49.

Mote, P. W., A. F. Hamlet, M. P. Clark, and D. P. Lettenmaier (2005), Declining mountain snowpack in western north America, *Bulletin of the American Meteorological Society*, *86*(1), 39.

O'Halloran, T. L., et al. (2012), Radiative forcing of natural forest disturbances, *Global Change Biology*, *18*(2), 555-565.

Painter, T. H., A. C. Bryant, and S. M. Skiles (2012), Radiative forcing by light absorbing impurities in snow from MODIS surface reflectance data, *Geophysical Research Letters*, *39*(17).

Painter, T. H., A. P. Barrett, C. C. Landry, J. C. Neff, M. P. Cassidy, C. R. Lawrence, K. E. McBride, and G. L. Farmer (2007), Impact of disturbed desert soils on duration of mountain snow cover, *Geophysical Research Letters*, *34*(12), L12502.

Pederson, G. T., J. L. Betancourt, and G. J. McCabe (2013), Regional patterns and proximal causes of the recent snowpack decline in the Rocky Mountains, US, *Geophysical Research Letters*, 1-6.

Pomeroy, J., X. Fang, and C. Ellis (2012), Sensitivity of snowmelt hydrology in Marmot Creek, Alberta, to forest cover disturbance, *Hydrological Processes*, *26*(12), 1892-1905.

Preston, C., and M. Schmidt (2006), Black (pyrogenic) carbon: a synthesis of current knowledge and uncertainties with special consideration of boreal regions, *Biogeosciences*, *3*(4), 397-420.

References (continued)

Serreze, M. C., M. P. Clark, R. L. Armstrong, D. A. McGinnis, and R. S. Pulwarty (1999), Characteristics of the western United States snowpack from snowpack telemetry (SNOTEL) data, *Water Resources Research*, *35*(7), 2145-2160.

Skidmore, P. B., K. Hansen, and W. Quimby (1994), *Snow accumulation and ablation under fire-altered lodgepole pine forest canopies*, Montana State University.

Skiles, S. M., T. H. Painter, J. S. Deems, A. C. Bryant, and C. C. Landry (2012), Dust radiative forcing in snow of the Upper Colorado River Basin: 2. Interannual variability in radiative forcing and snowmelt rates, *Water Resources Research*, *48*(7).

Sturm, M., J. Holmgren, and G. E. Liston (1995), A seasonal snow cover classification system for local to global applications, *Journal of Climate*, *8*(5), 1261-1283.

Taylor, G., and C. Hannan (1999), *The climate of Oregon: From rain forest to desert*, 211 pp., Oregon State University Press, Corvallis, Oregon.

Walters, S. P., N. J. Schneider, and J. D. Guthrie (2008), Geospatial Multi-Agency Coordination (GeoMAC) Wildland Fire Perimeters.

Warren, S. G., and W. J. Wiscombe (1980), A model for the spectral albedo of snow, 2. Snow containing atmospheric aerosols, *Journal of the Atmospheric Sciences*, *37*(12), 2734-2745.

Westerling, A. L., H. G. Hidalgo, D. R. Cayan, and T. W. Swetnam (2006), Warming and earlier spring increase western US forest wildfire activity, *Science*, *313*(5789), 940.

Westerling, A. L., B. P. Bryant, H. K. Preisler, T. P. Holmes, H. G. Hidalgo, T. Das, and S. R. Shrestha (2011), Climate change and growth scenarios for California wildfire, *Climatic Change*, *109*, 445-463.

Winkler, R. D. (2011), Changes in snow accumulation and ablation after a fire in south-central British Columbia, *Streamline Watershed Management Bulletin*, *14*(2), 1-7.

2.8 Figures

Figure 2.1. Burned woody debris (BWD) – pyrogenic carbon, charred woody detritis, burned branches, cones, and bark – accumulated on the snowpack surface.

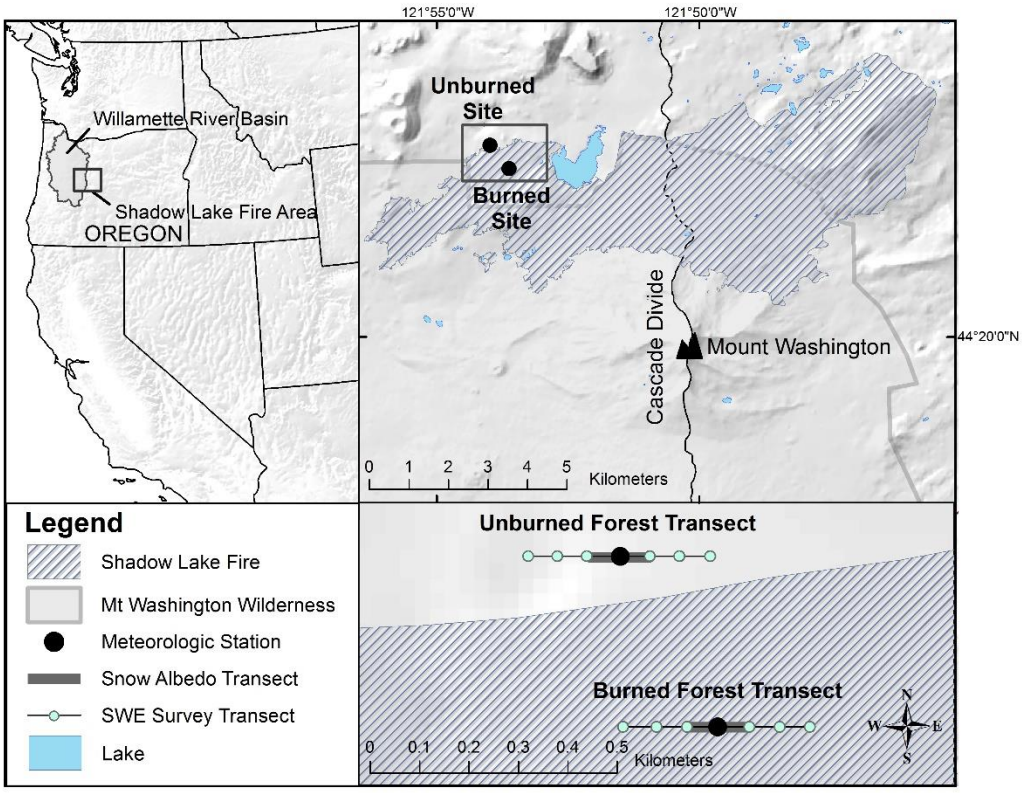

Figure 2.2. Burned and unburned forest sites are located in the Shadow Lake Fire area.

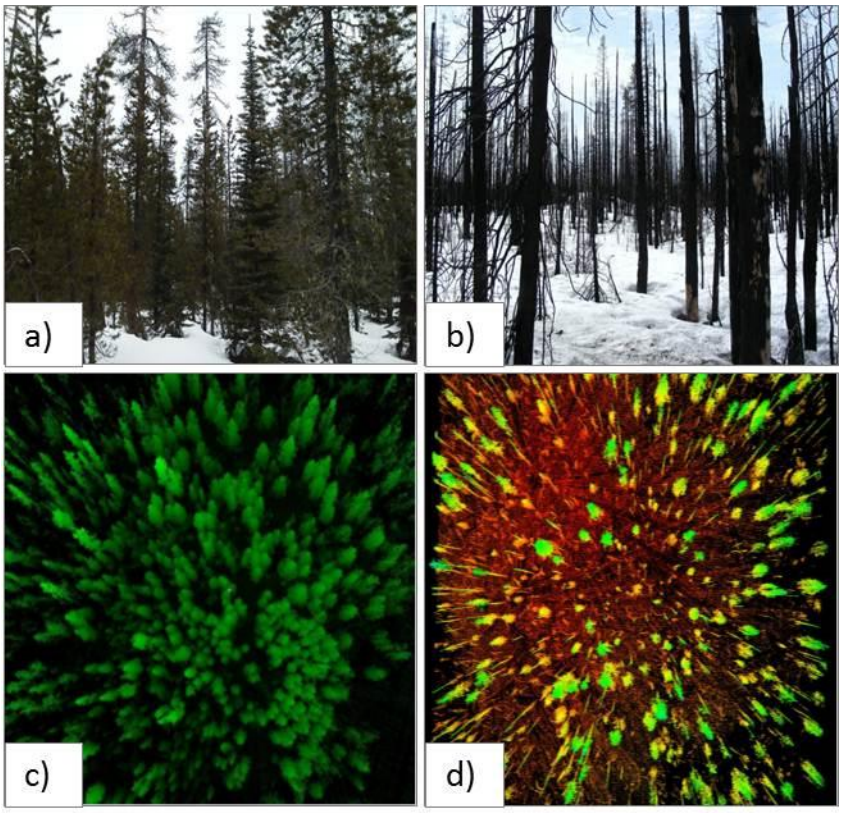

Figure 2.3. a & b) Unburned and burned forests, 04 May 2012; c & d) aerial representation of unburned forest and burned forest structure as determined by TLS surveys, colored by relative elevation (red=lowest elevation and green=highest elevation in scan area).

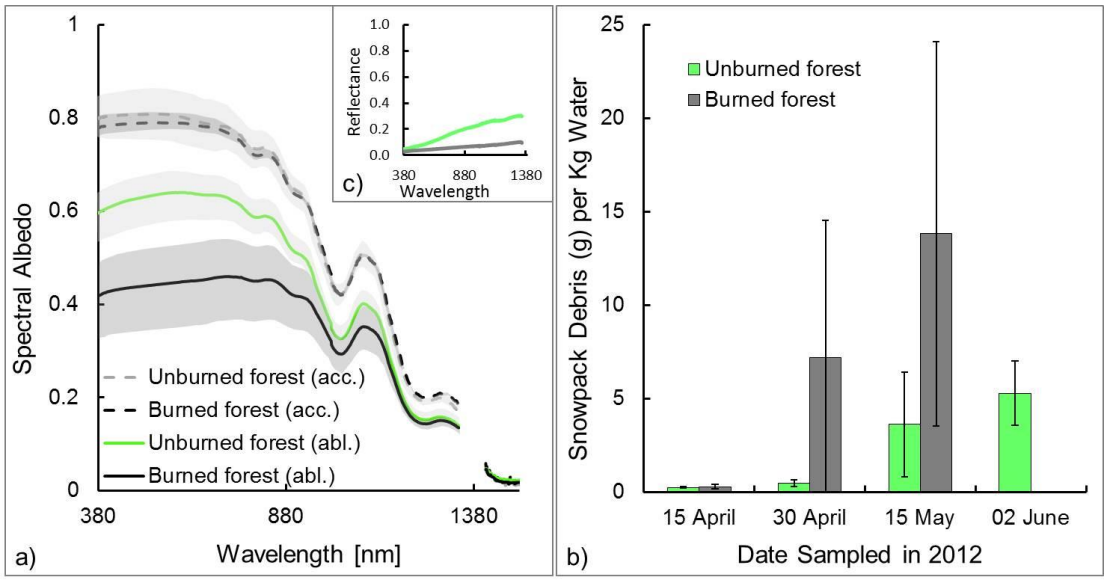

Figure 2.4. a) Mean ASD-FR-measured snow spectral albedo during accumulation (acc. 25 March 2013) and ablation (abl. 04 May 2012), shaded grey areas indicate range of measurements; b) Mean debris concentrations in ablation season snow samples, bars indicate one standard deviation; c) Reflectance factors of debris filtered from ablation season snow samples.

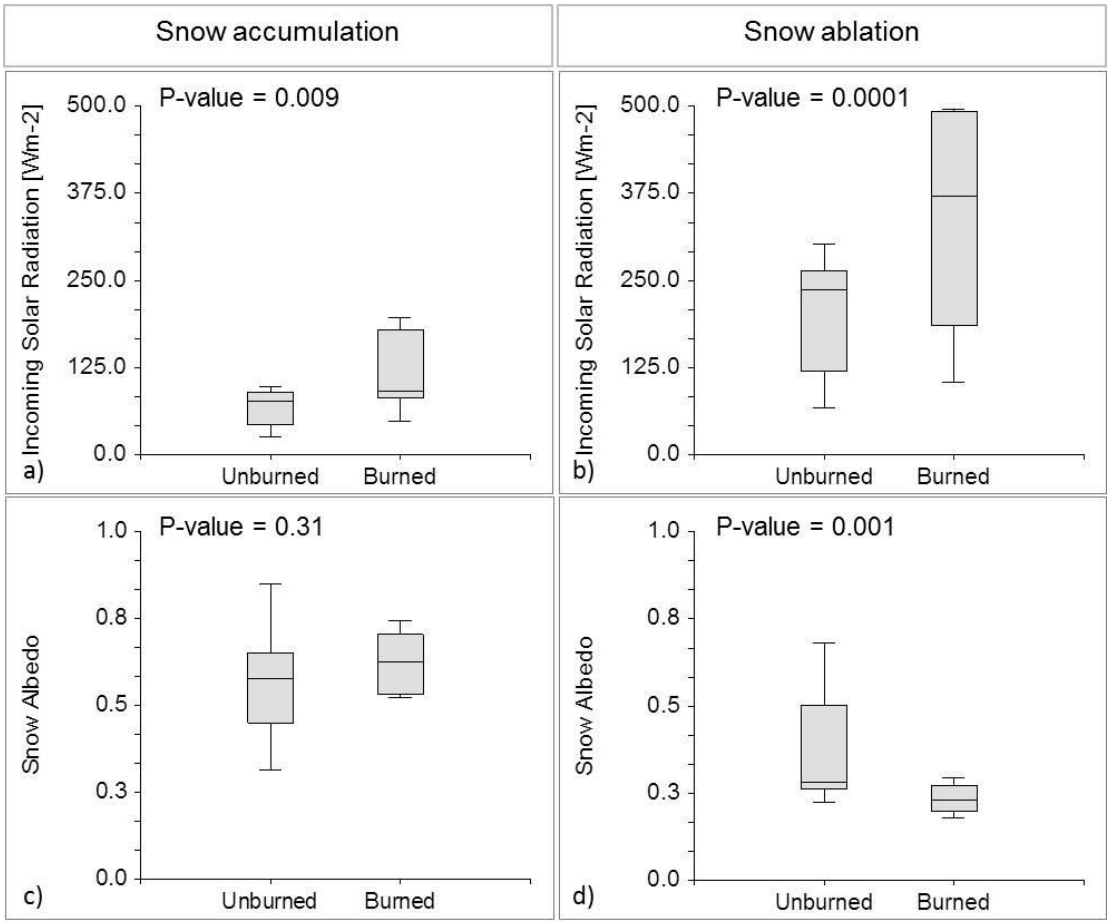

Figure 2.5. Box plots showing median and interquartile ranges in the distribution of pyranometer-measured incoming solar radiation during a) snow accumulation (04-27 February 2012) and b) snow ablation (08-31 May 2012); and snow albedo during c) snow accumulation (04-27 February 2012), and d) snow ablation (08-31 May 2012), in the burned and unburned forest plots.

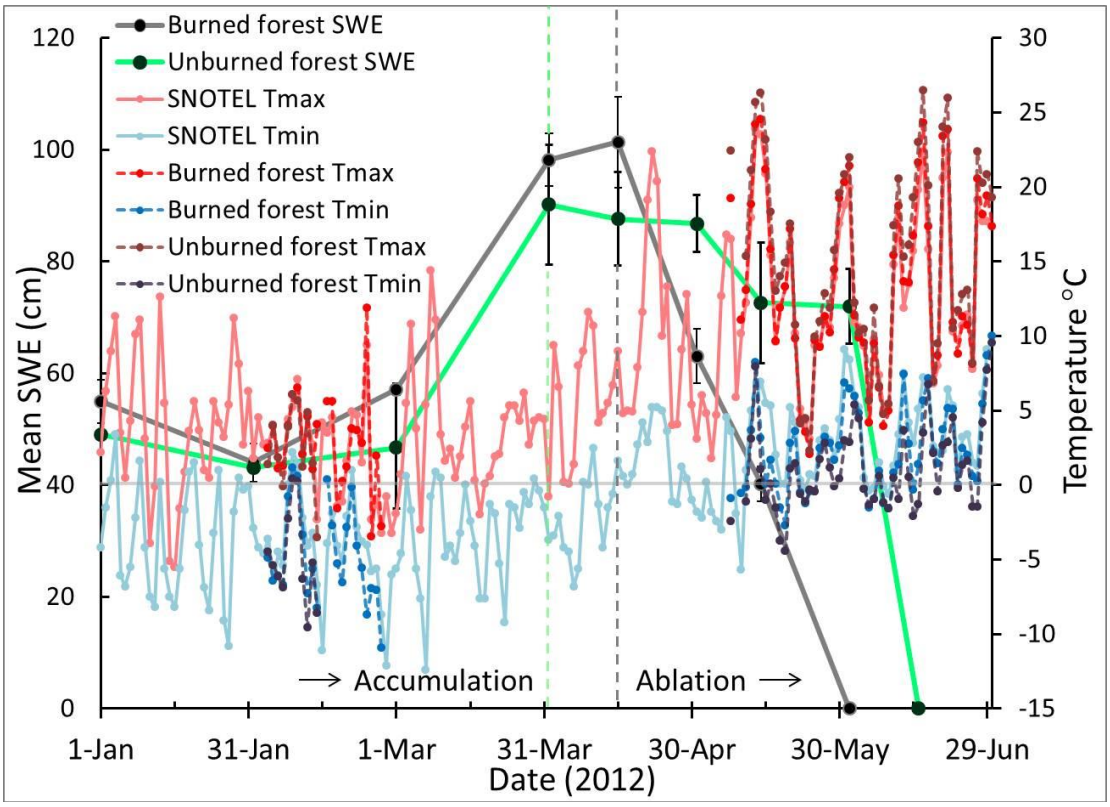

Figure 2.6. Measured mean snow water equivalent (SWE) in burned and unburned forests. Maximum SWE is indicated by vertical dashed lines. Minimum and maximum temperature data in burned and unburned forests, and retrieved from nearby NRCS-SNOTEL Hogg Pass Site. Horizontal grey line indicates 0º C.

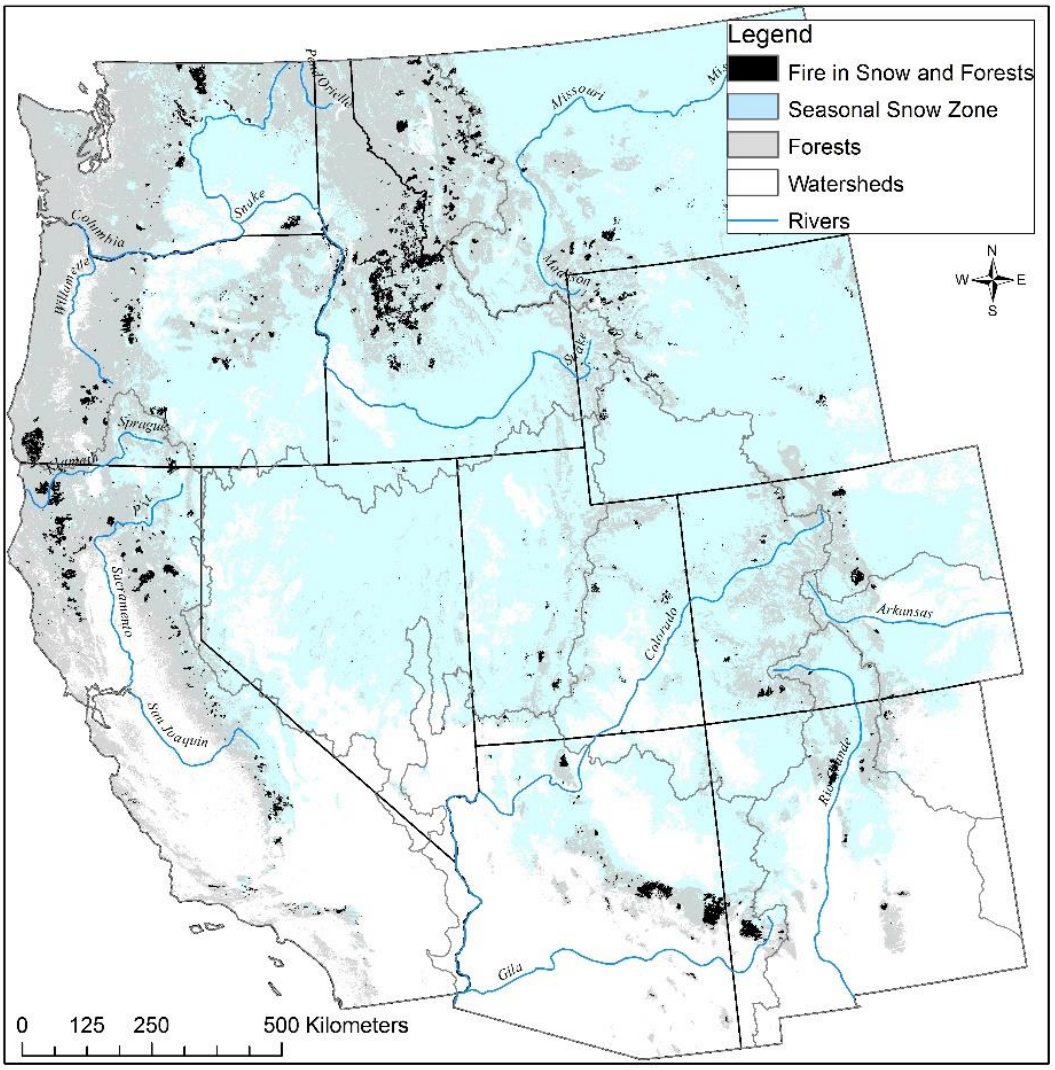

Figure 2.7. Forest fire area overlapping the seasonal snow zone in the western United States (2000-2012).

2.9 Tables

Table 2.1. Changes in net shortwave radiation due to the differences in snow albedo and incoming solar radiation in unburned and burned forest plots. Broadband mean snow albedo and radiation values were calculated for the snow accumulation period (04-27 February 2012), and snow ablation period (08-31 May 2012). ASD-FR mean albedo values were calculated for the snow accumulation period (25 March 2013), and snow ablation period (04 May 2012).

Measurement Period	Measurement Type	Forest Type	Mean Snow Albedo	Mean Incoming Shortwave Radiation [Wm-2]	Net Shortwave Radiation [Wm-2]
Accumulation	Pyranometer	Unburned forest	0.67	69	23
		Burned forest	0.68	114	36
		Change in net shortwave radiation			13
Accumulation	ASD-FR	Unburned forest	0.75	69	17
		Burned forest	0.74	114	30
		Change in net shortwave radiation			13
Ablation	Pyranometer	Unburned forest	0.38	203	126
		Burned forest	0.29	363	258
		Change in net shortwave radiation			132
Ablation	ASD-FR	Unburned forest	0.58	203	85
		Burned forest	0.42	363	211
		Change in net shortwave radiation			126

3 Charred Forests Increase Turbulent Energy Exchange over Snow: Sensible and Latent Heat Fluxes in a Burned and Unburned Montane Forest

Charred Forests Increase Turbulent Energy Exchange over Snow: Sensible and Latent Heat Fluxes in a Burned and Unburned Montane Forest

Kelly E. Gleason, Anne W. Nolin, Christoph Thomas, and Chad Higgins

Journal of Geophysical Research – Atmospheres
Submitted June 2015

3.1 Abstract

Snowmelt in the post-fire environment is accelerated by increased net shortwave radiation. However the role of post-fire turbulent fluxes over snow has not been quantified. In a paired burned/unburned forest study in the Oregon Cascades, we show that sensible and latent heat fluxes are roughly double the magnitude and variability in the burned forest compared with the unburned forest, yet they are still relatively small compared with shortwave radiative fluxes. Using eddy covariance and bulk-transfer techniques we measured sensible and latent heat in the paired sites during a cloudy pre-melt period (29 March 2013 to 03 April 2013) and during a clear sky snowmelt period (21 April 2013 to 02 May 2013). During the cloudy pre-melt period, turbulent fluxes contributed 35% of the net snowpack energy balance in the burned forest, and 22% of the net snowpack energy balance in the unburned forest. During the snowmelt period, turbulent fluxes represented -167% of the net snowpack energy balance in the burned forest, and -63% of the net snowpack energy balance in the unburned forest. The bulk aerodynamic method better resolved the sensible and latent heat fluxes over snow in the burned forest than the unburned forest, and overall better resolved the sensible fluxes than the latent fluxes. Bulk aerodynamic methods captured the relative differences in the sensible and latent heat fluxes between the burned and unburned forest during the pre-melt and snowmelt periods. Eddy covariance measurements demonstrated that the turbulent fluxes over snow can be periodically large and substantial over time. However the radiative fluxes dominate

the snowpack energy balance in burned and unburned forests. The contribution of sensible heat flux and loss of energy by the latent heat flux is responsible for a loss of snow mass of approximately 2% that measured snowmelt in the burned forest site during the clear-sky snowmelt period. Forest fires increase the net shortwave radiation over snow, decrease the net longwave radiation, and increase the sensible and latent heat fluxes over snow.

3.2 Introduction

Over the past decade, forest fires have been extensive across the seasonal snow zone in the western United States [*Gleason et al.*, 2013], and are likely to increase in extent, duration, and severity in a warming climate [*Semmens and Ramage*, 2012]. Although very little is known about how forest fire disturbance effects the snowpack energy balance and ultimately the persistence of seasonal snow cover in spring. Seasonal snow is an important reservoir of winter precipitation, and its persistence in spring is directly dependent on its surface energy balance and resulting change in the snowpack cold content. The radiative energy fluxes dominate the snowpack energy balance, although the turbulent energy exchange of heat and water vapor at the snow surface with the atmosphere is an important contribution to the snowpack energy balance, particularly in the snow melt season [*Garvelmann et al*., 2014; *Marks and Dozier*, 1992]. Measuring turbulent exchange in low flux environment such as above snow in mountain ecosystems, presents many challenges. Technical challenges such as power supply, icing and riming of sensors, as well as small perturbations in scalars that may be close to the detection limit of the sensors, are common. Theoretical challenges such as the relatively large flux loss because of small turbulence elements compared to finite separation distance [*Sakai et al.*, 2001], stable stratification leading to intermittency [*Sun et al.*, 2004], non-stationarities, and the presence of sub meso-scale atmospheric boundary layer motions [*Guettler and Belusic*, 2012; *L Mahrt*, 2010] are common and more difficult to quantify. Surface

heterogeneity and forest canopy architecture are additional structural challenges to measuring turbulent energy exchange over snow in forested mountain regions.

Forest canopies influence the snowpack energy balance in multiple ways, including by modifying the transmission of shortwave radiation through the canopy, the emission of longwave radiation from the canopy, and reducing wind speeds and therefore reducing the momentum driving the turbulent heat fluxes [*Burns et al.*, 2014; *Sicart et al.*, 2004]. Forest fire significantly alters the post-fire radiative regime over snow, by increasing canopy transmissivity, and decreasing the reflectivity of the snow surface through the deposition and concentration of organic debris [*Burles and Boon*, 2011; *Gleason et al.*, 2013; *Ueyama et al.*, 2014]. Despite recent progress in understanding and quantifying the key drivers of snowpack dynamics, there is still much uncertainty in how forest fire disturbance alters the turbulent energy exchange over snow. To date, no study thus far has evaluated the contribution of turbulent fluxes to snowpack energy balance snow in a very recently burned forest using eddy covariance methods, nor evaluated the ability of simple bulk aerodynamic methods to resolve the turbulent fluxes in these snow-dominated fire-disturbed forests. The objectives of this research were to:

1. Quantify and compare the turbulent energy fluxes over snow in a burned forest and in an adjacent unburned forest;
2. Evaluate the ability of a bulk aerodynamic method to resolve the turbulent fluxes over snow in a burned forest;

3. Evaluate the relative contribution of radiative and turbulent fluxes to the snowpack energy balance in a burned forest.

3.3 Background

3.3.1 Snowpack Energy Balance

The net snowpack energy balance Q* [W m^{-2}] is equal to the sum of the radiative, turbulent, conductive, and advective fluxes (Equation 3.1).

$$Q^* = Q_{radiative} + Q_{turbulent} + Q_{conductive} + Q_{advective} \quad \text{(Equation 3.1)}$$

Specifically, the net radiative flux includes the sum of the net shortwave (Q_K), and net longwave (Q_L) radiation, and the turbulent fluxes include the sensible (Q_H), and latent (Q_E) heat fluxes.

During the winter season snow accumulation period, when air temperatures are low (below 0°C) and humidity is low on non-storm days, snowpack energy balance is dominated by radiative fluxes [*Marks and Dozier*, 1992]. Even though new snow has an albedo of 0.8 or higher (integrated across the spectral range of 0.3–3.0 □m) [*Wiscombe and Warren*, 1980], and reflects the vast majority of the incoming solar radiation, net shortwave radiative fluxes provide the primary contribution to the snowpack energy balance [*Marks and Dozier*, 1992]. The net longwave radiative flux can be of equal magnitude, or even larger than the net shortwave radiative flux. While, the net longwave radiative flux is typically negative under clear-skies and in open areas, during warm cloudy days or under forest canopies, the longwave energy input can dominate the snowpack energy balance [*Lundquist et al.*, 2013; *Sicart et al.*, 2004]. During the winter accumulation period, and particularly in cold snow climates, turbulent energy fluxes over snow tend to be small, for there is no liquid

melt water for evaporation from the snowpack and little atmospheric water vapor for condensation onto the snow surface. Although, in dry windy environments, sublimation may cause a significant loss of latent energy from the snowpack even during the winter accumulation period [*Pomeroy et al.*, 1998]. In humid snow climates, if the snow surface temperature is below 0°C, water vapor may sublimate (deposit) onto the snow surface in the form of hoar frost. The latent heat released due to sublimation of vapor onto the surface is an energy input to the snowpack [*Oke*, 2002].

During the spring as air temperatures rise, sensible heat flux to the snow increases. Latent heat flux to the snowpack is positive when atmospheric saturation occurs, resulting in condensation or deposition onto the snowpack surface, thereby adding energy via the latent heat of vaporization or sublimation, respectively [*Leydecker and Melack*, 1999]. When the atmosphere is unsaturated, evaporation or sublimation may occur, resulting in a net energy loss from the snowpack [*DeWalle and Rango*, 2008]. The variability in turbulent energy exchange between the snowpack and the atmosphere depends on multiple scaling parameters, but is an important overall contribution to the snowpack energy balance. Accurately estimating the sensible and latent heat fluxes with the snowpack are critical for determining the rate of snowmelt and the snow disappearance date. [*Marks and Dozier*, 1992]. Under extreme events turbulent energy exchange can dominate the snowpack energy balance [*Garvelmann et al.*, 2014; *Marks et al.*, 1998; *Marks et al.*, 2001].

Compared with the radiative and turbulent energy fluxes to snow, other energy fluxes are relatively minor. Ground heat flux contributes very little to the total energy balance of a snowpack [*Marks and Dozier*, 1992]. The net advective flux contributions from rainfall, snowmelt, and refreezing also contribute little to the overall snowpack energy balance although such contributions may be sporadically important to snowpack energy balance during extreme rain-on-snow events [*Marks et al.*, 1998].

3.3.2 Forest Disturbance Influences to Snowpack Energy Balance

Forest canopies influence the snowpack energy balance by modifying the radiative and turbulent fluxes at the snowpack surface [*Ellis et al.*, 2010; *Lee and Mahrt*, 2004; *Mahrt and Vickers*, 2005a; b; *Pomeroy et al.*, 2003; *Turnipseed et al.*, 2003]. Forests influence the shortwave radiative fluxes over snow by altering the intensity and spectral composition of spectral irradiance [*Musselman et al.*, 2012; *Pomeroy and Dion*, 1996; *Seyednasrollah et al.*, 2013], and the reflectivity of the snow surface as a result of the deposition and concentration of organic debris [*Hardy et al.*, 2004; *Melloh et al.*, 2001]. Forests influence the longwave radiative fluxes over snow by altering the intensity of thermal irradiance as a function of forest structure, canopy and trunk temperature [*Garvelmann et al.*, 2014; *Lawler and Link*, 2011; *Pomeroy et al.*, 2009]. Forests influence the turbulent fluxes over snow by reducing wind speeds and turbulence through diminished shear generation, [*Blanken et al.*, 1998; *Garvelmann et al.*, 2014; *Harding and Pomeroy*, 1996; *Marks et al.*, 2008].

Marks et al. [2008], reported mean sensible heat fluxes of 7 [W m^{-2}] and latent heat fluxes of -6 [W m^{-2}] for the snow melt period, but with instantaneous measurements of up to +/- 30 [W m^{-2}]. *Launianen et al.*, [2005], reported sensible fluxes of greater magnitude, from -20 to 30 [Wm^{-2}], for the mid-winter period, but noted the magnitude and sign of fluxes were dependent on atmospheric stability. Open forest canopies are typically characterized by greater stability, while closed forests are almost always neutral within the canopy layer. Stable conditions are common over winter snowpack which can be cold, and are associated with near-surface temperature inversions that reduce turbulent mixing [*Mahrt and Thomas,* submitted 2015; *Male and Granger,* 1981].

Forest fire disturbance has been shown to increase streamflow primarily due to the reduction in evapotranspiration [*Holden et al.*, 2012; *Pomeroy et al.*, 2012; *Stoof et al.*, 2012]. Studies have shown changes to the land surface energy budget following fire using eddy covariance methods in a burned boreal forests [*Amiro,* 2001; *Amiro et al.*, 2006; *Chambers et al.*, 2005; *Liu et al.*, 2005; *Randerson et al.*, 2006; *Ueyama et al.*, 2014]. These studies showed a 10-31% reduction in net radiative, and a 55% reduction in turbulent flux contributions to the land surface energy balance in recently burned forests [*Chambers et al.*, 2005; *Liu et al.*, 2005]. Due to sign conventions, this reduction in the radiative and turbulent flux contributions to the land surface energy balance, corresponds to an increase in the radiative and turbulent flux contributions to the snowpack energy balance. These

measurements were made above the forest canopy, and therefore are most relevant to the land surface energy balance of the entire forest canopy. Few studies have investigated the sub-canopy snowpack energy balance and subsequent snowmelt in burned forests [*Burles and Boon*, 2011; *Gleason et al.*, 2013]. These studies were focused specifically on the net shortwave radiative flux over snow [*Gleason et al.*, 2013], or used simplified bulk aerodynamic approaches to resolve the turbulent flux contributions to the snowpack energy balance [*Burles and Boon*, 2011].

Most operational hydrological forecasters still use hydrology models which calculate snowpack energy balance using bulk aerodynamic methods for computational efficiency. However, due to the technological advancements over the past decades direct approaches of measuring the turbulent fluxes over snow using eddy covariance (EC) methods are becoming more common. EC measurements have been applied in snow covered conditions under varying terrain [*Burns et al.*, 2014; *Launiainen et al.*, 2005; *Molotch et al.*, 2007; *Pomeroy et al.*, 2003; *Turnipseed et al.*, 2002; *Turnipseed et al.*, 2003], but very few studies have evaluated the turbulent fluxes over snow using EC measurements under the forest canopy [*Burns et al.*, 2014; *Launiainen et al.*, 2005; *Marks et al.*, 2008].

3.3.3 Direct Approach: Eddy Covariance

The sensible and latent heat fluxes may be expressed as the covariance of fluctuations in the vertical velocity, *w*, of either temperature or water vapor concentration. The fluxes are defined as,

$$Q_H = C_p \rho_a \overline{w'T'} \quad \text{(Equation 3.2)}$$

$$Q_E = \lambda \, \rho_a \overline{w' \, q'} \quad \text{(Equation 3.3)}$$

Sensible heat (*w'T'*) exchange in energetic units [W m^{-2}] is the product of (*w'*) the vertical wind velocity, and (*T'*) temperature [K], as a function of (c_p) the specific heat of air, and (ρ_a) the density of air (Equation 3.2). The latent heat flux (*w'q'*) in energetic units is described as the kinematic water vapor transport as a function of (λ) latent heat of vaporization [J g^{-1}], and (ρ_a) the density of air (Equation 3.3).

The eddy covariance method is a direct flux determination method, as it computes the flux without the assumption of flux-gradient theories. The most important assumptions for this method are ergodicity of the flow, i.e., time and space averages converge, homogeneity of the flux source surface area, and stationary atmospheric conditions. The choice of the perturbation time scale and the size of the measurement footprint are associated with how well these assumptions are obeyed [*Vickers et al.*, 2009].

3.3.4 Indirect Approach: Bulk Aerodynamic Equations

The bulk aerodynamic equations for computing the flux density of sensible and latent heat exchange can be written as follows [*Foken*, 2008]. *Marks and Dozier* [1992], take a similar approach adapted from [*Brutsaert*, 1982].

$$Q_H = \rho c_p C_H(z) u(z) (T_z - T_{ss}) \quad \text{(Equation 3.4)}$$

$$Q_E = \rho \lambda C_E(z) u(z) (e_z - e_{ss}) \quad \text{(Equation 3.5)}$$

Where sensible heat flux density (Q_H) is the product of, (ρ_a) the density of air [kg m^{-3}], (c_p) the heat capacity of air [J kg^{-1} K^{-1}], (C_H) the Stanton number (bulk-coefficient), (u) wind speed [m s^{-1}], and ($T_z - T_{ss}$) the temperature difference between the measurement height (z) and the snow surface (Equation 3.4).The latent heat flux density (Q_E) is the product of, density of air, (λ_v) the latent heat of vaporization [2.48x10^6 J kg^{-1}], (C_E) the Dalton number (the bulk coefficient), wind speed, and ($e_a - e_{ss}$) the vapor pressure difference between the measurement height (z) and the snow surface (Equation 3.5).

Most hydrology models that explicitly resolve the snowpack energy balance use indirect approaches to calculate the sensible and latent heat fluxes at the snowpack surface. The bulk aerodynamic approach is a common indirect method, which uses measurements of wind speed, air temperature, and humidity at a fixed height above the snow surface to calculate the turbulent fluxes. Application of the bulk aerodynamic method to the computation of sensible and latent heat exchange over snow requires several assumptions including flux-gradient similarity, developed turbulence, and neutral stratification [*Moore*, 1983]. Despite its simplifications, the bulk-aerodynamic approach has been widely been used to approximate sensible and latent heat fluxes to the snowpack [*Anderson*, 1976; *Kustas et al.*, 1994; *Marks and Dozier*, 1992]. Functions for the bulk transfer coefficients have been empirically-derived by many authors [*Anderson*, 1976; *Brutsaert*, 1982; *Kustas et al.*, 1994; *Oke*, 2002], but are typically based on the roughness length, the von Karmán constant, and

stability parameters such as the dimensionless bulk Richardson number. The bulk-transfer coefficients C_H and $C_{E,}$ are stability dependent parameterizations, where a small error in determining the roughness length at the measurement height ($z_{0)}$ and the roughness length at the snow surface ($z_{0ss)}$ is largely influential in the calculations of turbulent fluxes.

3.4 Research Methods

3.4.1 Study Site

In a recently burned area near the crest of the western Oregon Cascades, we conducted an experiment monitoring turbulent fluxes over snow in paired burned and unburned forest sites (Figure 3.1), following the Shadow Lake Fire which burned over 11,000 acres of sub-alpine fir and pine forest at the headwaters of the McKenzie River, an important tributary of the Willamette River. The burned forest site was located in the largest contiguous high-severity burned patch within the Shadow Lake Fire burned area, which extended roughly for 700 m north-south and 200 m east-west of the burned forest study site. The unburned forest site was located in the center of the nearest contiguous patch of unburned sub-alpine fir and pine forest of similar area to burned forest site, approximately 1 km northwest of the burned forest site.

Terrestrial laser scanner data (Figure 3.2) confirmed the forest density was reduced by 500%, and hemispherical photography confirmed the canopy density was reduced by 300% in the burned forest as compared to the nearby unburned forest [*Gleason et al.*, 2013]. The mean overstory tree height is approximately 15 m in the remaining burned forest, and approximately 10 m in the nearby unburned forest. Lodgepole pine (*Pinus contorta*), sub-alpine fir (Abies *lasiocarpa*), and blue spruce (*Pinus pungens*), were dominant tree species, with a recent history of mountain pine beetle, and spruce budworm and frequent forest fires.

3.4.2 Eddy covariance, micrometeorological, and snow monitoring measurements

Snow energy balance stations were established in the burned and unburned forest sites, where we measured turbulent heat fluxes using eddy covariance, basic micrometeorological, and snow monitoring instruments. At 5 m above ground, in the sub-canopy of the burned and unburned forest sites, we measured the sensible and latent heat fluxes based upon turbulence observations at a 10 Hz sampling rate using a combination of a sonic anemometer and an open-path infrared gas analyzer (Model IRGASON, Campbell Scientific, Logan, UT, USA). At 5m and 2m above ground we measured temperature and relative humidity with a thermohygrometer (Model HMP 45, Vaisala Inc., Finland) in a custom-designed aspirated double-walled radiation shield [*Thomas and Smoot*, 2012]. At 5 m above ground we measured wind speed using a cup anemometer (Model MetOne XXX), incoming and outgoing solar radiation using pyranometers (Model LI-200s, LI-COR, Lincoln, NE, USA), and snow depth using a sonic depth sensor (Model Ultrasonic depth sensor, Judd Communications, Salt Lake City, UT, USA), every 10 s and recorded the 10-min averages of these measurements using a data logger (Model CR1000, Campbell Sci., Logan, UT, USA). At 5 m above the ground we maintained a four-component net radiometer to collect incoming and outgoing shortwave and longwave radiative fluxes (Model NR01, Hukseflux Thermal Sensors, The Netherlands) from 06 March 2013 to 20 April 2013. At approximately 5-m downslope of the micrometeorological

stations, we installed snowmelt lysimeters with a catchment area of 4.65 m^2, and measured snowmelt runoff from the lysimeters using a tipping bucket rain gage. Of the 60-day period of simultaneous data collection of eddy covariance and basic micrometeorological data in the burned and unburned forest, snowfall and rainfall restricted collection of biophysical eddy covariance flux data. Useable data were retrieved during a 6-day pre-melt period with cloudy atmospheric conditions from 29 March 2013 to 03 April 2013 (day-of-year (DOY) 88-93), and a 10 day period during snowmelt with clear-sky atmospheric conditions with strong diurnal fluctuations in temperature and humidity from 21 April 2013 to 02 May 2013 (DOY 111-121).

3.4.3 Flux Calculations and Analysis

In this paper, we follow the flux sign convention common in the hydrologic community and define energy fluxes directed towards the snow surface as positive, indicating a net energy gain for the snowpack [*Etchevers et al.*, 2004]. Latent and sensible heat fluxes from the 10 Hz high-frequency eddy covariance data were computed using a 300 s, i.e., 5 min perturbation time scale, and then linearly aggregated by averaging six subsequent 5-min intervals into 30min flux estimates to minimize both the random and systematic flux errors [*Vickers et al.*, 2009]. The flux calculation software included routines for 3D coordinate rotation, a despiking algorithm [*Vickers and Mahrt*, 1997], and a post-hoc flux density corrections [*Webb et al.*, 1980].

For comparison, sensible and latent heat fluxes were also calculated using simple bulk aerodynamic equations described above using the Thornthwaite-Holzman bulk transfer approach as described in [*Kustas et al.*, 1994], which parameterizes the turbulent transfer using stability criteria based on the bulk Richardson number [*Morris*, 1989]. This simple method was chosen because it is common in the snow hydrology models, and due to the uncertainty in selecting accurate roughness length values required in the stability corrections for the bulk-coefficients used in *Foken* [2008]. Temperature, relative humidity, and wind data from the energy balance stations were aggregated by computing a linear block-average over a one hour period prior to being entered into the formula. Hourly sensible and latent heat fluxes were tested for normality and evaluated between the burned and unburned forest from the EC and bulk aerodynamic methods using two-sample t-tests assuming unequal variances and 95% confidence limits.

Incoming and outgoing shortwave and longwave radiation measurements were also aggregated by computing a linear block-average over a one hour period and used to evaluate the contribution of net radiation to the snowpack energy balance. Incoming and outgoing shortwave radiation measurements were used to determine net shortwave radiation of the snowpack surface. Longwave radiation measurements were limited in their temporal extent (DOY 64-84 in the burned forest and DOY 84-110 in the unburned forest) therefore were used to determine the most effective method of calculating incoming longwave radiation in the burned and unburned

forests (Figure 3.3). The Crawford-Dilley method of calculating incoming longwave radiation performed best compared to measurements with the smallest RMSE [*Crawford and Duchon*, 1999; *Dilley and O'Brien*, 1998], and therefore was used to model incoming longwave radiation in the burned and unburned forests for the period consistent with biophysical EC data (DOY 88-93 & DOY 111-122).

3.5 Results

3.5.1 Eddy Covariance Sensible and Latent Heat Fluxes

Sensible and latent heat fluxes are of greater magnitude in the burned forest than in the unburned forest throughout the measurement period. During the cloudy pre-melt period, from DOY 88-93, both the sensible and latent heat fluxes were relatively small as compared to the clear-sky snowmelt period (Figure 3.4). During this period, the sensible and latent heat fluxes in the burned forest were more than double the magnitude of those in the unburned forest (H, p=0.004; Le, p= 1.04e-06) (Table 3.1).

During the clear sky snowmelt period, from DOY111-122, both the sensible and latent heat fluxes were of greater magnitude than in the cloudy pre-melt period (Figure 3.4). During this period, the sensible and latent fluxes in the burned forest were more than double the magnitude of those in the unburned forest (H, p=8.85e-04; Le, p= 1.39e-63) (Table 3.1). The variability in the sensible and latent fluxes was large in both forests and corresponded to diurnal and intra-seasonal variability in micrometeorological measurements both burned and unburned forest sites.

3.5.2 Bulk aerodynamic Sensible and Latent Heat Fluxes

During the cloudy pre-melt period, from DOY 88-93, the sensible and latent heat fluxes in the burned forest were approximately three times greater magnitude than those in the unburned forest (H, p= 4.47e-07; Le, p= 1.25e-12) (Table 3.1). During this cloudy period, the sensible heat fluxes derived from eddy covariance

measurements were significantly greater than those derived using the bulk aerodynamic equations in the burned forest but not in the unburned forest (BF, p= 0.01; UF, p= 0.14). Latent heat fluxes derived from EC measurements were significantly greater than those derived using the bulk equations in both the burned and unburned forests (BF, p= 5.52e-04; UF, p= 0.03).

During the clear-sky snowmelt period, from DOY 111-122, the sensible and latent heat fluxes in the burned forest were double the magnitude of those in the unburned forest (H, p= 8.15e-11; Le, p= 0.02) (Table 3.1). During this clear-sky period, the sensible heat fluxes derived from eddy covariance measurements were not significantly different than those derived using the bulk aerodynamic equations in both the burned and unburned forests. However, latent heat fluxes derived from EC measurements were almost double those calculated using the bulk approach in the burned and unburned forests (BF, p= 0.05; UF, p= 8.78e-07). The least squares regression lines of the sensible and latent heat fluxes in the burned forest relative to those in the unburned forest demonstrated that the bulk aerodynamic method captures the relative differences between the two forests in the sensible fluxes better than the relative differences in the latent fluxes (Figure 3.5). The latent and sensible heat fluxes are positively correlated in both the burned and unburned forests during both measurement periods (Figure 3.6).

3.5.3 Variability in Sensible and Latent Fluxes and Micrometeorology

The variability in the sensible and latent heat fluxes was dependent on diurnal and intra-seasonal variability in wind, temperature, humidity, and incoming solar radiation (Figure 3.7). The dependencies of the sensible and latent heat fluxes on the micrometeorological variables such as wind speed and the temperature and water vapor gradients over snow are embedded in the bulk aerodynamic equations. By evaluating the relationship of the eddy covariance fluxes to the parameters, we test the assumptions of flux-gradient similarity in its simplest form, the bulk method. Sensible fluxes measured with eddy covariance were well correlated with the temperature gradients, as well as the product of wind speed and the bulk-transfer coefficient over the snowpack, validating the flux-gradient similarity assumption implicit in bulk aerodynamic methods. Latent fluxes measured with eddy covariance were well correlated with the vapor pressure gradient, but were not well correlated with the product of wind speed and the bulk-transfer coefficient over snowpack, violating one important assumption implicit in the bulk aerodynamic approach.

Although sensible and latent heat fluxes in the burned forest are of consistently greater magnitude than in the unburned forest, ensemble averages demonstrated the burned and unburned forest have similar overall patterns of diurnal variability (Figure 3.8). During the cloudy pre-melt period (DOY 88-93), sensible and latent heat fluxes were mostly positive, while the greatest magnitude in both sensible and latent fluxes occurred in mid-day (Figure 3.8.a). During the clear-sky

snowmelt period (DOY 111-122), sensible fluxes were mostly positive, and latent fluxes were strongly negative. The greatest magnitude in both fluxes occurred in mid-day but with very large variability, particularly during the mid-day period when air temperatures and wind speeds are greatest (Figure 3.8.b). Negative sensible fluxes measured during the mid-day period, when air temperature was greater than the snowpack surface temperature, indicate the instruments captured fluxes not only from the snowpack surface but also from the surrounding forest canopy, and with an additional lag in the unburned forest site (Figure 3.8.b). The night-time variability in the latent fluxes estimated using the bulk aerodynamic method were likely due to the simplified stability parameters used in calculating the bulk coefficients for this method. Although daily average turbulent fluxes can be relatively small, these results showed that the turbulent fluxes over snow can be periodically large and substantial over time particularly during snowmelt.

3.5.4 Snowmelt and Sublimation

During the cloudy period, lysimeter data showed that minimal melt occurred from the snowpack in either the burned or unburned forest (Figure 3.7). During the clear-sky snowmelt period, lysimeter data showed that the snowpack in the burned forest was actively melting with diurnal variability positively correlated to air temperature and incoming solar radiation (Figure 3.7). Although there were two short periods on DOY 113 and DOY 119 which snowmelt occurred in the unburned forest, very little snowmelt occurred overall during the clear-sky snowmelt period (DOY

111-122). As air temperature and incoming solar radiation increased, one can infer the cold content of the snowpack in the burned forest was met each day, driving maximum instantaneous snowmelt of 0.6 [mm hr^{-1}]. Total daily snowmelt measured for the cloudy pre-melt period was 0.003 [mm day^{-1}] in the burned forest, and 1.6 [mm day^{-1}] in the unburned forest. Total daily snowmelt measured for the clear-sky snowmelt period was 3.85 [mm day^{-1}] in the burned forest, and 0.011 [mm day^{-1}] in the unburned forest. Although snowmelt in the unburned forest was greater during the cloudy pre-melt period than in the clear-sky snowmelt, snowmelt was greater overall in the burned forest than in the unburned forest. During the clear-sky period very little snowmelt occurred in the unburned forest even during periods of high air temperatures and incoming solar radiation, implying the cold content of the snowpack in the unburned forest had not yet been met.

Estimated sublimation was greater in the burned forest than the unburned forest (Figure 3.9). Estimated mean daily sublimation rates were negligible during the cloudy study period at 0.0025 [mm day^{-1}] in the burned forest and 0.0007 [mm day^{-1}] in the unburned forest. Estimated mean daily sublimation rates over the clear-sky study period were more substantial at 0.009 [mm day^{-1}] in the burned forest and 0.004 [mm day^{-1}] in the unburned forest. Total mass loss for the nine complete days of the clear sky sampling period was 3.62 [mm m^{-2}] in the burned forest and 1.81 [mm m^{-2}] in the unburned forest. The combined effects of increased transmissivity to solar

radiation with increased sensible and latent heat fluxes in the burned forest, induced greater sublimation and more rapid snowmelt than in the nearby unburned forest.

3.5.5 Snowpack Energy Balance: Error Analysis of Turbulent Fluxes

Throughout the measurement period the radiative fluxes dominated the snowpack energy balance. Net shortwave radiation is consistently greater in the burned forest, while net longwave radiation is consistently greater in the unburned forest (Figure 3.10). During the cloudy pre-melt period, the EC-derived turbulent fluxes contributed 35% in the burned forest and 22% in the unburned forest to the net snowpack energy balance (Table 3.2). Whereas the bulk-derived turbulent fluxes only contributed 15% in the burned forest and 7% in the unburned forest to the net snowpack energy balance. During this pre-melt period, the overall net snowpack energy balance was not significantly different between the burned and unburned forests. Nor was the net snowpack energy balance different when calculated using either the EC or bulk-derived sensible and latent heat fluxes in either forest site during this pre-melt period (Figure 3.11).

During the clear-sky snowmelt period, the EC-derived turbulent fluxes contributed -167% in the burned forest and -63% in the unburned forest to the net snowpack energy balance (Table 3.2).Whereas the bulk-derived fluxes only contributed 3% in the burned forest and -2% in the unburned forest to the net snowpack energy balance. During this snowmelt period, the overall net snowpack energy balance was greater during the peak daylight hours, and lesser during the peak

nighttime in the burned forest than the unburned forest (Figure 3.11). Overall the magnitude and variability in the net snowpack energy balance calculated using either the EC-derived or bulk-derived turbulent fluxes were similar because they are dominated by net shortwave and net longwave radiative fluxes. However these results were punctuated by periods in which the net snowpack energy balance derived from these two methods diverged and provided very different outcomes (i.e. DOY 113-114 and DOY 119-120).

3.6 Discussion and Conclusions

Forest fire disturbance increased the magnitude and variability of sensible and latent heat fluxes over snow, particularly during the spring snowmelt period. During the cloudy pre-melt period the turbulent fluxes were small compared to the clear-sky snowmelt period when turbulent fluxes substantially contributed to the net snowpack energy balance. Our results from the unburned forest were similar to those of previous authors who measured fluxes over snow with eddy covariance under a forest canopy [*Launiainen et al.*, 2005; *Marks et al.*, 2008]. The variability between the few below-canopy studies that have been conducted is likely due to the differences in forest structure and composition where the measurements were taken. *Garvelmann et al.*, [2014], investigated the spatial variability in complex terrain of energy balance components in relation to forest conditions and complex topography. They showed snowpack energy balance was dominated by shortwave radiation in open areas, but dominated by longwave radiation and turbulent fluxes in forested areas. We found similar results, where the snowpack energy balance was dominated by the radiative fluxes (shortwave radiation in the burned forest, and longwave radiation in the unburned forest). Eddy covariance measurements demonstrated that the turbulent fluxes over snow can be periodically large and substantial over time, however the radiative fluxes dominate the snowpack energy balance in burned and unburned forests. The diurnal fluctuations expressed in the ensemble mean results indicate extreme temporal variability in both the sensible and latent heat fluxes over snow,

where there are large fluxes at the 30 min time scale and relatively small fluxes at the daily time scale. The contribution of energy by the sensible heat flux and loss of energy by the latent heat flux during the snowmelt period, was responsible for a loss of snow mass of approximately 2% than that of measured snowmelt in the burned forest site, and 36% of measured snowmelt in the unburned forest site. Measured sublimation values from the unburned forest site were consistent with those found by *Molotch et al.,* [2007], for average daily sub-canopy sublimation rates in an unburned forest.

Although the direct eddy covariance methods of measuring turbulent fluxes over snow are preferable to indirect bulk aerodynamic methods of calculating the turbulent fluxes because they depend on fewer assumptions, there are many challenges in operating these eddy covariance systems, particularly in rugged forested montane watersheds. In this study, the bulk aerodynamic method captured the sign and relative magnitude, but not the appropriate variability in the sensible and latent heat fluxes, and therefore does not fully represent the fluxes at sub-daily time scales, during stable atmospheric conditions, or perhaps even during extreme storm events. The bulk approach did not capture the overall sub-daily scale magnitude or variability in the latent heat fluxes or in the sensible heat fluxes, but overall, the net snowpack energy balance calculated using the bulk aerodynamic method is highly correlated with the net snowpack energy balance calculated using EC measured turbulent fluxes. The few places for which the net snowpack energy balance diverged between these

two methods was during periods of high magnitude turbulent fluxes, which were generally not well represented by the bulk aerodynamic approach. Particularly for operational purposes, for which models are typically run on a daily time step, the bulk aerodynamic approach sufficiently estimates the mean sensible and latent heat fluxes in both burned and unburned forests. However, the direct eddy covariance approach is still preferred, particularly when accurately capturing the variability in the sensible and latent heat fluxes is required, such as during extreme rain-on-snow events.

Forest fire disturbance increases both the radiative and turbulent energy contributions to the snowpack energy balance, increases sublimation, and contributes to faster and earlier snow melt in the burned forests. These disturbance effects to snow ablation and the snowpack energy balance are important to consider in hydrologic models to accurately predict the volume and availability of water-resources in burned snow-dominated watersheds. Future work is required to identify the main drivers of the existing uncertainty in measuring sensible and particularly latent heat fluxes using simple bulk aerodynamic approaches in dense unburned forests with rugged terrain typical of forested montane watersheds of the Pacific Northwest.

3.7 References

Amiro, B. D. (2001), Paired-tower measurements of carbon and energy fluxes following disturbance in the boreal forest, *Global Change Biology*, *7*(3), 253-268.

Amiro, B. D., et al. (2006), Carbon, energy and water fluxes at mature and disturbed forest sites, Saskatchewan, Canada, *Agricultural and Forest Meteorology*, *136*(3-4), 237-251.

Anderson, E. A. (1976), A point of energy and mass balance model of snow cover, *NOAA Techical Report, National Weather Service*, *19*, 1-150.

Blanken, P. D., T. A. Black, H. H. Neumann, G. Den Hartog, P. C. Yang, Z. Nesic, R. Staebler, W. Chen, and M. D. Novak (1998), Turbulent flux measurements above and below the overstory of a boreal aspen forest, *Boundary-Layer Meteorology*, *89*(1), 109-140.

Brutsaert, W. (1982), Evaporation into the Atmosphere, 299 pp, *D. Reidel, Norwell, Mass*.

Burles, K., and S. Boon (2011), Snowmelt energy balance in a burned forest plot, Crowsnest Pass, Alberta, Canada, *Hydrological Processes*, *25*(19), 3012-3029.

Burns, S. P., N. P. Molotch, M. W. Williams, J. F. Knowles, B. Seok, R. K. Monson, A. A. Turnipseed, and P. D. Blanken (2014), Snow temperature changes within a seasonal snowpack and their relationship to turbulent fluxes of sensible and latent heat, *Journal of Hydrometeorology*, *15*(1), 117-142.

Chambers, S. D., J. Beringer, J. T. Randerson, and F. S. Chapin (2005), Fire effects on net radiation and energy partitioning: Contrasting responses of tundra and boreal forest ecosystems, *Journal of Geophysical Research - Atmospheres*, *110*(D9).

Crawford, T. M., and C. E. Duchon (1999), An improved parameterization for estimating effective atmospheric emissivity for use in calculating daytime downwelling longwave radiation, *Journal of Applied Meteorology*, *38*(4), 474-480.

DeWalle, D. R., and A. Rango (2008), *Principles of snow hydrology*, Cambridge University Press.

References (Continued)

Dilley, A. C., and D. M. O'Brien (1998), Estimating downward clear sky long-wave irradiance at the surface from screen temperature and precipitable water, *Quarterly Journal of the Royal Meteorological Society*, *124*(549), 1391-1401.

Ellis, C. R., J. W. Pomeroy, R. L. H. Essery, and T. E. Link (2010), Effects of needleleaf forest cover on radiation and snowmelt dynamics in the Canadian Rocky Mountains, *Canadian Journal of Forest Research-Revue Canadienne De Recherche Forestiere*, *41*(3), 608-620.

Etchevers, P., et al. (2004), Validation of the energy budget of an alpine snowpack simulated by several snow models (SnowMIP project), in *Annals of Glaciology, Vol 38, 2004*, edited by P. M. B. Fohn, pp. 150-158.

Foken, T. (2008), *Applied meteorology: micrometeorological methods*, Springer.
Garvelmann, J., S. Pohl, and M. Weiler (2014), Variability of Observed Energy Fluxes during Rain-on-Snow and Clear Sky Snowmelt in a Midlatitude Mountain Environment, *Journal of Hydrometeorology*, *15*(3), 1220-1237.

Gleason, K. E., A. W. Nolin, and T. R. Roth (2013), Charred forests increase snowmelt: Effects of burned woody debris and incoming solar radiation on snow ablation, *Geophysical Research Letters*, *40*(17), 4654-4661.

Guettler, I., and D. Belusic (2012), The nature of small-scale non-turbulent variability in a mesoscale model, *Atmospheric Science Letters*, *13*(3), 169-173.

Harding, R. J., and J. W. Pomeroy (1996), Energy balance of the winter boreal landscape, *Journal of Climate*, *9*(11), 2778-2787.

Hardy, J. P., R. Melloh, G. Koenig, D. Marks, A. Winstral, J. W. Pomeroy, and T. Link (2004), Solar radiation transmission through conifer canopies, *Agricultural and Forest Meteorology*, *126*(3-4), 257-270.

Holden, Z. A., C. H. Luce, M. A. Crimmins, and P. Morgan (2012), Wildfire extent and severity correlated with annual streamflow distribution and timing in the Pacific Northwest, USA (1984-2005), *Ecohydrology*, *5*(5), 677-684.

Kustas, W. P., A. Rango, and R. Uijlenhoet (1994), A simple energy budget algorithm for the snowmelt runoff model, *Water Resources Research*, *30*(5), 1515-1527.

References (Continued)

Launiainen, S., J. Rinne, J. Pumpanen, L. Kulmala, P. Kolari, P. Keronen, E. Siivola, T. Pohja, P. Hari, and T. Vesala (2005), Eddy covariance measurements of CO2 and sensible and latent heat fluxes during a full year in a boreal pine forest trunk-space, *Boreal Environment Research*, *10*(6), 569-588.

Lawler, R. R., and T. E. Link (2011), Quantification of incoming all-wave radiation in discontinuous forest canopies with application to snowmelt prediction, *Hydrological Processes*, *25*(21), 3322-3331.

Lee, Y. H., and L. Mahrt (2004), An evaluation of snowmelt and sublimation over short vegetation in land surface modelling, *Hydrological Processes*, *18*(18), 3543-3557.

Leydecker, A., and J. M. Melack (1999), Evaporation from snow in the central Sierra Nevada of California, *Nordic Hydrology*, *30*(2), 81-108.

Liu, H. P., J. T. Randerson, J. Lindfors, and F. S. Chapin (2005), Changes in the surface energy budget after fire in boreal ecosystems of interior Alaska: An annual perspective, *Journal of Geophysical Research - Atmospheres*, *110*(D13).

Lundquist, J. D., S. E. Dickerson-Lange, J. A. Lutz, and N. C. Cristea (2013), Lower forest density enhances snow retention in regions with warmer winters: A global framework developed from plot-scale observations and modeling, *Water Resources Research*, *49*(10), 6356-6370.

Mahrt, L. (2010), Computing turbulent fluxes near the surface: needed improvements, *Agricultural and Forest Meteorology*, *150*(4), 501-509.

Mahrt, L., and D. Vickers (2005a), Moisture fluxes over snow with and without protruding vegetation, *Quarterly Journal of the Royal Meteorological Society*, *131*(607), 1251-1270.

Mahrt, L., and D. Vickers (2005b), Boundary-layer adjustment over small-scale changes of surface heat flux, *Boundary-Layer Meteorology*, *116*(2), 313-330.

Male, D. H., and R. J. Granger (1981), Snow-surface energy exchange, *Water Resources Research*, *17*(3), 609-627.

References (Continued)

Marks, D., and J. Dozier (1992), Climate and energy exchange at the snow surface in the alpine region of the Sierra Nevada, 2, Snow cover energy balance, *Water Resources Research*, *28*(11), 3043-3054.

Marks, D., J. Kimball, D. Tingey, and T. Link (1998), The sensitivity of snowmelt processes to climate conditions and forest cover during rain-on-snow: a case study of the 1996 Pacific Northwest flood, *Hydrological Processes*, *12*(10-11), 1569-1587.

Marks, D., T. Link, A. Winstral, and D. Garen (2001), Simulating snowmelt processes during rain-on-snow over a semi-arid mountain basin, in *Annals of Glaciology, Vol 32, 2001*, edited, pp. 195-202.

Marks, D., M. Reba, J. Pomeroy, T. Link, A. Winstral, G. Flerchinger, and K. Elder (2008), Comparing Simulated and Measured Sensible and Latent Heat Fluxes over Snow under a Pine Canopy to Improve an Energy Balance Snowmelt Model, *Journal of Hydrometeorology*, *9*(6), 1506-1522.

Melloh, R. A., J. P. Hardy, R. E. Davis, and P. B. Robinson (2001), Spectral albedo/reflectance of littered forest snow during the melt season, *Hydrological Processes*, *15*(18), 3409-3422.

Molotch, N. P., P. D. Blanken, M. W. Williams, A. A. Turnipseed, R. K. Monson, and S. A. Margulis (2007), Estimating sublimation of intercepted and sub-canopy snow using eddy covariance systems, *Hydrological Processes*, *21*(12), 1567-1575.

Moore, R. D. (1983), On the use of bulk aerodynamic formulas over melting snow, *Nordic Hydrology*, *14*(4), 193-206.

Morris, E. (1989), Turbulent transfer over snow and ice, *Journal of Hydrology*, *105*(3), 205-223.

Musselman, K. N., N. P. Molotch, S. A. Margulis, P. B. Kirchner, and R. C. Bales (2012), Influence of canopy structure and direct beam solar irradiance on snowmelt rates in a mixed conifer forest, *Agricultural and Forest Meteorology*, *161*, 46-56.

Oke, T. R. (2002), *Boundary layer climates*, Routledge.

References (Continued)

Pomeroy, J. W., X. Fang, and C. Ellis (2012), Sensitivity of snowmelt hydrology in Marmot Creek, Alberta, to forest cover disturbance, *Hydrological Processes*, *26*(12), 1892-1905.

Pomeroy, J. W., and K. Dion (1996), Winter radiation extinction and reflection in a boreal pine canopy: Measurements and modelling, *Hydrological Processes*, *10*(12), 1591-1608.

Pomeroy, J. W., B. Toth, R. J. Granger, N. R. Hedstrom, and R. L. H. Essery (2003), Variation in surface energetics during snowmelt in a subarctic mountain catchment, *Journal of Hydrometeorology*, *4*(4), 702-719.

Pomeroy, J. W., D. M. Gray, K. R. Shook, B. Toth, R. L. H. Essery, A. Pietroniro, and N. Hedstrom (1998), An evaluation of snow accumulation and ablation processes for land surface modelling, *Hydrological Processes*, *12*(15), 2339-2367.

Pomeroy, J. W., D. Marks, T. Link, C. Ellis, J. Hardy, A. Rowlands, and R. Granger (2009), The impact of coniferous forest temperature on incoming longwave radiation to melting snow, *Hydrological Processes*, *23*(17), 2513-2525.

Randerson, J. T., et al. (2006), The impact of boreal forest fire on climate warming, *Science*, *314*(5802), 1130-1132.

Sakai, R. K., D. R. Fitzjarrald, and K. E. Moore (2001), Importance of low-frequency contributions to eddy fluxes observed over rough surfaces, *Journal of Applied Meteorology*, *40*(12), 2178-2192.

Semmens, K. A., and J. Ramage (2012), Investigating correlations between snowmelt and forest fires in a high latitude snowmelt dominated drainage basin, *Hydrological Processes*, *26*(17), 2608-2617.

Seyednasrollah, B., M. Kumar, and T. E. Link (2013), On the role of vegetation density on net snow cover radiation at the forest floor, *Journal of Geophysical Research - Atmospheres*, *118*(15), 8359-8374.

Sicart, J. E., J. W. Pomeroy, R. L. H. Essery, J. Hardy, T. Link, and D. Marks (2004), A sensitivity study of daytime net radiation during snowmelt to forest canopy and atmospheric conditions, *Journal of Hydrometeorology*, *5*(5), 774-784.

References (Continued)

Stoof, C. R., R. W. Vervoort, J. Iwema, E. van den Elsen, A. J. D. Ferreira, and C. J. Ritsema (2012), Hydrological response of a small catchment burned by experimental fire, *Hydrology and Earth System Sciences*, *16*(2), 267-285.

Sun, J., D. H. Lenschow, S. P. Burns, R. M. Banta, R. K. Newsom, R. Coulter, S. Frasier, T. Ince, C. Nappo, and B. B. Balsley (2004), Atmospheric disturbances that generate intermittent turbulence in nocturnal boundary layers, *Boundary-Layer Meteorology*, *110*(2), 255-279.

Thomas, C. K., and A. R. Smoot (2012), An effective, economic, aspirated radiation shield for air temperature observations and its spatial gradients, *Journal of Atmospheric and Oceanic Technology*, *30*(3), 526-537.

Turnipseed, A. A., P. D. Blanken, D. E. Anderson, and R. K. Monson (2002), Energy budget above a high-elevation subalpine forest in complex topography, *Agricultural and Forest Meteorology*, *110*(3), 177-201.

Turnipseed, A. A., D. E. Anderson, P. D. Blanken, W. M. Baugh, and R. K. Monson (2003), Airflows and turbulent flux measurements in mountainous terrain Part 1. Canopy and local effects, *Agricultural and Forest Meteorology*, *119*(1-2), 1-21.

Ueyama, M., K. Ichii, H. Iwata, E. S. Euskirchen, D. Zona, A. V. Rocha, Y. Harazono, C. Iwama, T. Nakai, and W. C. Oechel (2014), Change in surface energy balance in Alaska due to fire and spring warming, based on upscaling eddy covariance measurements, *Journal of Geophysical Research-Biogeosciences*, *119*(10), 1947-1969.

Vickers, D., and L. Mahrt (1997), Quality control and flux sampling problems for tower and aircraft data, *Journal of Atmospheric and Oceanic Technology*, *14*(3), 512-526.

Vickers, D., C. Thomas, and B. E. Law (2009), Random and systematic CO2 flux sampling errors for tower measurements over forests in the convective boundary layer, *Agricultural and Forest Meteorology*, *149*(1), 73-83.

Webb, E. K., G. I. Pearman, and R. Leuning (1980), Correction of flux measurements for density effects due to heat and water vapour transfer, *Quarterly Journal of the Royal Meteorological Society*, *106*(447), 85-100.

References (Continued)

Wiscombe, W. J., and S. G. Warren (1980), A model for the spectral albedo of snow. I: Pure snow, *Journal of the Atmospheric Sciences, 37*(12), 2712-2733.

3.8 Figures

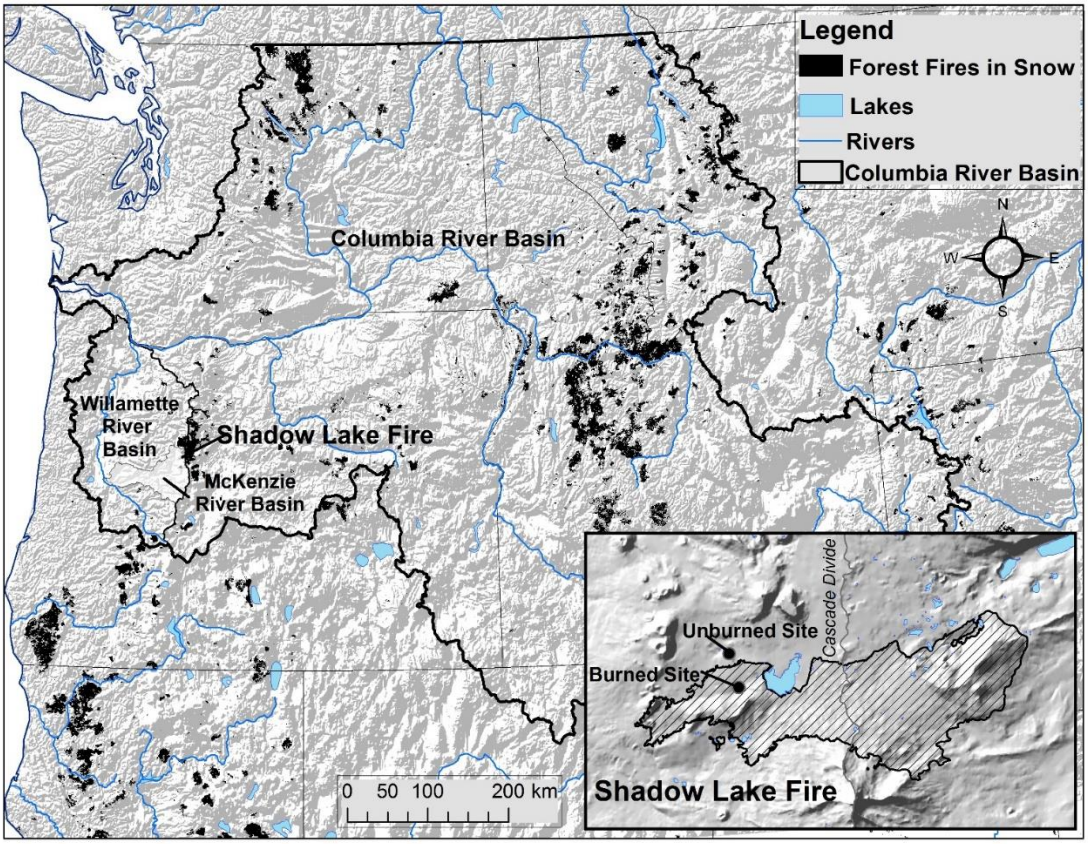

Figure 3.1. The Shadow Lake Fire burned at the headwaters of the McKenzie River Basin, a major tributary of the Willamette River Basin.

Figure 3.2. Terrestrial laser scanner data of unburned and burned forest measured June 2012 (shown as a bird's-eye perspective of both forests sites with the station location located under the orange X in each image).

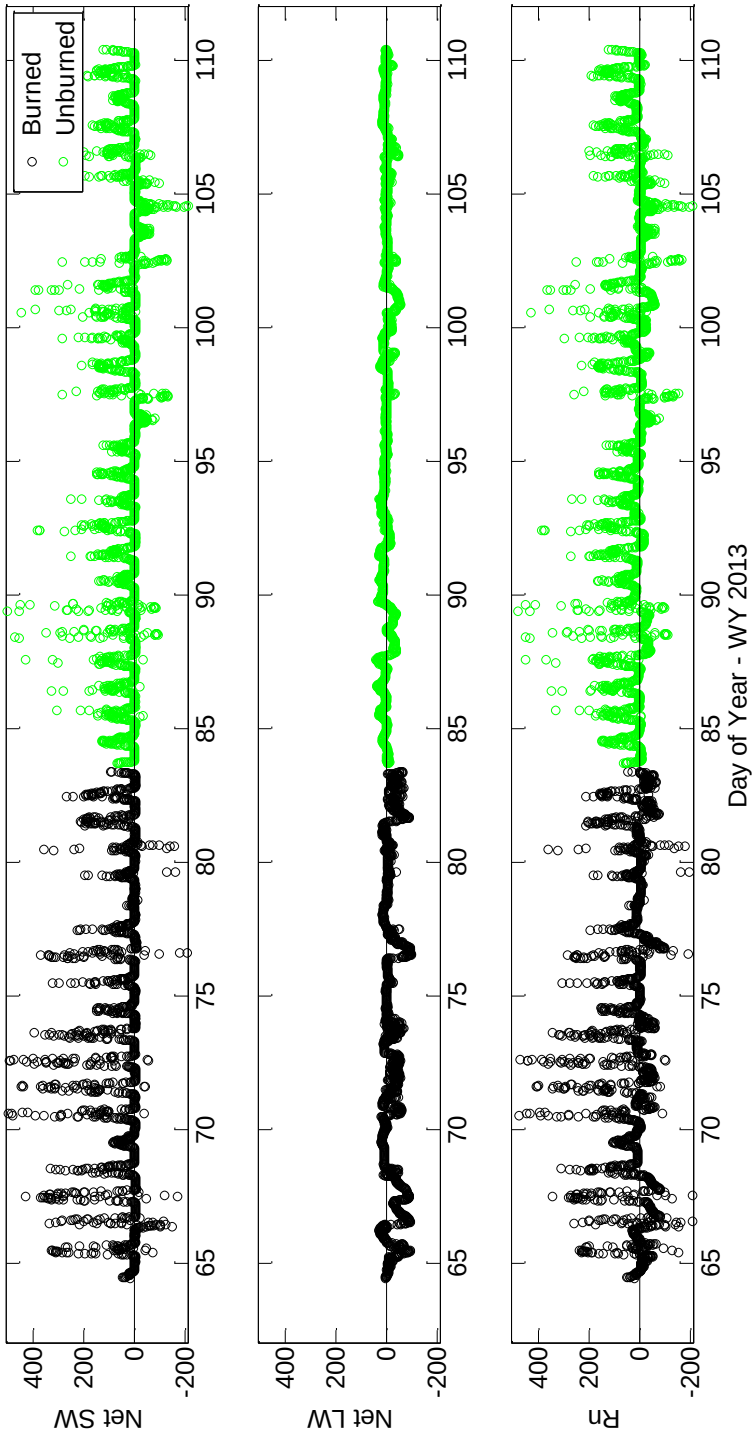

Figure 3.3. Four component net-radiometer data during the two month period from DOY 65 – 110 used to validate the method of modeling longwave radiation in the burned forest and nearby unburned forest showing measured data of a) net shortwave radiation [W m^{-2}], b) net longwave radiation [W m^{-2}], and c) net all-wave radiation [W m^{-2}].

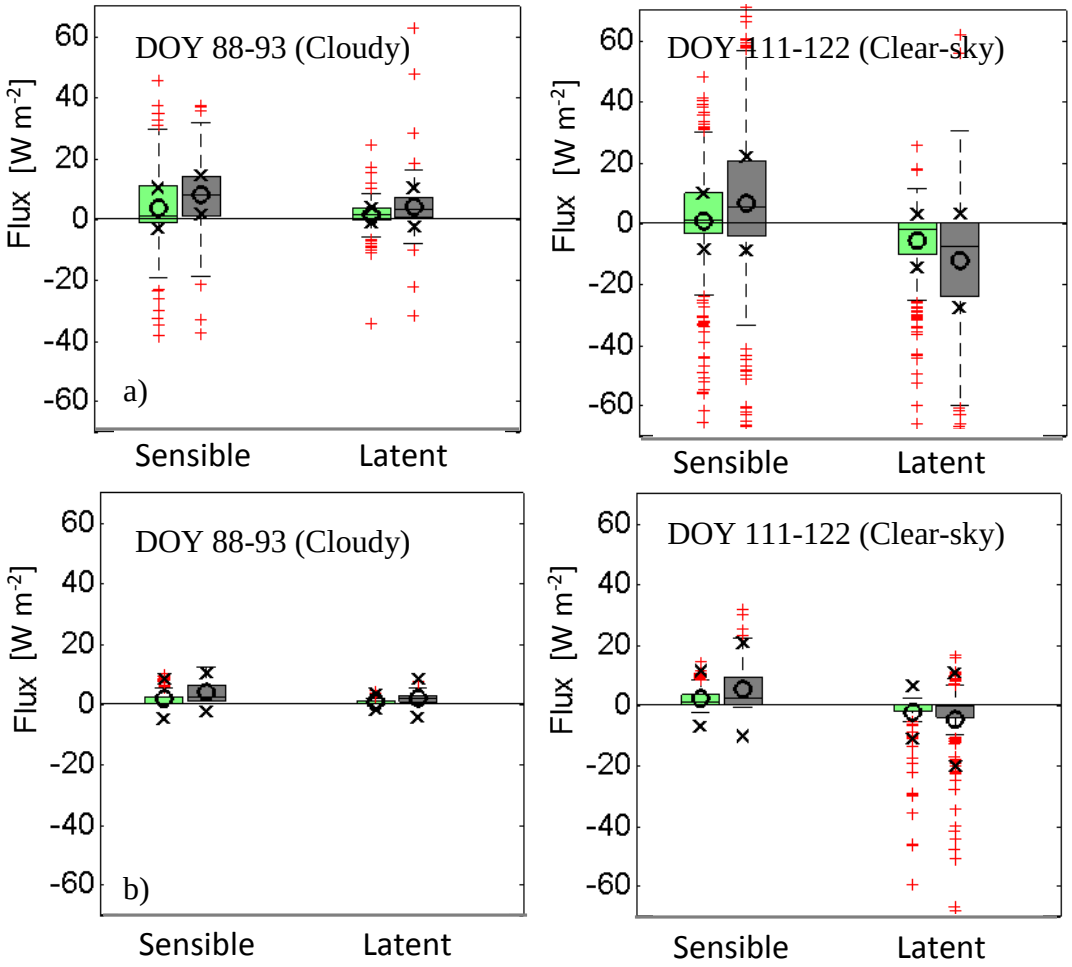

Figure 3.4. Standard box plots of the sensible and latent heat fluxes show the turbulent fluxes are double the magnitude in the burned forest (grey) compared to the unburned forest site. Box plots show the 25, median, 50, and 75 percentiles, shown with mean (black circle) and one standard deviation around the mean (black x) from a) eddy covariance measurements during the cloudy pre-melt period (DOY 88-93), and b) the eddy covariance measurements from the clear-sky period (DOY 111-122).

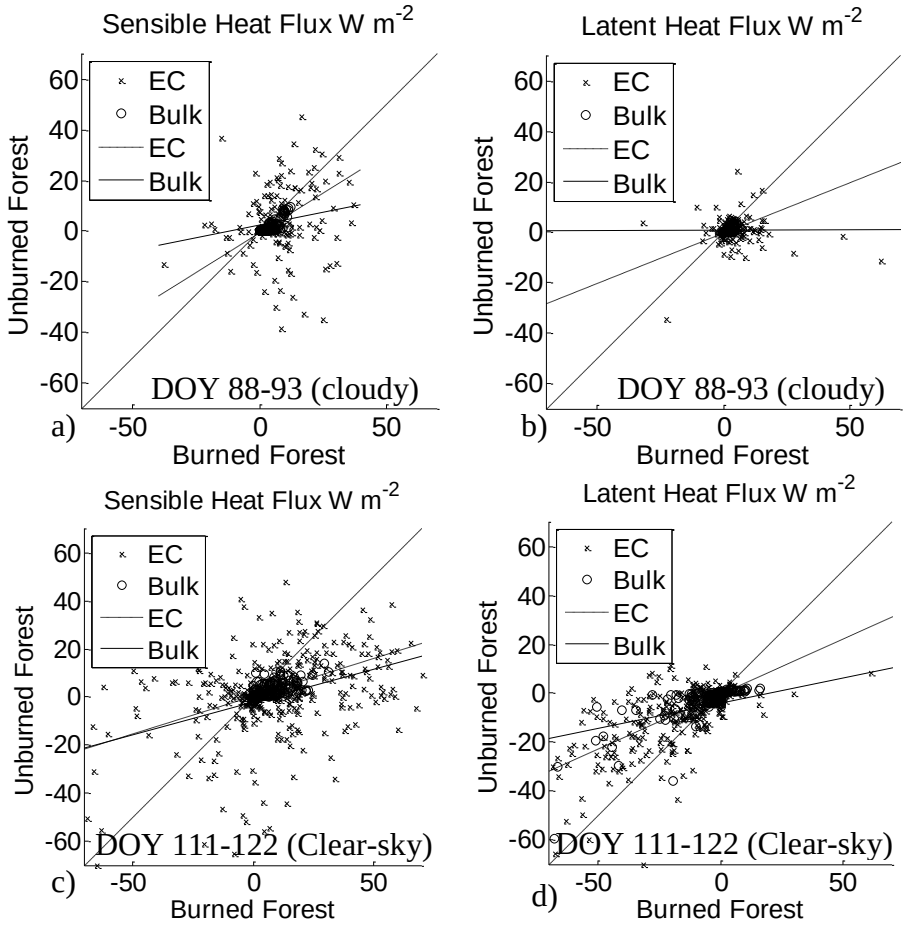

Figure 3.5. Scatter plots show the a) sensible heat fluxes and b) latent heat fluxes during the cloudy period (DOY 88-93), c) sensible heat fluxes, and d) latent heat fluxes during the clear-sky period (DOY 111-122), in the burned forest are double those in the unburned forest for both EC and bulk methods. Dashed reference line shows a 1:1 ratio between the burned and unburned forest, least squares regression lines for both EC (dashed) and bulk (solid) methods are shown.

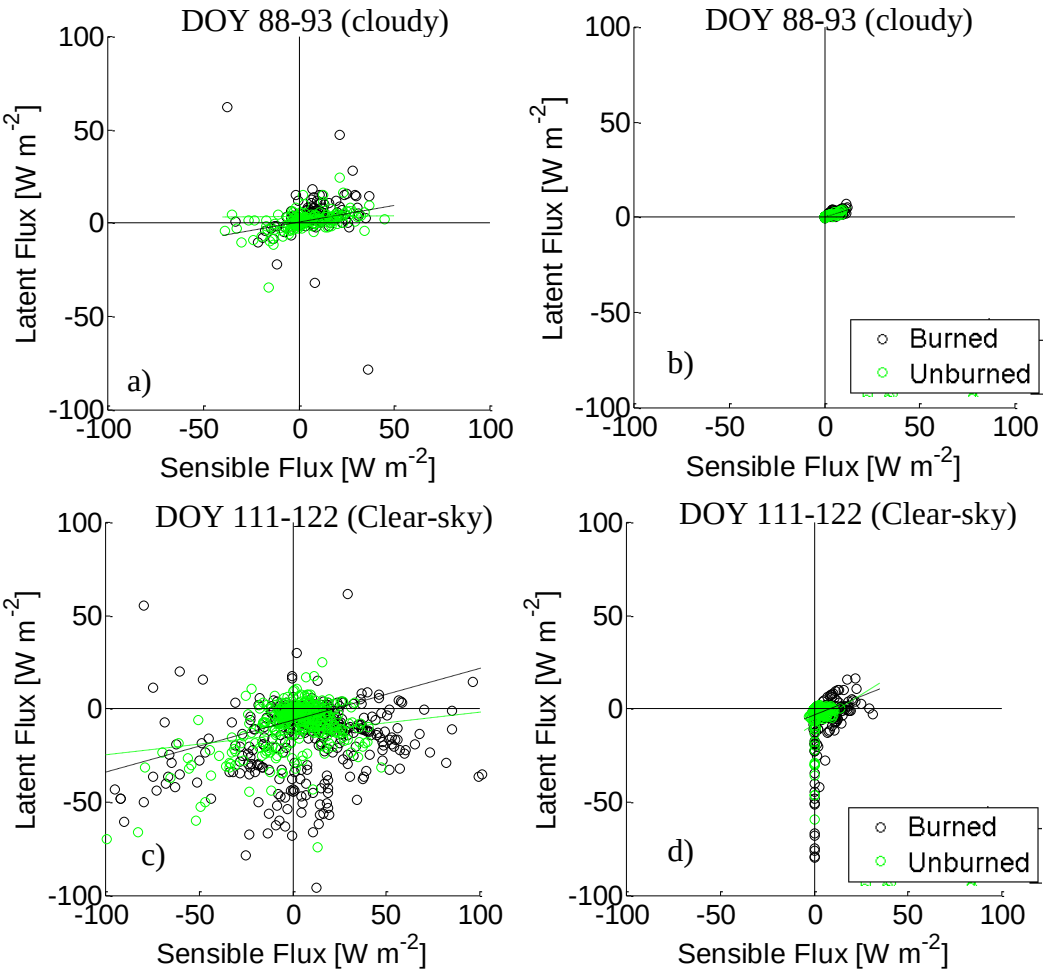

Figure 3.6. Quadrant plots of latent and sensible heat fluxes for the burned forest (black) and unburned forest (green) sites show the turbulent fluxes are positively correlated for the, a) eddy covariance measured fluxes during the cloudy period (DOY 88-93), b) bulk aerodynamic calculated fluxes during the cloudy period (DOY 88-93), c) eddy covariance measured fluxes during the clear-sky period (DOY 111-122), and d) bulk aerodynamic calculated fluxes during the clear-sky period (DOY 111-122).

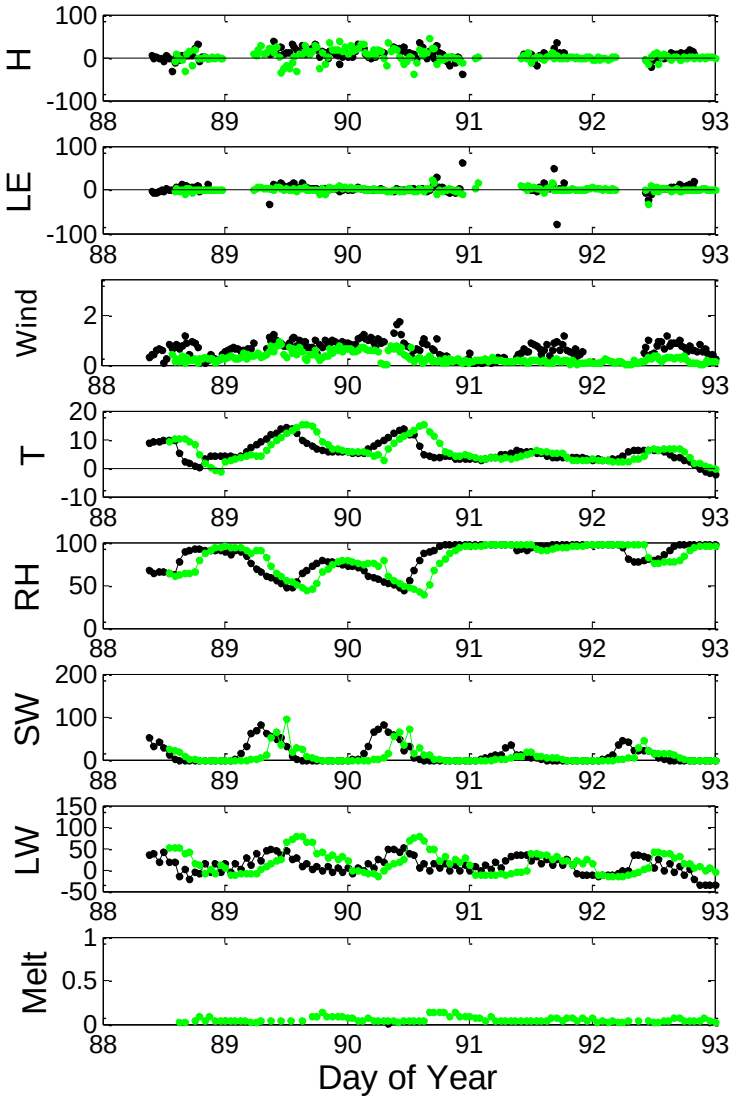

Figure 3.7.a. Fluxes and micrometeorological variables shown for the cloudy pre-melt period (DOY 88-93) for the burned forest (black) and unburned forest (green) sites. Variables from top to bottom, include the sensible heat flux [W m^{-2}] (30 min EC aggregates), latent heat fluxes [W m^{-2}] (30 min EC aggregates), Wind speed [m s^{-1}] (30 min EC aggregates), temperature [°C] (60 min met aggregates), relative humidity [%] (60 min met aggregates), net shortwave radiation [W m^{-2}] (60 min met aggregates), and snowmelt [mm/hour] (lysimeter measured). Missing data in the snowmelt record are due to no snowmelt measured by the lysimeter.

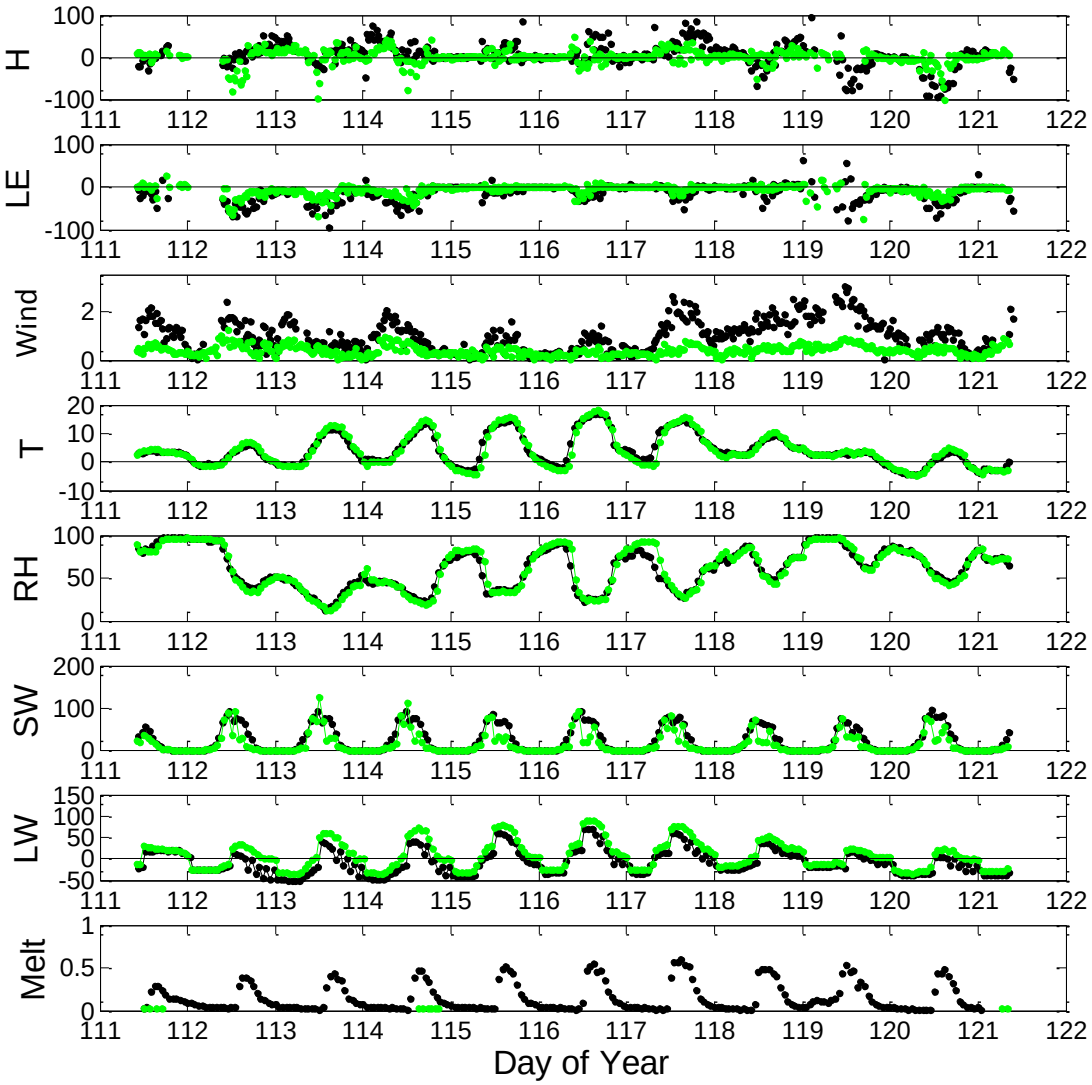

Figure 3.7.b. Fluxes and micrometeorological variables shown for the clear-sky snowmelt period (DOY 111-122) for the burned forest (black) and unburned forest (green) sites. Variables from top to bottom, include the sensible heat flux [W m^{-2}] (30 min EC aggregates), latent heat fluxes [W m^{-2}] (30 min EC aggregates), Wind speed [m s^{-1}] (30 min EC aggregates), temperature [°C] (60 min met aggregates), relative humidity [%] (60 min met aggregates), net shortwave radiation [W m^{-2}] (60 min met aggregates), and snowmelt [mm/hour] (lysimeter measured). Missing data in the snowmelt record are due to no snowmelt measured by the lysimeter.

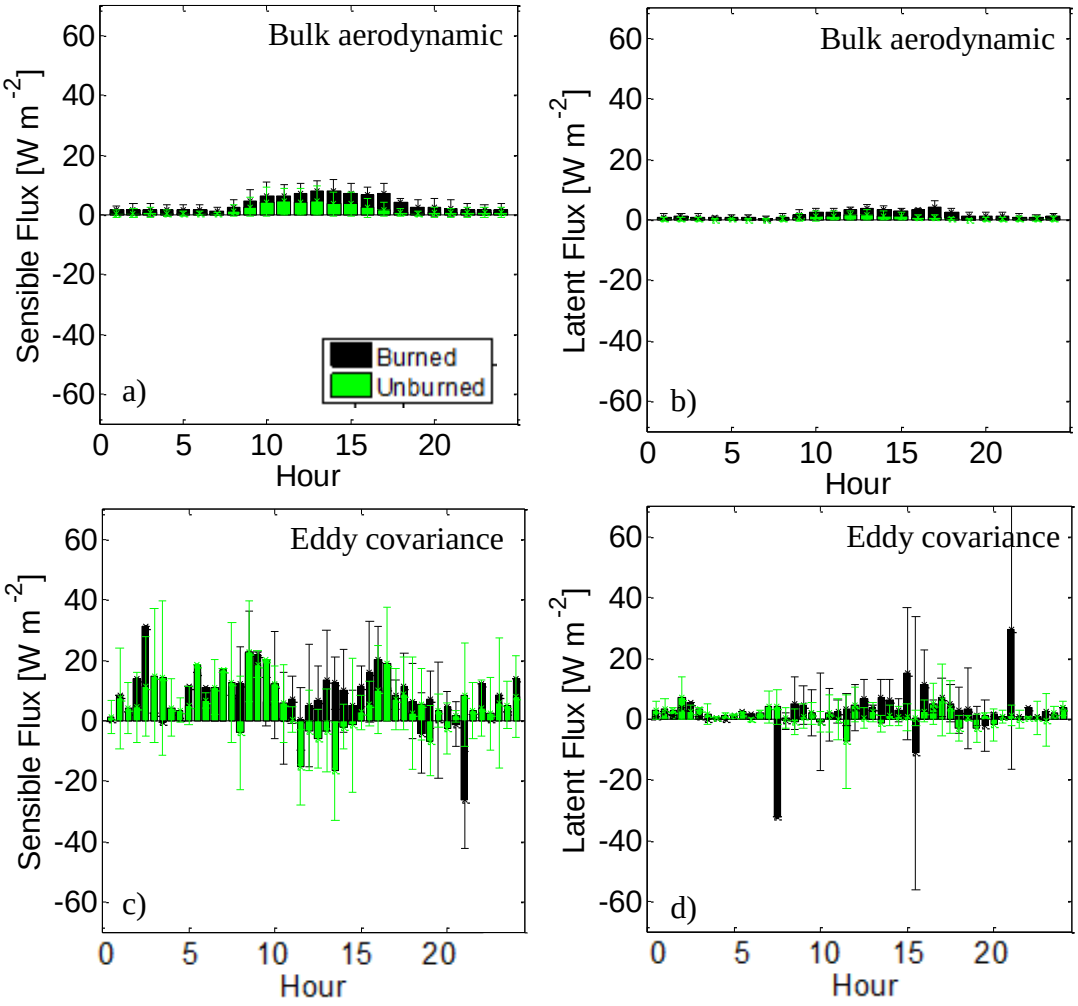

Figure 3.8.a. Hourly ensemble mean values of a) sensible heat fluxes and b) latent heat fluxes derived from the bulk aerodynamic method, and 30 minute ensemble mean values of c) sensible heat fluxes, and d) latent heat fluxes derived from the eddy covariance measurements, for burned (black) and unburned (green) forests during the cloudy pre-melt period (DOY 88-93). Standard deviation for the fluxes are shown as error bars in the burned forest (black) and unburned (green) forest.

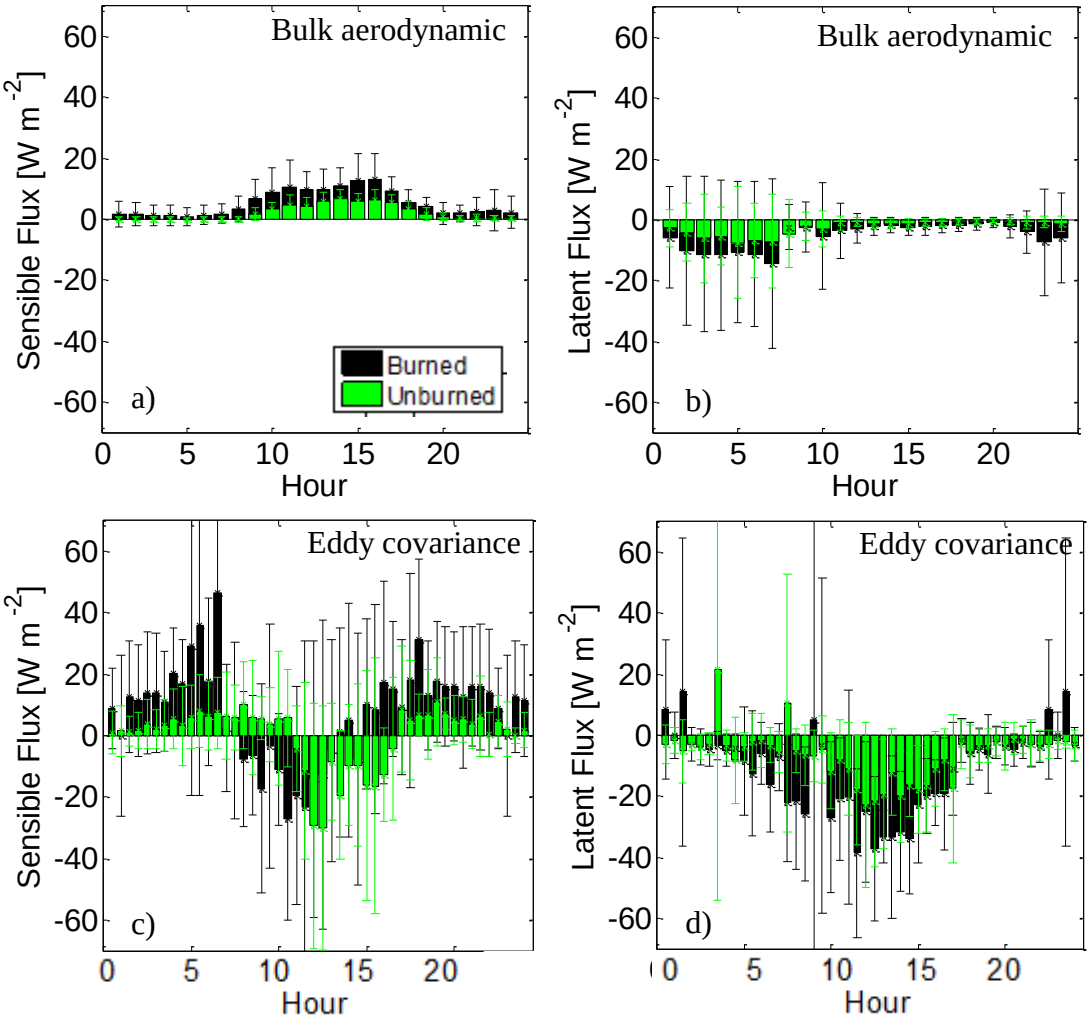

Figure 3.8.b. Hourly ensemble mean values of a) sensible heat fluxes and b) latent heat fluxes derived from the bulk aerodynamic method, and 30 minute ensemble mean values of c) sensible heat fluxes, and d) latent heat fluxes derived from the eddy covariance measurements, for burned (black) and unburned (green) forests during the clear-sky snowmelt period (DOY 111-122). Standard deviation for the fluxes are shown as error bars in the burned forest (black) and unburned (green) forest.

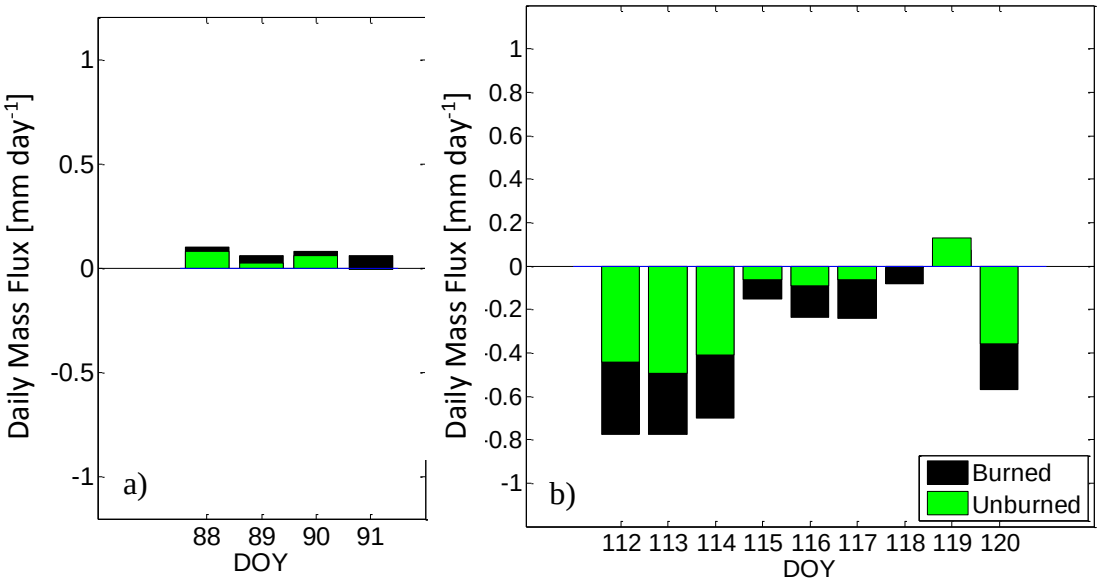

Figure 3.9. Daily mass flux during, a) the cloudy pre-melt period (DOY 88-91) and b) the clear-sky snowmelt period (DOY 112-120).

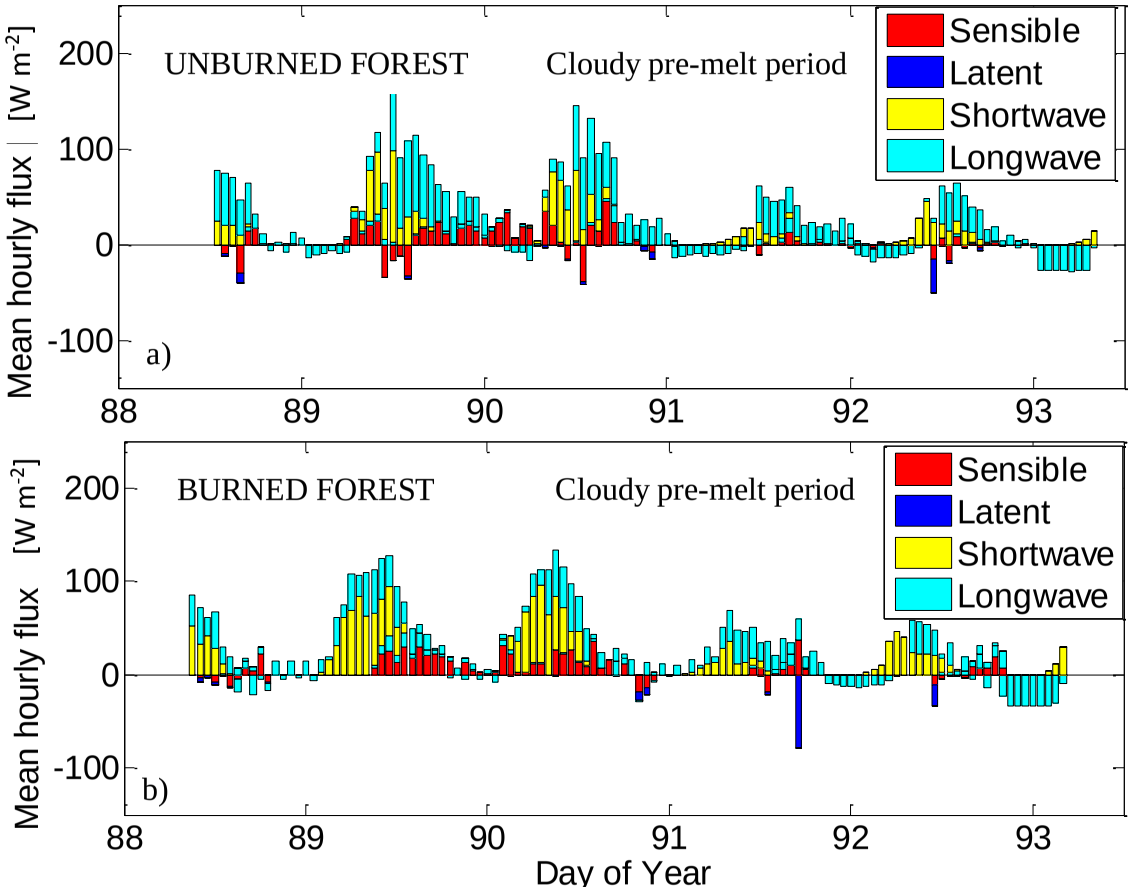

Figure 3.10.a. In the, a) unburned forest, and b) burned forest during the cloudy pre-melt period (DOY 88-93), the hourly mean sensible (EC-derived), latent (EC-derived), shortwave (measured), and longwave (calculated) fluxes [W m^{-2}].

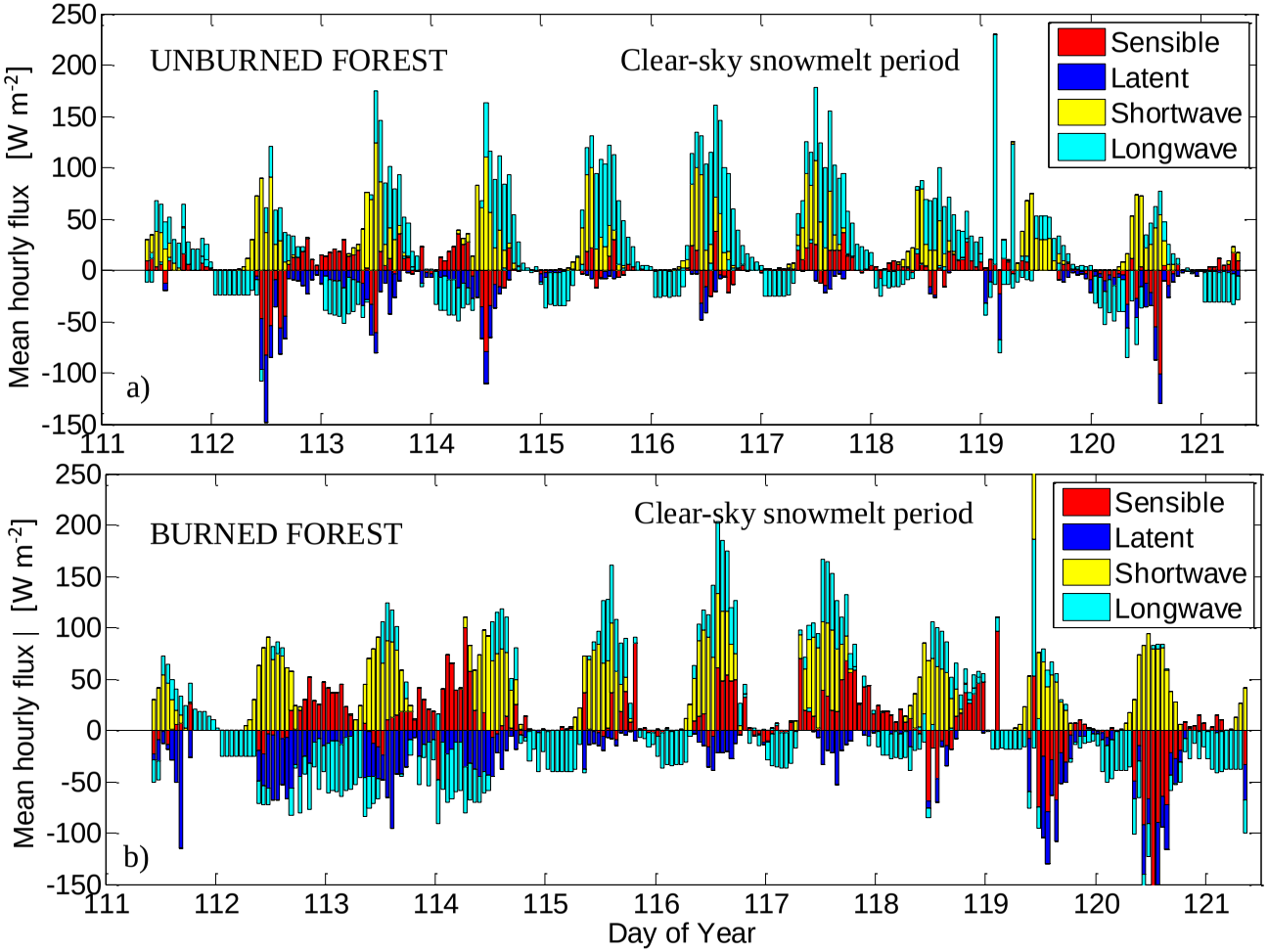

Figure 3.10.b. In the a) unburned forest, and b) burned forest during the clear-sky snowmelt period (DOY 111-122), the hourly mean sensible (EC-derived), latent (EC-derived), shortwave (measured), and longwave (modeled) fluxes [W m^{-2}].

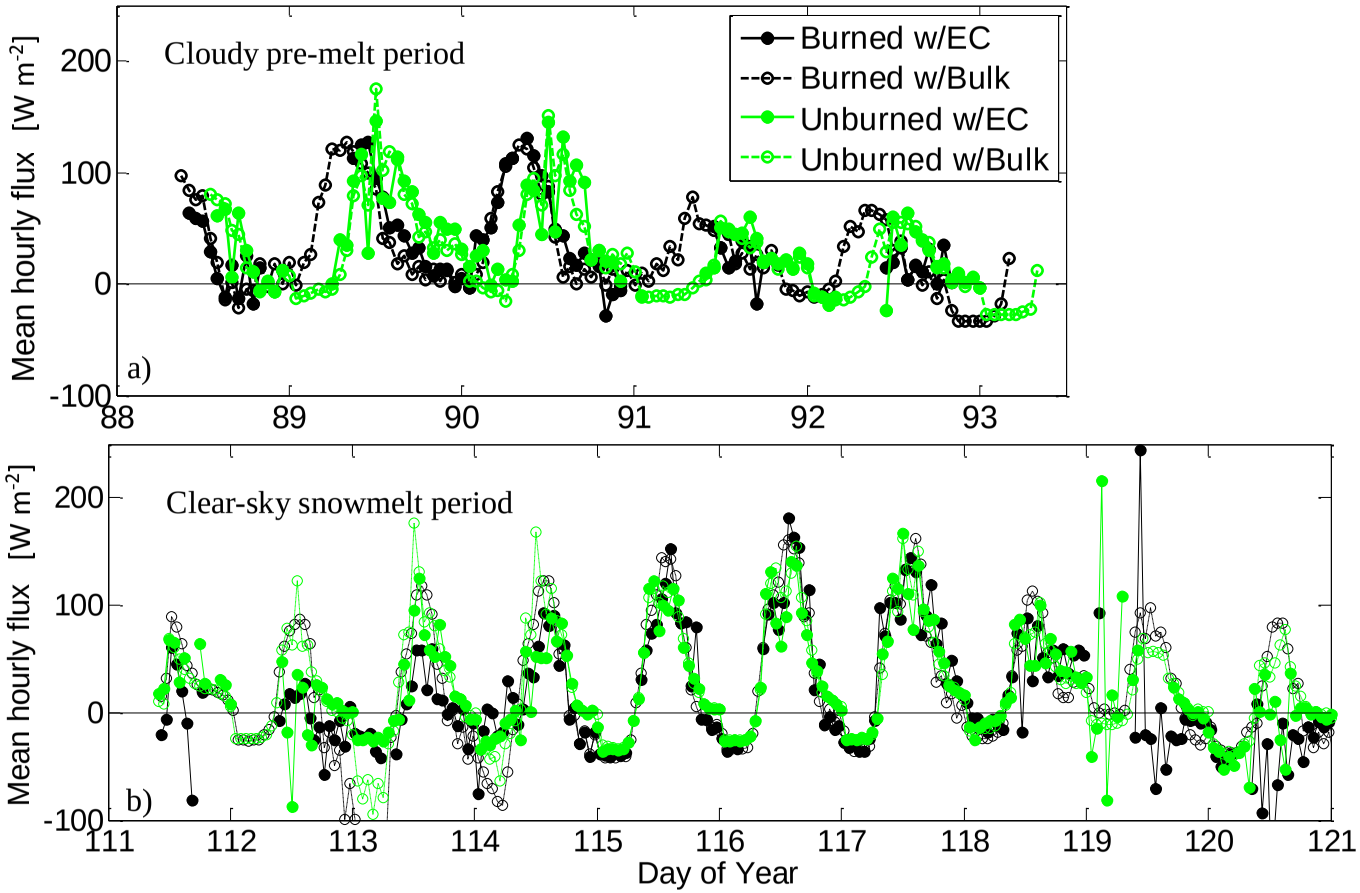

Figure 3.11. The hourly mean net energy balance during, a) DOY 88-93, and b) DOY 111-122, the for the burned and unburned forests calculated with eddy covariance measured turbulent fluxes shown as a solid line with filled circles, and with bulk aerodynamic calculated turbulent fluxes shown as a dashed line with open circles.

Table 3.1. Mean (μ) and standard deviation (σ) of direct (eddy covariance) and indirect (bulk aerodynamic) measured sensible and latent heat flux measurements in the burned and unburned forests.

METHOD	**BURNED**				**UNBURNED**			
	Sensible		**Latent**		**Sensible**		**Latent**	
DOY 88-93	**μ**	**σ**	**μ**	**σ**	**μ**	**σ**	**μ**	**σ**
Eddy Covariance	7.8	12.7	3.9	11.9	3.5	13.3	1.2	5.2
Bulk Aerodynamic	3.7	3.5	1.8	1.5	1.6	2.6	0.5	0.9
DOY 111-122								
Eddy Covariance	6.4	30.9	-12.4	28.7	0.6	18.3	-5.8	17
Bulk Aerodynamic	5.1	6.4	-4.9	14.6	2.1	2.9	-2.5	7.6

Table 3.2. Mean daily sum of energy balance components for sensible (H), latent (Le), and net turbulent flux (Turb) derived from the eddy covariance (EC) and bulk (B) methods, in addition to net shortwave radiation (SW), net longwave radiation (LW), net radiative flux (Rn), and net snowpack energy balance for the burned and unburned forests during the cloudy pre-melt period (DOY 88-93) and the clear-sky snowmelt period (DOY 111-122).

	H (EC)	**Le (EC)**	**Turb (EC)**	**H (B)**	**Le (B)**	**Turb (B)**	**SW**	**LW**	**Rn**	**Net**
Cloudy pre-melt period (DOY 88-93)										
UF	97	30	128	31	11	42	172	280	453	581
BF	168	80	248	72	35	106	271	191	463	711
BF/UF	1.7	2.2	1.9	2.3	3.1	2.5	1.6	0.7	1.0	1.2
Clear-sky snowmelt period (DOY 111-122)										
UF	25	-251	-226	49	-59	-9	363	218	581	355
BF	248	-503	-255	121	-117	4	584	-173	410	155
BF/UF	9.9	2.0	1	2.5	2.0	-0.4	1.6	-0.8	0.7	0.4

4 Charred Forests Accelerate Snow Albedo Decay: A New Parameterization of the Post-Fire Radiative Forcing on Snow

Charred Forests Accelerate Snow Albedo Decay: A New Parameterization of the Post-Fire Radiative Forcing on Snow

Kelly E. Gleason, and Anne W. Nolin

Hydrological Processes
Submitted June 2015

4.1 Abstract

As forest fires increase and snowpacks become increasingly vulnerable across much of the western US, it is imperative that we understand forest fire disturbance effects to snowpack hydrology. The objectives of this study were to characterize, parameterize, model, and validate the post-fire radiative forcing on snow as a function of days-since-snowfall with the ultimate goal of better representing the effects of forest fire disturbance in hydrologic modeling of snow-dominated watersheds. Following a high-severity forest fire in the Oregon Cascades, we conducted snow albedo measurements, snow and micrometeorological monitoring, snow surface debris sampling, and snow energy and mass balance modeling in adjacent burned and unburned forest sites. For three winters following the fire, charred debris in the burned forest reduced the maximum and minimum mean snow albedo, accelerated snow albedo decay, increased snow melt rates, and advanced the date of snow disappearance compared to the nearby unburned forest. We developed a new parameterization of post-fire snow albedo decay as a function of days-since-snowfall and net snowpack energy balance using an empirically-based exponential decay function. To evaluate forest fire effects to snowpack duration across the extent of the recent burn, we employed our variable snow albedo parameterization in a spatially distributed energy and mass balance snow model. By incorporating our variable snow albedo parameterization, the model better predicted the snow cover duration and spatial variability of snow water equivalent across the burned forest, particularly

during the late snow melt period. Field measurements, snow model results, and a remote sensing data demonstrated that charred forests increase snowpack radiative forcing and advance the timing of snow disappearance for several years following fire.

4.2 Introduction

In response to warmer temperatures and declining snowpacks, large wildfires are increasing in frequency, intensity, and extent across the western US [*Semmens and Ramage*, 2012; *Trouet et al.*, 2010; *Westerling et al.*, 2006; *Westerling et al.*, 2011]. In turn, forest fire disturbance affects patterns of snow accumulation and ablation by reducing canopy interception, increasing turbulent fluxes, and modifying the net radiation balance [*Boon*, 2009; *Burles and Boon*, 2011; *Gleason et al.*, 2013; *Liu et al.*, 2005; *Ueyama et al.*, 2014; *Winkler et al.*, 2005].

Forest fire disturbance significantly alters the net radiation balance of the underlying snowpack by increasing the transmission of incoming solar radiation through the canopy, decreasing the emission of longwave radiation by the canopy, and decreasing snow surface shortwave albedo by deposition of organic debris from the canopy [*Burles and Boon*, 2011; *Kelly E. Gleason et al.*, 2013; *Pomeroy and Dion*, 1996; *R Winkler et al.*, 2010]. Charred forests increase snow melt and drive earlier date of snow disappearance, [*Gleason et al.*, 2013; *Harpold et al.*, 2014; *Micheletty et al.*, 2014; *Winkler et al.*, 2010], which may feedback and contribute to alterations of the atmosphere-terrestrial-hydrology [*Dery and Brown*, 2007; *Liu et al.*, 2005; *O'Halloran et al.*, 2012; *Ueyama et al.*, 2014].

Although forest fire disturbance is abundant in the snow-dominated headwaters [*Gleason et al.*, 2013] of most of the western US water supply [*Serreze et al.*, 1999], and forest fire disturbance is projected to increase across the western US

[*Abatzoglou and Kolden*, 2013; *Dennison et al.*, 2014; *Moritz et al.*, 2012], forest fire effects to snow accumulation and snow melt patterns are rarely incorporated into snow energy and mass balance models. The objective of this study was to **characterize**, **parameterize**, **model**, and **validate** the **post-fire radiative forcing on snow** as a function of time-since-snowfall to better represent forest fire disturbance in hydrologic modeling of snow-dominated watersheds.

4.3 Background

4.3.1 Characterization of Snow Albedo

Snow surface shortwave albedo is tightly coupled with snowpack energy balance, snowpack metamorphism, and snow melt hydrology [*Wiscombe and Warren*, 1980]. Because snow is so highly reflective in the visible wavelengths (0.4–0.7 μm), even a small decrease in visible albedo will significantly increase net shortwave radiation [*Dozier et al.,* 2009]. Snow surface shortwave albedo is a function of snow grain size, concentration and type of light absorbing impurities; solar zenith angle and cloud conditions; and, for optically thin snow, the albedo of the substrate below the snowpack [*Warren*, 1982]. Newly fallen, fine-grained snow has an albedo of 0.8-0.9, but over days-to-weeks, this albedo decreases exponentially. As snow grain growth occurs to reduce the surface free energy of individual grains and grain clusters is function of the temperature and vapor pressure gradient between the snowpack and boundary-layer atmosphere at the snow surface [*Colbeck,* 1986]. The rate of "snow albedo decay" depends both on grain growth [*Wiscombe and Warren*, 1980], and the deposition and concentration rates of dust [*Painter et al.*, 2010], soot [*Hansen and Nazarenko*, 2004; *Warren and Wiscombe*, 1980], and burned and unburned forest debris [*Gleason et al.*, 2013; *Hardy et al.*, 2004]. During the mid-winter period when air temperatures are cold and dry the snowpack energy balance is predominately negative, and snow metamorphism and associated snow albedo decay occur slowly. However during the spring snowmelt period when air temperatures are warm and

humid, the snowpack energy balance is predominately positive, and therefore snow metamorphism and associated snow albedo decay occur more rapidly.

Recent work has shown that dust and soot deposition on snow can lead to substantial radiative heating and faster snow melt rates [*Deems et al.*, 2013; *Flanner et al.*, 2009; *Painter et al.*, 2012; *Painter et al.*, 2013; *Painter et al.*, 2010; *Painter et al.*, 2007; *Skiles et al.*, 2012]. Compared with mineral dust, carbon soot is an order of magnitude more effective at absorbing solar energy in the visible wavelengths [*Warren and Wiscombe*, 1980]. Atmospheric deposition of soot on snow results in concentrations of 100 ppmw or less [*Rosen et al.*, 1981], but even smaller amounts may increase absorbed solar radiation [*Hadley and Kirchstetter*, 2012; *Xu et al.*, 2009], leading to radiative heating in snow and ice [*Flanner et al.*, 2009; *Hansen and Nazarenko*, 2004; *Hansen et al.*, 2005].

Snow albedo in forested regions is often much lower than the more pristine snow in open areas and above tree line. Forest litter (bark, needles, cones, lichen, etc.) is shed from the canopy, accumulates on the snowpack, and further concentrates on the snowpack surface during snow ablation. [*Melloh et al.*, 2002] found that forest litter reduced the snow albedo from a maximum of about 0.9 during snow accumulation to as low as 0.25 during snow ablation. After a forest fire, large quantities of burned woody debris (BWD) sheds from standing charred trees and accumulates on the snowpack, even further reducing snow albedo [*Gleason et al.*, 2013].

Although far more coarse than dust and soot, the deposition and concentration of pyrogenic carbon, charcoal, charred woody detritus, and partially charred needles, cones, and bark in burned forests significantly increases net shortwave radiation of the snowpack surface in the first winter after a forest fire [*Gleason et al.*, 2013], and may persist for decades following fire disturbance [*Acker et al.*, 2013; *Dunn and Bailey*, 2012]. Charred forests increase snow melt and advance the date of snow disappearance [*Gleason et al.*, 2013; *Harpold et al.*, 2014; *Micheletty et al.*, 2014; *Winkler et al.*, 2010]. However, we still have no parameterization of post-fire radiative forcing on snow, and therefore no method of evaluating forest fire disturbance effects to snowpack hydrology.

4.3.2 Parameterization of Snow Albedo Decay

Because snow albedo decay has such a large influence on the snowpack energy balance [*Wiscombe and Warren*, 1980], it is an important parameter in snow hydrology models to accurately capture variability in snowmelt [*Essery et al.*, 2013]. Using a range of tunable/fixed algorithms, i.e. SNTHERM [*Jordan*, 1991], and SnowModel [*Liston and Elder*, 2006]; empirically-based variable algorithms, i.e. CLASS [*Verseghy*, 1991], DHSVM [*Wigmosta et al.*, 1994], VIC [*Andreadis et al.*, 2009], iSNOBAL [*Marks and Dozier*, 1992], SNOWPACK [*Bartelt and Lehning*, 2002]; or pseudo to fully physically-based algorithms, i.e. SNICAR and others [*Anderson*, 1976; *Flanner and Zender*, 2006; *Warren and Wiscombe*, 1981], many different parameterizations have been shown to improve the accuracy of snowmelt

models. Although a physically-based solution may be preferred, most models were written with computational limitations. Therefore nearly all operational models and the majority of research models use simple solutions to estimate snow albedo.

A commonly used representation of snow albedo in many models is shown in Equation 1, where the first term to the right represents the refreshment of snow albedo as a result of new snowfall, the second term on the right represents snow albedo decay over time. In Equation 4.1, the change in snow albedo, (α_{snow}); over the change in time, (Δt); is a function of the rate of snowfall, (q_{snow} [kg m $^{-2}$ s $^{-1}$]); the mass required for albedo refreshment, (S_{ref} [kg m^{-2}]); the albedo decay rate, (K_{α} [s $^{-1}$]); and the maximum and minimum snow albedo, $(\alpha_{snow,max})$ and ($\alpha_{snow,min}$) [*Mendoza et al.*, 2014].

$$\frac{d\alpha_{snow}}{dt} = \frac{q_{snow}}{S_{ref}}\left(\alpha_{snow,max} - \alpha_{snow,min}\right) - K_{\alpha}\left(\alpha_{snow} - \alpha_{snow,min}\right) \quad \text{(Equation 4.1)}$$

Many models use this exponential decay scheme to calculate snow albedo. This scheme uses an empirically-derived aging coefficient based on one or more snow properties including SUMMA [*Clark et al.*, 2015]; SNOWPACK [*Lehning et al.*, 2002]; CLASS [*Verseghy*, 1991]; DHSVM [*Wigmosta et al.*, 1994]. Some models assume that diffuse and direct snow albedo values are similar, and calculate a single snow albedo value for shortwave radiation [*Lehning et al.*, 2002; *Verseghy*, 1991; *Wigmosta et al.*, 1994] while others differentiate diffuse and direct snow albedo [*Marks and Dozier*, 1992; *Wiscombe and Warren*, 1980]. Visible and near-infrared

snow albedo are combined in some models [*Lehning et al.*, 2002; *Verseghy*, 1991; *Wigmosta et al.*, 1994], while others distinguish visible and near-infrared shortwave radiation [*Marks and Dozier*, 1992; *Yang et al.*, 1997]. *Garen and Marks* [2005], incorporated an albedo reduction of approximately half the albedo calculated for open areas to account for surface debris in forested regions as represented in iSNOBAL based on previously published albedo decay estimates [*Hardy et al.*, 2000; *Melloh et al.*, 2001]. Painter *et al.* [2010] included an additional forcing parameter in the VIC model [*Liang et al.*, 1994] to account for the effect of black carbon and dust deposition on snow albedo decay. Due to the uncertainty in the interactions and feedbacks of snowpack radiative forcing parameters that typically have little physical basis [*Mendoza et al.*, 2014], a simple exponential decay function as shown in Equation 4.1, may best capture the range of observational data (Figure 4.2) in applicable framework for many snow hydrology models.

Although snow albedo decay has been parameterized in many models and strongly influences snowpack energy balance, it is often used as a tuning parameter, albeit one not based on observations or physical snow properties. This may explain the wide range of coefficients seen in the literature. Charred forests increase the net shortwave radiation at the snowpack surface, driving earlier and more rapid snow melt in burned areas, however very few hydrologic models explicitly incorporate forest fire disturbance effects in snowpack energy and mass balance models [*Lanini et al.*, 2009]. No prior investigation has parameterized the post-fire snow albedo decay

to evaluate forest fire disturbance effects to snow ablation as a result of deposition and concentration of burned woody debris and subsequent acceleration of snow albedo decay.

4.4 Site Description

Our study area is located in the western Oregon Cascades, at the volcanic headwaters of the McKenzie River Basin (Figure 4.1), a 3000-km^2 predominant tributary of the Willamette River. Especially in recent decades, fires occur frequently in the Cascadian sub-alpine forests of western Oregon, where deep and relatively warm winter snowpack accumulates most winters. Our paired study sites include a high elevation (1450 m) burned forest, disturbed by the Shadow Lake Fire, which burned 11,000 acres of sub-alpine fir/pine forest in September 2011, and a nearby unburned sub-alpine fir/pine forest. Structural differences between the two forests are described in *Gleason et al.,* [2013]. Our research extended continuously through the snow-cover season (October-July) of water years (WY) 2012, 2013, and 2014. We also used data from a nearby micrometeorological tower, and the nearest Natural Resources Conservation Service snowpack telemetry (SNOTEL) site, Hogg Pass, as forcing data for snow energy and mass balance model evaluations.

4.5 Research Methods

Our approach was to empirically characterize and statistically parameterize post-fire snow albedo decay using extensive field measurements. We then leveraged these results using a physically-based spatially distributed snow model to evaluate forest fire disturbance effects to snow ablation at our burned and unburned forest sites, as well as across the extent of a recent burned forest. We validated the spatial and temporal variability of our model results using field measurements and remotely sensed data products before and after fire disturbance across the extent of the burned area.

4.5.1 Characterization of the Post-fire Snow Albedo

To empirically characterize the post-fire radiative forcing on snow we conducted in-situ spectral and broadband snow albedo and micrometeorological measurements, as well as snow water equivalent (SWE) and snowpack surface debris monitoring.

Spectral Albedo Measurements

We measured snow spectral albedo using an Analytical Spectral Devices™ Full-Range Portable Field Spectroradiometer (ASD-FR) equipped with a cosine receptor mounted. The ASD-FR has a spectral resolution of 1 nm over a spectral range of 350-2500 nm. Measurements were acquired every 20 m along a 200-m transect through each research site. The cosine receptor was mounted at the end of a 110-cm long horizontally leveled rod that was rotated to obtain upward and

downward hemispherical fluxes that were then ratioed to compute spectral albedo. The rod-mounted system was used to minimize the effect of the operator in the instrument field of view. Measurements were made at height of 1 m above the snowpack surface. All spectral albedo measurements were made within one hour of solar noon under clear sky conditions. For each study year we obtained albedo measurements multiple times during the accumulation and ablation periods, as conditions permitted. Sampling efforts were focused on the ablation period, when albedo decay was considerable, compared with the accumulation period when frequent snowfall would reset the albedo to its initial high value. High quality spectral albedo measurements were made on 25 March 2013, 04 April 2013, 21 April 2013, 1 May 2013, and 5 May 2013. Broadband albedo measurements, described below were acquired continuously over the study period. For each of these spectral data acquisitions snowpack surface debris concentrations were determined from snow surface samples following the method of *Gleason et al.,* [2013].

Broadband Albedo and Meteorological Measurements

Micrometeorological stations were operated at both the burned and unburned forest sites. For WY 2012, 2013, and 2014 each station recorded 10-min averaged data of 1-min measurements of air temperature, relative humidity, incoming and outgoing shortwave radiation, wind speed and direction, and snow depth using CSC™ CR1000 loggers. We used upward- and downward-facing LI-COR™ 200s pyranometers to measure incoming and outgoing shortwave radiation, which have a

spectral range of 400-1100 nm and a 180º field-of view. We used a MetOne™ 034B wind vane to measure wind speed and direction, and a Judd™ sonic snow depth sensor to measure snow depth. All instruments were installed at 5 m above the ground surface on a tower located at the transect center in each study site (Figure 4.1). Because of power supply problems during WY 2012, data collection was restricted to the period 04 February to 28 February and 08 May to snowmelt. Continuous micrometeorological data were collected for both sites for WY 2013 and WY 2014, with the exception of two one-week periods in WY 2013, and one two-week period in WY 2014. These data were used to empirically calculate post-fire snow albedo decay and to provide input data for snow energy and mass balance modeling.

Snowpack and Snow Surface Debris Monitoring

We conducted regular snow course transects through the burned and unburned forest sites. Along each transect we measured SWE, snow depth, and snow surface debris concentrations. Measurements were made on a monthly basis during the accumulation period and every two weeks during the ablation period (April 1 – date of snow disappearance). Each 500-m long transect was centered on the micrometeorological tower site. Along each transect, snow depth measurements were collected every 5 m using a snow probe and SWE measurements were collected every 50 m using a Federal snow sampler. As with the spectral albedo measurements, we collected snow samples coincident with the SWE measurements and determined

snowpack surface debris concentrations following the method of *Gleason et al.*, [2013].

4.5.2 Parameterization of Post-fire Snow Albedo Decay

Daily mean broadband snow albedo, as the ratio of outgoing to incoming solar radiation, was calculated for the burned and unburned forest sites using hourly mean data. Quality control of the data limited the values to time of day when the solar elevation angle >30°, snow depth was >30 cm, and the upward-facing pyranometer was snow-free. Mean broadband snow albedo values were computed separately for periods of negative and positive net energy balance. Snow albedo decay was then computed based on these mean values. A snowfall depth threshold of 3 cm d^{-1} was used to reset the snow albedo to its maximum value. This depth was selected based on previous work showing that 3 cm produces an adequate optical depth to reset the snow surface albedo. Snow depth measurements from the micrometeorological stations were used to determine new snowfall.

Because the snowpack energy balance, snowpack metamorphism, and snow albedo decay are intricately connected, positive and negative net snowpack energy balance periods were determined using the sum of net shortwave, longwave, sensible, latent and ground heat fluxes. Net shortwave radiation was calculated as the incoming shortwave radiation minus outgoing shortwave radiation. Net longwave radiation was computed using the Crawley-Dilley method [*Crawford and Duchon*, 1999; *Dilley and O'Brien*, 1998; *Flerchinger et al.*, 2009]. This method was selected

because it best approximated data from a two-month period (06 March - 20 April 2013) when we maintained longwave measurements at the burned and unburned sites. Sensible and latent heat fluxes were calculated using the bulk aerodynamic method with a stability based bulk coefficient [*Boon,* 2009; *Kustas,* 1994], from temperature, humidity, and wind speed measurements.

Albedo decay functions were derived using daily mean albedo as a function of days-since- snowfall. Exponential regression was used to compute the best-fit function to the albedo data: one for each negative and positive energy balance period, for each site. The decay rate was derived from the exponential coefficient of the best-fit polynomial least-squares regression function. The maximum albedo was derived from the intercept of the best-fit function. The minimum albedo was selected based on an asymptotic slope threshold of 1% per day.

As noted by previous authors [*Burles and Boon*, 2011; *Gleason et al.*, 2013], the upwelling radiation measurements provided unusually low estimates of snow surface albedo. These measurements were inconsistent with our aggregated spectral albedo measurements, particularly during the low snow years. Because the unburned forest station is located in a sub-alpine forest with a canopy closure of 82%, the field of view of the downward-facing pyranometers was influenced by the forest canopy. To correct for this bias, we developed a control that allowed us to compute a correction factor. By measuring reflected shortwave radiation close to the snow surface, we reduced the effect of forest within the field of view of the downward-

looking pyranometer. For this control, we installed an additional set of upward- and downward-facing pyranometers at our unburned forest station during WY 2014 field season at 2 m above ground. The mean difference in mean daily snow albedo measurements between the 2-m and 5-m pyranometers was used to bias-correct the 5-m albedo measurements during WY 2013 and WY 2014 (Figure 4.3). The correction factor was derived from data acquired from 18 February to 30 March 2014 which was centered over the date of peak SWE in WY 2014. The correction factor was determined to be $\mu = 1.54$; $\sigma = 0.24$. Mean daily snow albedo measurements from WY 2012 were not bias corrected due to the scarcity of data, and the assumption that the deep snowpack during the above average snow year may have reduced bias by burying much of the sub-alpine forest.

4.5.3 Modeling Post-fire Snow Albedo Decay

The new parameterization of post-fire snow albedo decay was employed in a snow energy and mass balance model to evaluate forest fire disturbance effects to snow accumulation, snow melt, and snowpack energy balance across the extent of the burned area. A physically-based spatially-distributed snowpack energy and mass balance model, SnowModel was used [*Liston and Elder*, 2006], because it has demonstrated moderate accuracy in the western Oregon Cascades [*Sproles et al.*, 2013], and is broadly-used across the scientific and operational snow hydrology community.

SnowModel uses a hierarchical modeling architecture that aggregates four submodels: *MicroMet, EnBal, SnowPack-ML,* and *SnowTran-3d*. *MicroMet* interpolates observations of temperature, precipitation, wind speed, wind direction, and relative humidity to a DEM, and estimates incoming shortwave and longwave radiation and surface pressure in each gid cell [*Liston and Elder*, 2006]. *Enbal* uses the gridded meteorological surfaces to compute the mass and energy balance of the snowpack in each grid cell for every timestep [*Liston and Hall*, 1995]. *SnowTran-3D* is a surface model for snow redistrubution by wind [*Liston and Sturm*, 1998; 2002]. *SnowPack-ML* is a multilayer snowpack model which simulates the refreezing of meltwater of snow as a function of permeabilty and cold content [*Liston and Mernild*, 2012]. A full description of each sub-model, governing equations, approximations, and assumptions can be found in the associated cited papers. We used SnowModel 3.2.1 released April 2014, including a 5-layer maximum multi-layer snowpack and conduction terms.

SnowModel uses the leaf area index (LAI) parameter to modify the incoming shortwave and longwave radiation based on empirically-derived scaling function of canopy transmissivity and emissivity in different forest types. SnowModel uses a default temperature threshold of 2°C to delineate the phase of incoming precipitation as rain or snow. SnowModel uses a default temperature threshold of 0°C to differentiate fixed snow albedo values used to represent non-melting ($\alpha = 0.8$) and melting (non-forest $\alpha = 0.6$; unburned forest $\alpha = 0.45$) snow conditions. The model

was minimally tuned to best represent the snow and forest conditions in the western Oregon Cascades.

Snow Modeling and Post-fire Modifications

SnowModel runs were conducted at a 30-m resolution for a 262.4 km^2 modeling domain, from Three Fingered Jack to Mount Washington across the crest of the Oregon High Cascades. Land cover data was obtained from the National Land Cover Database (NLCD) 2011, with land class values reassigned to the equivalent SnowModel land cover class values. The Monitoring Trends in Burn Severity (MTBS) fire perimeter data were used to delineate burned area within the modeling domain [*Eidenshink et al.,* 2007]. The burned area from the Shadow Lake Fire was reclassified to a new "burned forest" class recognized by our modified SnowModel. These combined data resulted in non-forest (NF), unburned forest (UF), and burned forest (BF) land covers in our high elevation sub-alpine modeling domain.

The LAI parameter was modified to 0.5 in the burned forest and 2.8 in the unburned forest across the modeling domain to match converted measurements from hemispherical photos [*Gleason et al.,* 2013] and published values from a nearby forest [*Waring et al.,* 2013]. Finally, the new variable parameterization of snow albedo decay was incorporated into the existing framework of the net shortwave radiation calculation within the *Enbal* sub-model of SnowModel, by modifying the maximum and minimum snow albedo and snow albedo decay parameters to be representative of measured values in the burned and unburned forests.

4.5.4 Validation of Post-fire Snow Albedo and Snowmelt across the Extent of the Burned Forest

The new post-fire snow albedo decay parameterization was validated across the extent of the burned area using field measurements and remote sensing data.

Validation Using Measured Data

Model results of snow albedo, snow water equivalent, and date of snow disappearance derived using the default fixed albedo function, were compared to model results using the improved post-fire snow albedo decay parameterization at the burned and unburned micrometeorological station locations. We used Root Mean Square Error (RMSE) to compare modeled SWE at the station locations to measured SWE along the snow course transect to evaluate model performance using the default and improved post-fire snow albedo decay parameterizations. Spatial variability of snow albedo, SWE, and the date of snow disappearance were evaluated across the extent of the burned forest in comparison to remote sensing data.

Validation Using Snow Cover Frequency

Forest fire effects to snow ablation, snow cover duration, and the date of snow disappearance were evaluated using a monthly snow cover frequency (SCF) data product derived from the Moderate Resolution Imaging Spectroradiometer (MODIS) MOD10A1 8-day composite 250-m snow cover product. Monthly SCF was derived from the frequency of snow cover present amongst all valid measurements from all MOD10A1 snow cover data for each month within the Shadow Lake Fire perimeter

from 2007-2012. The difference in mean monthly SCF for March, April, May, and June were averaged for the period of five years prior to burn occurrence (2007-2011). These mean monthly SCF for the period before fire occurrence were compared to the first year following fire occurrence (WY 2012) using probability distribution functions and analysis of variance for pixels across the extent of the burn.

4.6 Results

Charred forests accelerate snow albedo decay, and increase the post-fire radiative forcing to snow. By incorporating fire disturbance effects to the snow energy balance, we improved the accuracy and confidence in our snow energy and mass balance model results.

4.6.1 Characterization of Post-fire Snow Albedo Decay

Measured Snow Spectral Albedo Decay

Particularly across the visible wavelengths, measured spectral albedo of the snowpack surface decreased throughout the ablation season in both burned and unburned forests. However, snow spectral albedo was significantly lower overall and decreased more rapidly after snowfall in the burned forest than in the unburned forest during snow ablation (Figure 4.2a). The extent to which snow albedo was reduced in the burned forest can be only be explained by charred debris deposition on the snowpack surface, and concentration during snow ablation in the burned forest (Figure 4.2b). A snowfall event of 6 cm in the burned forest and 5 cm in the unburned forest occurred between the 03 April and 21 April spectral measurements; however, snow spectral albedo continued to decrease throughout this rapid melt period in the burned forest.

Measured Broadband Snow Albedo Decay

Measured mean daily broadband albedo was variable, but was consistently reset to near 0.9 with new snowfall and gradually decreased over time as a function of

days-since-snowfall at both sites in all years (Figure 4.4). During the accumulation period (negative net energy balance periods), there was no difference in mean snow albedo (Figure 4.5a), or snow albedo decay (Figure 4.5b), between the burned and unburned forests. However during snow ablation (positive net energy balance periods), both mean snow albedo and minimum snow albedo were significantly lower (Figure 4.5c), and snow albedo decay was significantly accelerated (Figure 4.5d) in the burned forest compared to the nearby, unburned forest. The temporal variability in both spectral and broadband albedo measurements in the unburned forest likely corresponds to irregular timing of sloughing events of intercepted snow from the canopy to the snow surface.

Snowpack and Snow Surface Debris

Peak SWE was 11% greater in the burned forest than in the unburned forest the first year following fire, a slightly above average snow year. The second and third years following fire, which were relatively warm, below average snow years, with many mid-winter melt events (Figure 4.6), peak SWE was greater in the unburned forest. For all years following fire, the date of snow disappearance ranged from 11-28 days earlier in the burned forest than in the unburned forest (Table 4.2). Assuming a consistent deposition rate of BWD and interannual variability in SWE, greater concentrations of snow surface debris would accumulate during low snow years. Therefore, at least immediately following fire disturbance, the total snow surface

debris load may have a greater post-fire radiative impact during years of low snow accumulation.

During the accumulation period, the mean snow surface debris concentration in the burned forest (0.08 [g/kg]) was approximately 35% of that measured in the unburned forest (0.23 [g/Kg]) for the first, second, and third years following fire. During the ablation period, snow surface debris concentrations increased in both forests, but were 2.5 times greater in the burned forest (4.4 [g/kg]) than in the unburned forest (1.7 [g/kg]) for the first and second years following fire (Figure 4.7). Snow surface debris concentrations in the first post-fire year (WY 2012) were double those measured in the same area during the second post-fire year (WY 2013), when snowpack was shallower [*Gleason et al.*, 2013], although there was no significant difference in surface debris in the nearby unburned forest between years. Snow surface debris concentrations where not significantly different between the burned and unburned forests during the third year post-fire, except for an extremely large sample of debris collected during 01 May 2014 snow course in the burned forest. This 298 [g/kg] measurement consisted of a section of a 3-m long and 28-cm wide strip of bark, which had fallen across the sampling area.

4.6.2 Parameterization of Post-fire Snow Albedo Decay

The new post-fire snow albedo decay parameterization solves for daily mean snow albedo using a time-varying exponential decay coefficient, and maximum and minimum snow albedo parameters. After new snowfall of 0.001m of SWE per day,

albedo refreshment resets the snow albedo (α_{snow}) to the maximum albedo ($\alpha_{snow,max}$), and thereafter snow albedo decays over time to the minimum albedo ($\alpha_{snow,min}$), as a function of an exponential albedo decay coefficient ($-K_{\alpha}$) and daily time step (Δt) (Equation 4.2).

$$(\alpha_{snow})^{n+1} = \alpha_{snow,min} + ((\alpha_{snow})^{n} - \alpha_{snow,min})^{(-\mathrm{K}_{\alpha}\,\Delta t)} \qquad \text{(Equation 4.2)}$$

The actual parameters used for the unburned forest melt albedo decay were maximum albedo, 0.7; minimum albedo, 0.4; K = 0.018, for the burned forest melt albedo decay were maximum albedo, 0.58; minimum albedo, 0.3; and K = 0.038, and for non-forest melt albedo decay maximum albedo, 0.8; minimum albedo, 0.5; and K = 0.01 (Table 4.2). The post-fire snow albedo decay parameterization drives faster exponential decrease in albedo as a function of days-since-snowfall and permits a lower minimum albedo value to account for the deposition and concentration of charred debris on the post-fire snowpack surface.

4.6.3 Modeled Post-fire Snow Energy Balance, Snow Albedo Decay, and Snow Hydrology

Modeled Snow Albedo Decay and SWE Accumulation and Ablation

Modeled daily snow albedo values using the default fixed albedo parameterization are unphysical and thus not representative of measured snow albedo variability (Figure 4.8a). By including our variable post-fire snow albedo decay parameterization, the maximum snow albedo, minimum snow albedo, and snow albedo decay rates were more representative of measured snow albedo values in both

the burned and unburned forests (Figure 4.8b). SnowModel with the modified LAI values performed well overall in predicting measured SWE values in the burned and unburned forests, even using default the fixed albedo. The variable albedo decay parameterization more accurately represents the variability in snow albedo, and, particularly in the burned forest site, it more accurately predicts SWE than the fixed albedo decay parameterization.

Modeled Snow Albedo and SWE across the Burned Forest

Using the fixed snow albedo parameterization, there was no difference in the spatial variability of albedo and SWE between the unburned and burned forest areas during snow accumulation and snow ablation periods. However, by reducing the LAI and using the variable post-fire snow albedo decay parameterization, the model more accurately captures the mean albedo as well as the temporal (Figure 4.9) and spatial (Figure 4.10) variability observed in measured snow albedo data (Figure 4.4). The most profound differences in snow albedo and SWE values between the fixed and variable post-fire snow albedo decay parameterization occurred during the snow ablation period. Using the fixed albedo parameterization, on 5 May 2013, the date of measured snow disappearance from our snow course transect, the model predicted SWE across the burned forest. By incorporating the variable post-fire snow albedo decay parameterization, the model more accurately predicted the accelerated snow albedo decay during ablation, as well as advanced date of snow disappearance in the burned forest.

4.6.4 Validation of Post-fire Radiative Forcing to Snow

Across the extent of the burned area, differences in pre- and post-fire snow cover frequency varied by month. There was no difference in April pre- and post-fire snow cover frequency. However, there was a significantly lower May and June post-fire snow cover frequency (Figure 4.11). The probability distribution function of the difference in snow cover frequency before and after the fire disturbance showed that mean snow cover frequency across the burned area was about 20% less in May and June in the year after fire disturbance than prior to the forest fire disturbance. The areas with greatest change in snow cover frequency in May and June correspond to areas of highest forest fire severity to overstory trees. Across the extent of the burned area, snow melted off faster and earlier in spring, advancing the date of snow disappearance.

4.7 Discussion

Snow albedo decay, a predominate driver of snow metamorphism and snow melt processes, increased during snow ablation in both burned and unburned forests. Although charred forests even further accelerated spectral and broadband snow albedo decay during ablation for at least three years following high severity fire disturbance. Considerable variability exists in daily mean snow albedo values in both the burned and unburned forests through the winter seasons. Overall snow albedo decay is strongly correlated with days-since-snowfall and snow surface debris concentrations, both highly multi-collinear in the burned and unburned forests. Our results for three years following fire were consistent with those found the first year following fire [*Gleason et al.*, 2013]. During snow accumulation, spectral and broadband snow albedo values were similar in the burned and unburned forests. However during snow ablation, mean spectral and broadband snow albedo values were significantly lower in the burned forest for all three years following fire. As observed by both our extensive field measurements and remotely sensed data, snow melted off faster and earlier in the year across the extent of the burned forest for many years following fire.

Three years following fire disturbance, snow surface albedo and related snow surface debris concentrations in the burned forest appeared to be recovering to values near those in the unburned forest site. By the third year post-fire, snow surface debris concentrations in the burned forest were not significantly different than in the

unburned forest with the exception of a large outlier. Although we did not specifically quantify particulate size in our sampling strategy, we observed a changing pattern in post-fire debris deposition over time. Immediately following the fire, the greatest mass of debris deposition occurred and was comprised of mostly fine particulates. During the second winter after fire, mass of debris deposition was reduced, but the general size of the debris increased. During the third winter after fire, debris concentration was much less overall, but was punctuated by very large pieces of bark and branches falling near standing burned trees. Considering unburned forest debris also reduces snow surface albedo, it is likely the post-fire snow albedo decay will eventually resemble that of an open area with lower radiative forcing due to surface debris than in the nearby unburned forest. *Burles and Boon*, [2011], showed broadband snow albedo was greater in the burned forest than the unburned forest 5-7 years following fire disturbance.

We derived a new parameterization of the post-fire snow albedo decay using three winters of measured data, which used a lower maximum snow albedo and a greater recession coefficient than in the unburned forest. We effectively parameterized the entire snow surface albedo, by using one integrated post-fire snow albedo decay coefficient representative of both snow albedo decay from grain growth, as well as from debris deposition and concentration of light absorbing impurities on the snow surface. More data are needed to characterize and parameterize the temporal and spatial variability of first-order post-fire debris deposition in relation to

physiography and forest fire disturbance characteristics. For now, an empirically-derived exponential decay function is the most representative and parsimonious solution that fits in to the existing framework of most land surface hydrology models.

Although the focus of this investigation was snow albedo decay in the burned forest environment, we also developed snow albedo parameters based on the bias-corrected measured data from the unburned forest. As noted by *Gleason et al.,* [2013] and *Burles and Boon,* [2011], snow albedo derived from hemispherical radiation measurements in dense forest canopies integrate a large proportion of the forest canopy and are not representative of the true snow surface albedo. The bias-corrected broadband snow albedo data was more consistent with integrated spectral albedo measurements, and improves our confidence in the evaluation of snow albedo decay in the unburned forest. However, the sloughing of snow intercepted by the forest canopy is not represented in the days-since-snowfall metric derived from the sonic snow depth measurements, and may have introduced additional variability in measured values by "resetting" snow surface albedo to that of fresh snowfall when no new snowfall was measured. Although this study effectively parameterized an unburned forest for comparison to our burned forest site, more research into snow albedo decay processes in unburned forests is required to be confident in its representation.

Using a variable snow albedo decay parameterization better represents the temporal and spatial variability of snow albedo and SWE in relation to snowfall

timing and snow ablation as a function of disturbance history and landscape physiography. Because snowmelt and snow cover duration are so sensitive to snowpack net energy balance, which is dominated by net shortwave radiation, particularly during the ablation period, it is critical that our hydrologic models accurately represent snow albedo decay. Particularly under variable disturbance regimes, our ability to accurately parameterize snow albedo decay, improves our confidence in our model results.

4.8 Conclusions

For three years following high severity fire disturbance in the western Oregon Cascades, we characterized forest fire effects to snow albedo decay and subsequent snow ablation. With these data we developed a new parameterization of post-fire radiative forcing on snow to enable quantification of disturbance effects to high elevation winter water storage. Although forest structure and inter-annual variability were influential to snow melt processes [*Maurer and Bowling*, 2014], the post-fire radiative forcing on snow has a profound influence to snow melt timing, snow cover duration, and date of snow disappearance in the years immediately following fire disturbance.

Significant spatial and temporal variability in the post-fire snow albedo decay rates will surely result from different snow climates, forest composition and structure, and forest fire burn severity. More research is needed to determine the temporal variability in the post-fire recovery of snow albedo decay for the decades following fire disturbance, and to evaluate how these results from a Pacific Northwest maritime snow climate corresponds to intercontinental mountain west and desert systems in the western US. Lack of high-resolution temporally and spatially distributed data restrict our models to empirically-based parameterizations of the post-fire radiative forcing to snow, we need a first-order physically based mechanistic understanding of this process to enable confident application of the function across variable snow climates.

4.9 References

Abatzoglou, J. T., and C. A. Kolden (2013), Relationships between climate and macroscale area burned in the western United States, *International Journal of Wildland Fire*, *22*(7), 1003-1020.

Acker, S. A., J. Kertis, H. Bruner, K. O'Connell, and J. Sexton (2013), Dynamics of coarse woody debris following wildfire in a mountain hemlock (*Tsuga mertensiana*) forest, *Forest Ecology and Management*, *302*, 231-239.

Anderson, E. A. (1976), A point of energy and mass balance model of snow cover, *NOAA Techical Report, National Weather Service*, *19*, 1-150.

Andreadis, K. M., P. Storck, and D. P. Lettenmaier (2009), Modeling snow accumulation and ablation processes in forested environments, *Water Resources Research*, *45*.

Bartelt, P., and M. Lehning (2002), A physical SNOWPACK model for the Swiss avalanche warning Part I: numerical model, *Cold Regions Science and Technology*, *35*(3), 123-145.

Boon, S. (2009), Snow ablation energy balance in a dead forest stand, *Hydrological Processes*, *23*(18), 2600-2610.

Burles, K., and S. Boon (2011), Snowmelt energy balance in a burned forest plot, Crowsnest Pass, Alberta, Canada, *Hydrological Processes*, *25*(19), 3012-3029.

Clark, M. P., B. Nijssen, J. D. Lundquist, D. Kavetski, Rupp, D. E., R. A. Woods, J. E. Freer, E. D. Gutmann, A. W. Wood, L. D. Brekke, J. R. Arnold, D. J. Gochis, and R. M. Rasmussen (2015), A unified approach for process-based hydrologic modeling: 1. Modeling concept, *Water Resources Research*, published online, DOI: 10.1002/2015WR017198.

Colbeck, S. C. (1986), Classification of seasonal snow cover crystals, *Water Resources Research*, *22*(9), S59-S70.

Crawford, T. M., and C. E. Duchon (1999), An improved parameterization for estimating effective atmospheric emissivity for use in calculating daytime downwelling longwave radiation, *Journal of Applied Meteorology*, *38*(4), 474-480.

REFERENCES (Continued)

Deems, J. S., T. H. Painter, J. J. Barsugli, J. Belnap, and B. Udall (2013), Combined impacts of current and future dust deposition and regional warming on Colorado River Basin snow dynamics and hydrology, *Hydrology and Earth System Sciences*, *17*(11), 4401-4413.

Dennison, P. E., S. C. Brewer, J. D. Arnold, and M. A. Moritz (2014), Large wildfire trends in the western United States, 1984-2011, *Geophysical Research Letters*, *41*(8), 2928-2933.

Dery, S. J., and R. D. Brown (2007), Recent Northern Hemisphere snow cover extent trends and implications for the snow-albedo feedback, *Geophysical Research Letters*, *34*(22).

Dilley, A. C., and D. M. O'Brien (1998), Estimating downward clear sky long-wave irradiance at the surface from screen temperature and precipitable water, *Quarterly Journal of the Royal Meteorological Society*, *124*(549), 1391-1401.

Dozier, J., R. O. Green, A. W. Nolin, and T. H. Painter (2009), Interpretation of snow properties from imaging spectrometry, *Remote Sensing of Environment*, *113*, S25-S37.

Dunn, C. J., and J. D. Bailey (2012), Temporal dynamics and decay of coarse wood in early seral habitats of dry-mixed conifer forests in Oregon's Eastern Cascades, *Forest Ecology and Management*, *276*, 71-81.

Eidenshink, J., B. Schwind, K. Brewer, Z.-L. Zhu, B. Quayle, and S. Howard (2007), project for monitoring trends in burn severity, *Fire Ecology*.

Essery, R., S. Morin, Y. Lejeune, and C. B. Menard (2013), A comparison of 1701 snow models using observations from an alpine site, *Advances in Water Resources*, *55*, 131-148.

Flanner, M. G., and C. S. Zender (2006), Linking snowpack microphysics and albedo evolution, *Journal of Geophysical Research - Atmospheres*, *111*(D12).

Flanner, M. G., C. S. Zender, P. G. Hess, N. M. Mahowald, T. H. Painter, V. Ramanathan, and P. J. Rasch (2009), Springtime warming and reduced snow cover from carbonaceous particles, *Atmospheric Chemistry and Physics*, *9*(7), 2481-2497.

REFERENCES (Continued)

Flerchinger, G. N., W. Xaio, D. Marks, T. J. Sauer, and Q. Yu (2009), Comparison of algorithms for incoming atmospheric long-wave radiation, *Water Resources Research*, *45*.

Garen, D. C., and D. Marks (2005), Spatially distributed energy balance snowmelt modelling in a mountainous river basin: estimation of meteorological inputs and verification of model results, *Journal of Hydrology*, *315*(1-4), 126-153.

Gleason, K. E., A. W. Nolin, and T. R. Roth (2013), Charred forests increase snowmelt: Effects of burned woody debris and incoming solar radiation on snow ablation, *Geophysical Research Letters*, *40*(17), 4654-4661.

Gleason, K. E., A. W. Nolin, and T. Roth (2013), Charred forests increase snowmelt: effects of burned woody debris and incoming solar radiation on snow ablation, *Geophysical Research Letters*.

Hadley, O. L., and T. W. Kirchstetter (2012), Black-carbon reduction of snow albedo, *Nature Climate Change*, *2*(6), 437-440.

Hansen, J., and L. Nazarenko (2004), Soot climate forcing via snow and ice albedos, *Proceedings of the National Academy of Sciences of the United States of America*, *101*(2), 423-428.

Hansen, J., et al. (2005), Efficacy of climate forcings, *Journal of Geophysical Research - Atmospheres*, *110*(D18).

Hardy, J., R. Melloh, P. Robinson, and R. Jordan (2000), Incorporating effects of forest litter in a snow process model, *Hydrological Processes*, *14*(18), 3227-3237.

Hardy, J. P., R. Melloh, G. Koenig, D. Marks, A. Winstral, J. W. Pomeroy, and T. Link (2004), Solar radiation transmission through conifer canopies, *Agricultural and Forest Meteorology*, *126*(3-4), 257-270.

Harpold, A. A., J. A. Biederman, K. Condon, M. Merino, Y. Korgaonkar, T. Nan, L. L. Sloat, M. Ross, and P. D. Brooks (2014), Changes in snow accumulation and ablation following the Las Conchas Forest Fire, New Mexico, USA, *Ecohydrology*, *7*(2), 440-452.

Jordan, R. (1991), A one-dimensional temperature model for a snow cover: Technical documentation for SNTHERM. 89*Rep.*, DTIC Document.

REFERENCES (Continued)

Lanini, J. S., E. A. Clark, and D. P. Lettenmaier (2009), Effects of fire-precipitation timing and regime on post-fire sediment delivery in Pacific Northwest forests, *Geophysical Research Letters*, *36*(1).

Lehning, M., P. Bartelt, B. Brown, C. Fierz, and P. Satyawali (2002), A physical SNOWPACK model for the Swiss avalanche warning Part II: Snow microstructure, *Cold Regions Science and Technology*, *35*(3), 147-167.

Liang, X., D. P. Lettenmaier, E. F. Wood, and S. J. Burges (1994), A simple hydrologically based model of land-surface water and energy fluxes for general-circulation models, *Journal of Geophysical Research - Atmospheres*, *99*(D7), 14415-14428.

Liston, G. E., and D. K. Hall (1995), An energy-balance model of lake-ice evolution, *Journal of Glaciology*, *41*(138), 373-382.

Liston, G. E., and M. Sturm (1998), A snow-transport model for complex terrain, *Journal of Glaciology*, *44*(148), 498-516.

Liston, G. E., and M. Sturm (2002), Winter precipitation patterns in arctic Alaska determined from a blowing-snow model and snow-depth observations, *Journal of Hydrometeorology*, *3*(6), 646-659.

Liston, G. E., and K. Elder (2006), A distributed snow-evolution modeling system (SnowModel), *Journal of Hydrometeorology*, *7*(6), 1259-1276.

Liston, G. E., and S. H. Mernild (2012), Greenland Freshwater Runoff. Part I: A Runoff Routing Model for Glaciated and Nonglaciated Landscapes (HydroFlow), *Journal of Climate*, *25*(17), 5997-6014.

Liu, H. P., J. T. Randerson, J. Lindfors, and F. S. Chapin (2005), Changes in the surface energy budget after fire in boreal ecosystems of interior Alaska: An annual perspective, *Journal of Geophysical Research - Atmospheres*, *110*(D13).

Marks, D., and J. Dozier (1992), Climate and energy exchange at the snow surface in the alpine region of the Sierra Nevada, 2, Snow cover energy balance, *Water Resources Research*, *28*(11), 3043-3054.

REFERENCES (Continued)

Maurer, G. E., and D. R. Bowling (2014), Seasonal snowpack characteristics influence soil temperature and water content at multiple scales in interior western US mountain ecosystems, *Water Resources Research*, *50*(6), 5216-5234.

Melloh, R. A., J. P. Hardy, R. E. Davis, and P. B. Robinson (2001), Spectral albedo/reflectance of littered forest snow during the melt season, *Hydrological Processes*, *15*(18), 3409-3422.

Melloh, R. A., J. P. Hardy, R. N. Bailey, and T. J. Hall (2002), An efficient snow albedo model for the open and sub canopy, *Hydrological Processes*, *16*(18), 3571-3584.

Mendoza, P. A., B. Rajagopalan, M. P. Clark, G. Cortes, and J. McPhee (2014), A robust multimodel framework for ensemble seasonal hydroclimatic forecasts, *Water Resources Research*, *50*(7), 6030-6052.

Micheletty, P. D., A. M. Kinoshita, and T. S. Hogue (2014), Application of MODIS snow cover products: wildfire impacts on snow and melt in the Sierra Nevada, *Hydrology and Earth System Sciences*, *18*(11), 4601-4615.

Moritz, M. A., M.-A. Parisien, E. Batllori, M. A. Krawchuk, J. Van Dorn, D. J. Ganz, and K. Hayhoe (2012), Climate change and disruptions to global fire activity, *Ecosphere*, *3*(6), art49.

O'Halloran, T. L., et al. (2012), Radiative forcing of natural forest disturbances, *Global Change Biology*, *18*(2), 555-565.

Painter, T. H., A. C. Bryant, and S. M. Skiles (2012), Radiative forcing by light absorbing impurities in snow from MODIS surface reflectance data, *Geophysical Research Letters*, *39*.

Painter, T. H., F. C. Seidel, A. C. Bryant, S. M. Skiles, and K. Rittger (2013), Imaging spectroscopy of albedo and radiative forcing by light-absorbing impurities in mountain snow, *Journal of Geophysical Research - Atmospheres*, *118*(17), 9511-9523.

REFERENCES (Continued)

Painter, T. H., J. S. Deems, J. Belnap, A. F. Hamlet, C. C. Landry, and B. Udall (2010), Response of Colorado River runoff to dust radiative forcing in snow, *Proceedings of the National Academy of Sciences of the United States of America*, *107*(40), 17125-17130.

Painter, T. H., A. P. Barrett, C. C. Landry, J. C. Neff, M. P. Cassidy, C. R. Lawrence, K. E. McBride, and G. L. Farmer (2007), Impact of disturbed desert soils on duration of mountain snow cover, *Geophysical Research Letters*, *34*(12), L12502.

Pomeroy, J. W., and K. Dion (1996), Winter radiation extinction and reflection in a boreal pine canopy: Measurements and modelling, *Hydrological Processes*, *10*(12), 1591-1608.

Rosen, H., T. Novakov, and B. Bodhaine (1981), Soot in the Arctic, *Atmospheric Environment (1967)*, *15*(8), 1371-1374.

Semmens, K. A., and J. Ramage (2012), Investigating correlations between snowmelt and forest fires in a high latitude snowmelt dominated drainage basin, *Hydrological Processes*, *26*(17), 2608-2617.

Serreze, M. C., M. P. Clark, R. L. Armstrong, D. A. McGinnis, and R. S. Pulwarty (1999), Characteristics of the western United States snowpack from snowpack telemetry (SNOTEL) data, *Water Resources Research*, *35*(7), 2145-2160.

Skiles, S. M., T. H. Painter, J. S. Deems, A. C. Bryant, and C. C. Landry (2012), Dust radiative forcing in snow of the Upper Colorado River Basin: 2. Interannual variability in radiative forcing and snowmelt rates, *Water Resources Research*, *48*.

Sproles, E. A., A. W. Nolin, K. Rittger, and T. H. Painter (2013), Climate change impacts on maritime mountain snowpack in the Oregon Cascades, *Hydrology and Earth System Sciences*, *17*(7), 2581-2597.

Trouet, V., A. H. Taylor, E. R. Wahl, C. N. Skinner, and S. L. Stephens (2010), Fire-climate interactions in the American West since 1400 CE, *Geophysical Research Letters*, *37*.

REFERENCES (Continued)

Ueyama, M., K. Ichii, H. Iwata, E. S. Euskirchen, D. Zona, A. V. Rocha, Y. Harazono, C. Iwama, T. Nakai, and W. C. Oechel (2014), Change in surface energy balance in Alaska due to fire and spring warming, based on upscaling eddy covariance measurements, *Journal of Geophysical Research-Biogeosciences*, *119*(10), 1947-1969.

U.S. Army Corps of Engineers (1956), *Snow hydrology. Summary report of the snow investigations of the North Pacific Division, Portland, OR.*

Verseghy, D. L. (1991), CLASS-A Canadian land surface scheme for GCMS, 1. Soil model, *International Journal of Climatology*, *11*(2), 111-133.

Waring, R., B. Law, and B. Bond (2013), NPP Temperate Forest: OTTER Project Sites, Oregon, USA, 1989-1991, *Data set. Available on-line [http://daac. ornl. gov] from Oak Ridge National Laboratory Distributed Active Archive Center, Oak Ridge, Tennessee, USA.*

Warren, S. G. (1982), Optical properties of snow, *Reviews of Geophysics*, *20*(1), 67-89.

Warren, S. G., and W. J. Wiscombe (1980), A model for the spectral albedo of snow, 2. Snow containing atmospheric aerosols, *Journal of the Atmospheric Sciences*, *37*(12), 2734-2745.

Warren, S. G., and W. J. Wiscombe (1981), Comment on radiative properties of snow for clear sky solar-radiation, *Cold Regions Science and Technology*, *5*(2), 177-180.

Westerling, A. L., H. G. Hidalgo, D. R. Cayan, and T. W. Swetnam (2006), Warming and earlier spring increase western US forest wildfire activity, *Science*, *313*(5789), 940.

Westerling, A. L., B. P. Bryant, H. K. Preisler, T. P. Holmes, H. G. Hidalgo, T. Das, and S. R. Shrestha (2011), Climate change and growth scenarios for California wildfire, *Climatic Change*, *109*, 445-463.

Wigmosta, M. S., L. W. Vail, and D. P. Lettenmaier (1994), A distributed hydrology-vegetation model for complex terrain, *Water Resources Research*, *30*(6), 1665-1680.

REFERENCES (Continued)

Winkler, R., S. Boon, B. Zimonick, and K. Baleshta (2010), Assessing the effects of post-pine beetle forest litter on snow albedo, *Hydrological Processes, 24*(6), 803-812.

Winkler, R. D., D. L. Spittlehouse, and D. L. Golding (2005), Measured differences in snow accumulation and melt among clearcut, juvenile, and mature forests in southern British Columbia, *Hydrological Processes*, *19*(1), 51-62.

Wiscombe, W. J., and S. G. Warren (1980), A model for the spectral albedo of snow. I: Pure snow, *Journal of the Atmospheric Sciences, 37*(12), 2712-2733.

Xu, B. Q., et al. (2009), Black soot and the survival of Tibetan glaciers, *Proceedings of the National Academy of Sciences of the United States of America, 106*(52), 22114-22118.

Yang, Z. L., R. E. Dickinson, A. Robock, and K. Y. Vinnikov (1997), Validation of the snow submodel of the biosphere-atmosphere transfer scheme with Russian snow cover and meteorological observational data, *Journal of Climate, 10*(2), 353-373.

4.10 Figures

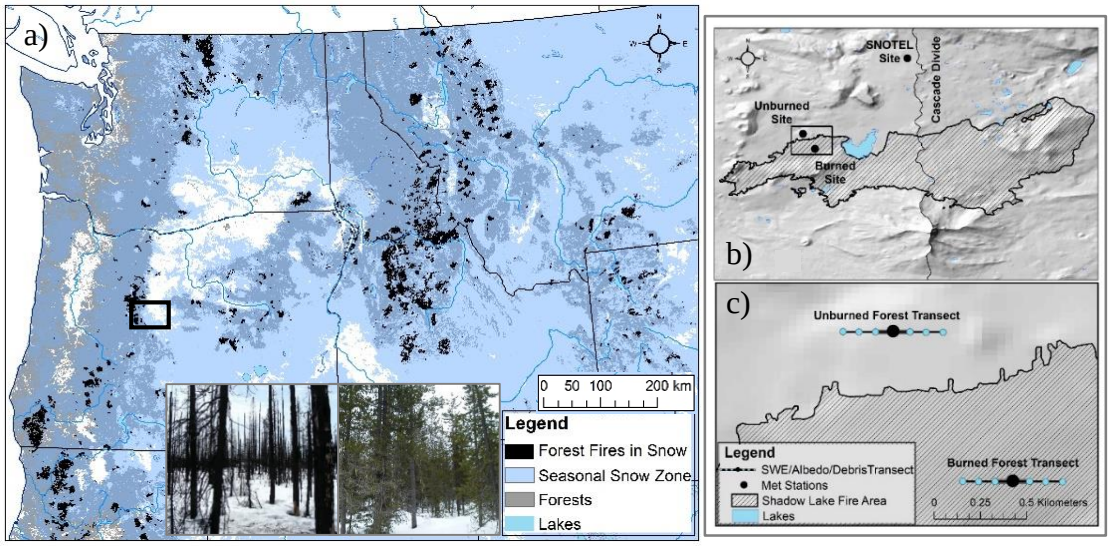

Figure 4.1. Burned area in the Pacific Northwest, b) unburned and burned forest sites in the Shadow Lake Fire area, c) locations of the micrometeorological stations, spectral and snow course transects in the burned and unburned forest sites.

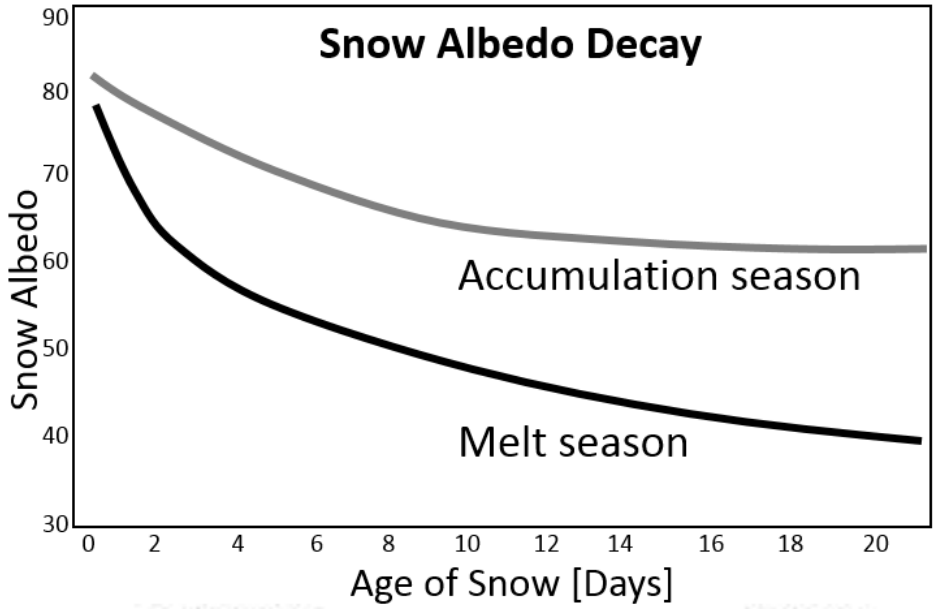

Figure 4.2. Snow albedo decay curves adapted from *US Army Corps of Engineers*, [1956].

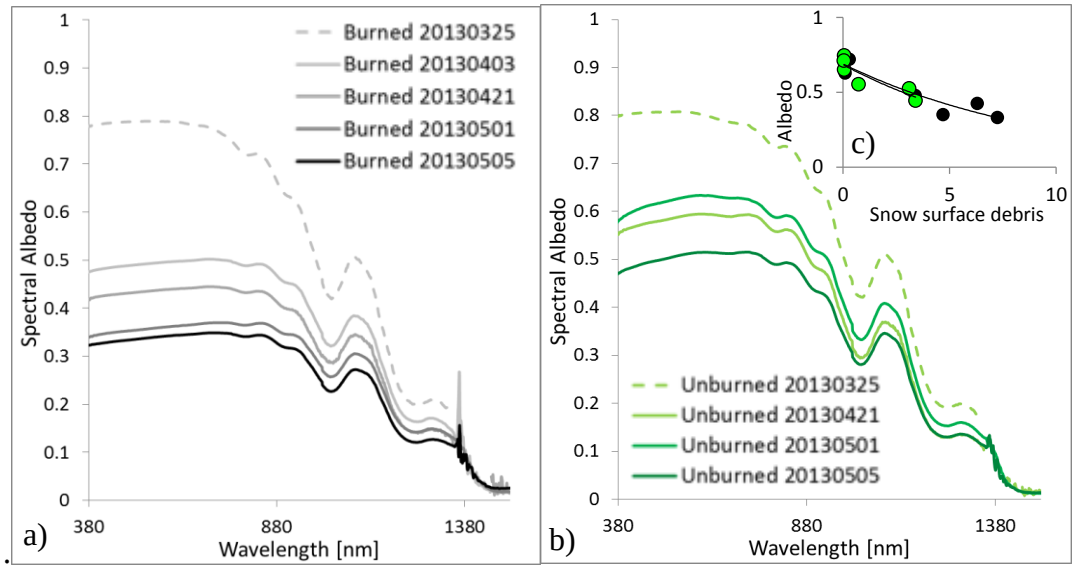

Figure 4.3. a) Mean spectral albedo of the burned forest, and b) mean spectral albedo of the unburned forest measured on spectrometer surveys on 25 March, 03 April, 21 April, 1 May, and 5 May 2013. New snowfall greater than 3cm occurred on 22 March 2013, 09 April 2013, and 14 April 2013. c) Integrated mean spectral albedo for all surveys in 2013 and 2014 over snow surface debris concentration [g/Kg].

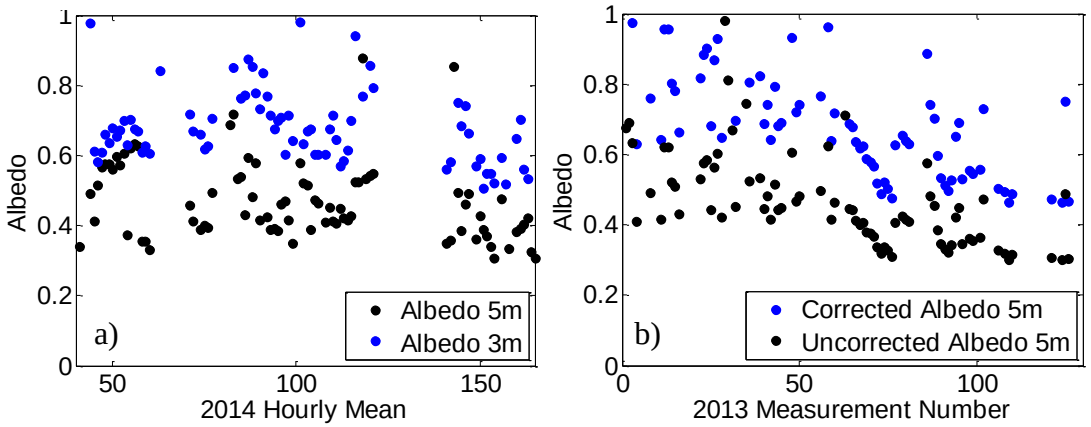

Figure 4.4. a) Hourly mean broadband albedo values calculated from pyranometers measurements at 5 m and 3 m above ground in the unburned forest, and b) corrected and uncorrected hourly mean broadband albedo values calculated from pyranometers at 5 m above ground.

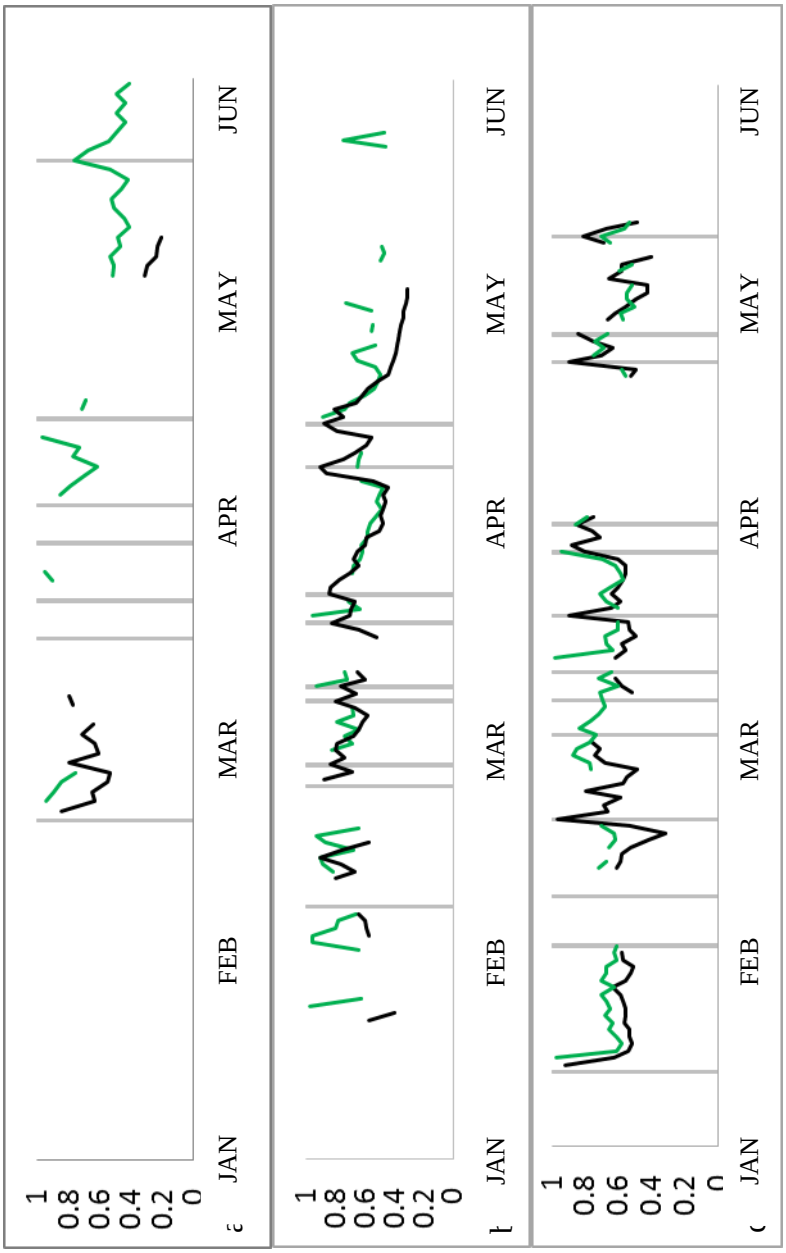

Figure 4.5. Measured daily mean snow albedo in burned and unburned forests for a) 2012, b) 2013, and c) 2014 (only quality measurements included).

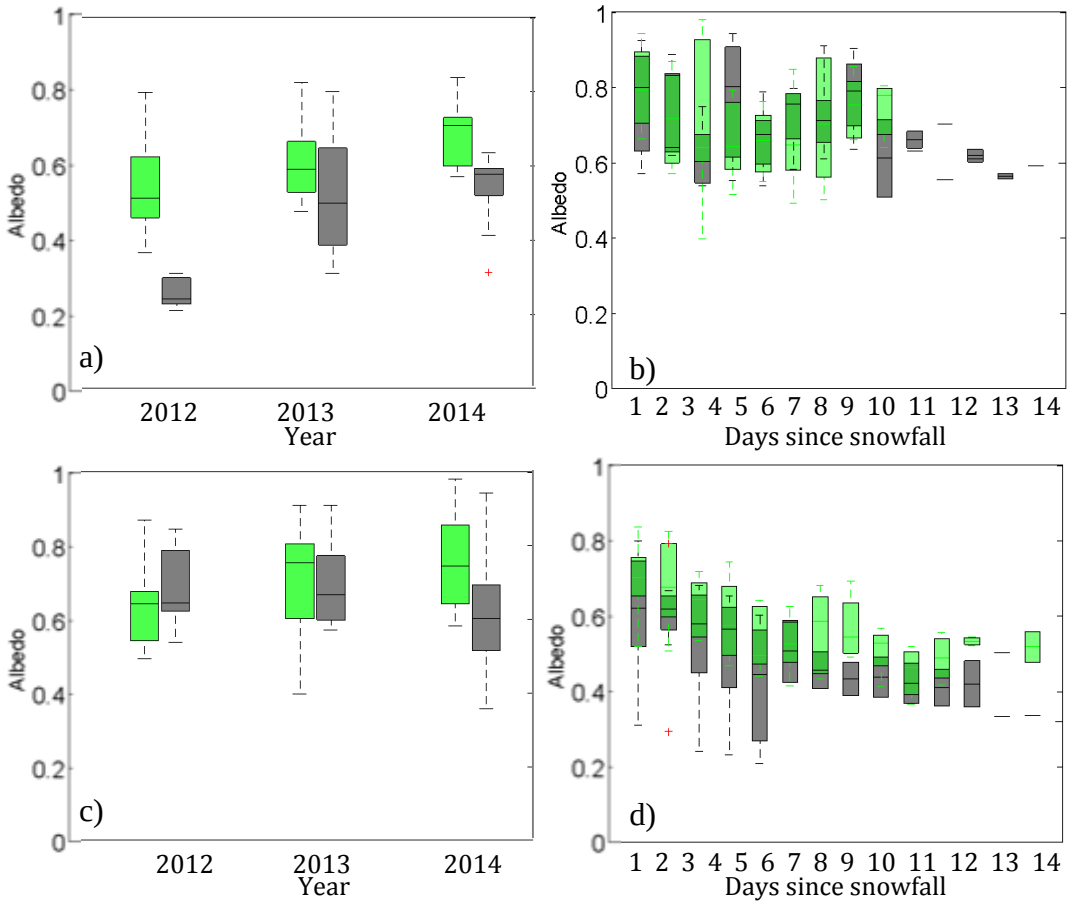

Figure 4.6. a) Measured mean daily snow albedo for days with positive energy balance, and b) negative energy balance for each year of measurements. c) Measured snow albedo decay (mean daily snow albedo vs. days-since-snowfall) during positive energy balance periods, and during d) negative energy balance periods for all years of measurements. Burned forest measurements shown in dark grey and unburned forest measurements shown in green.

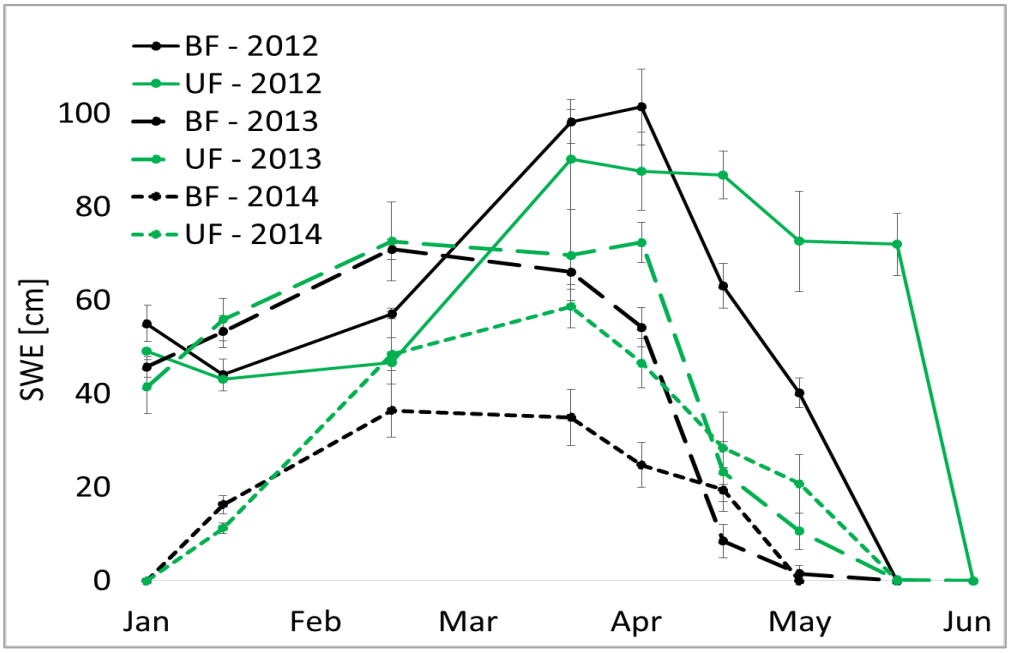

Figure 4.7. Mean SWE along the burned and unburned forest snow course transects measured during the water years 2012, 2013, and 2014.

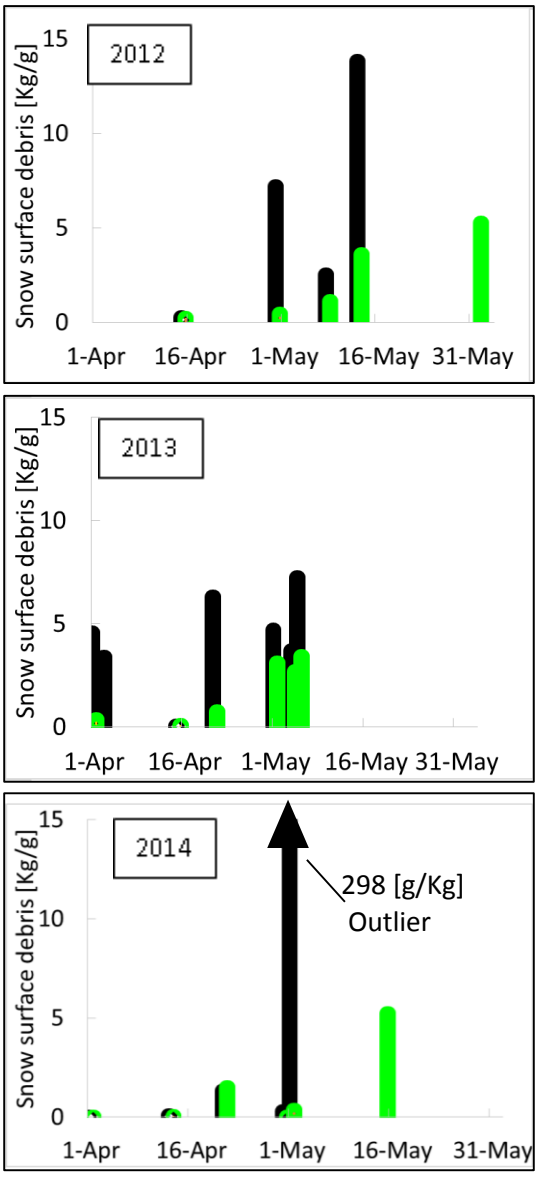

Figure 4.8. All measured snowpack surface debris concentrations from ablation season snow course and spectral snow albedo transects during each measurement year (2012, 2013, and 2014).

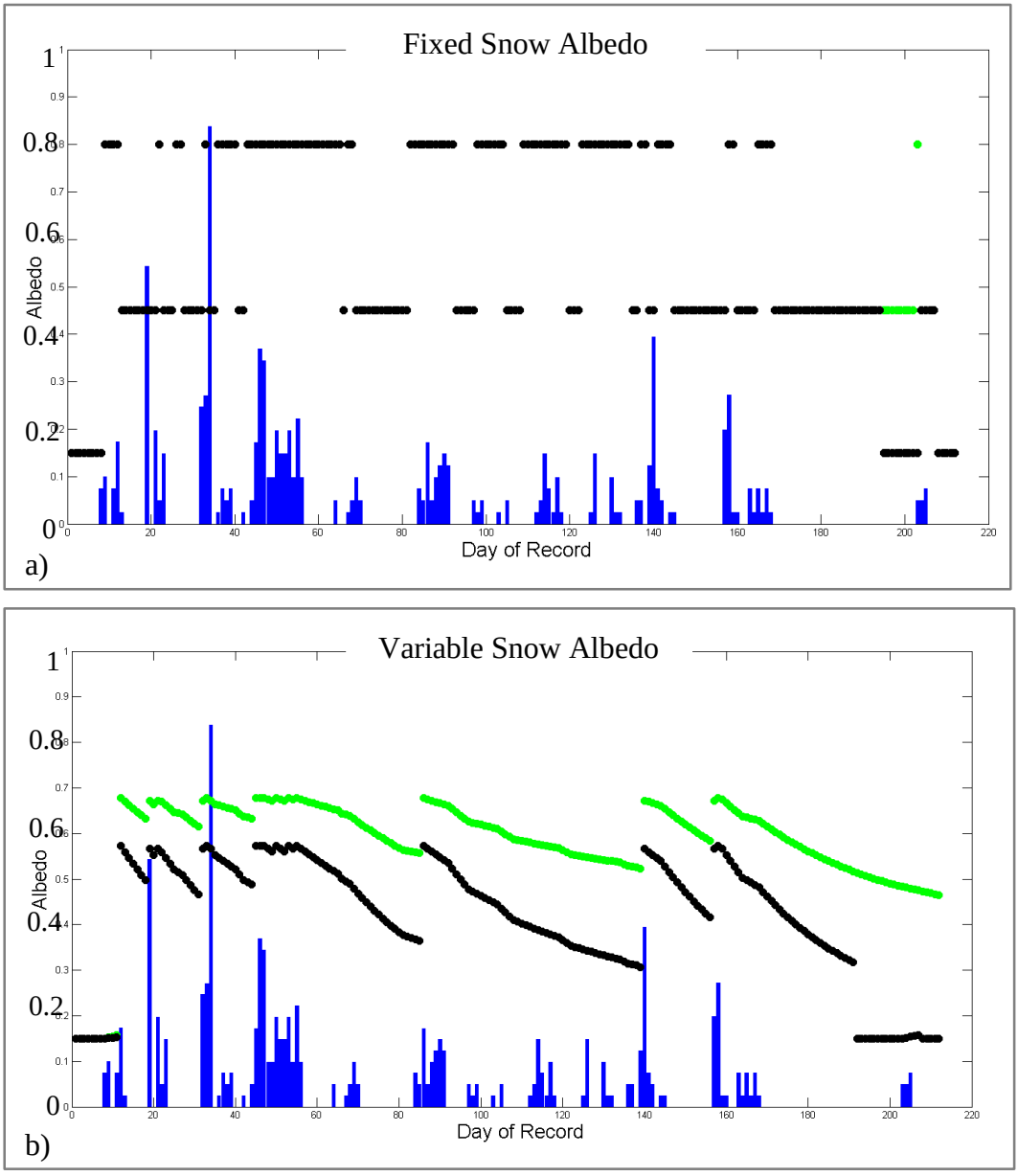

Figure 4.9. SnowModel results of snow albedo for the WY 2013 snow season derived using the, a) default fixed albedo parameterization, and the b) new variable albedo decay parameterization. Results are shown with snowfall * 1000 for scale shown in blue, to demonstrate the resetting of the snow albedo with sufficient new snowfall.

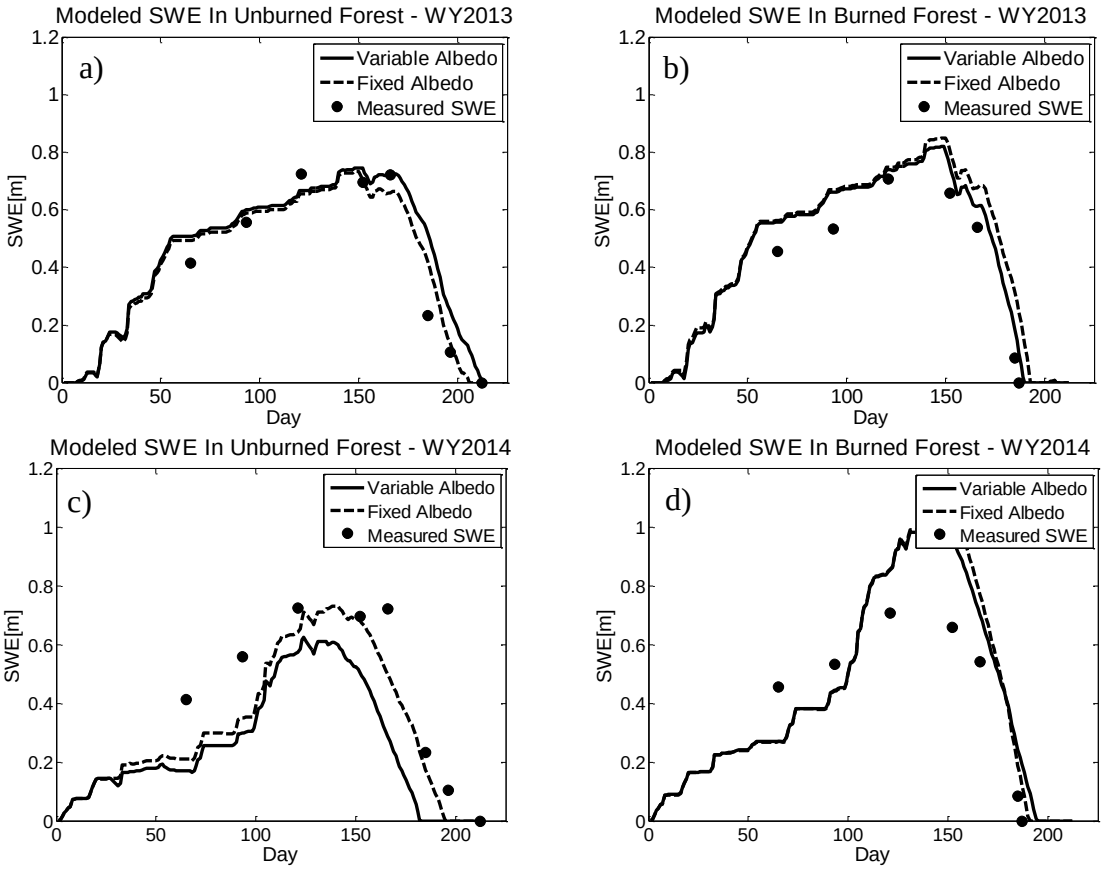

Figure 4.10. Modeled results of SWE from SnowModel using fixed and variable snow albedo decay parameterizations, and measured SWE from snow course data, in the a) & c) unburned forest, and b) & d) burned forests sites for WY 2013 and WY 2014 snow seasons.

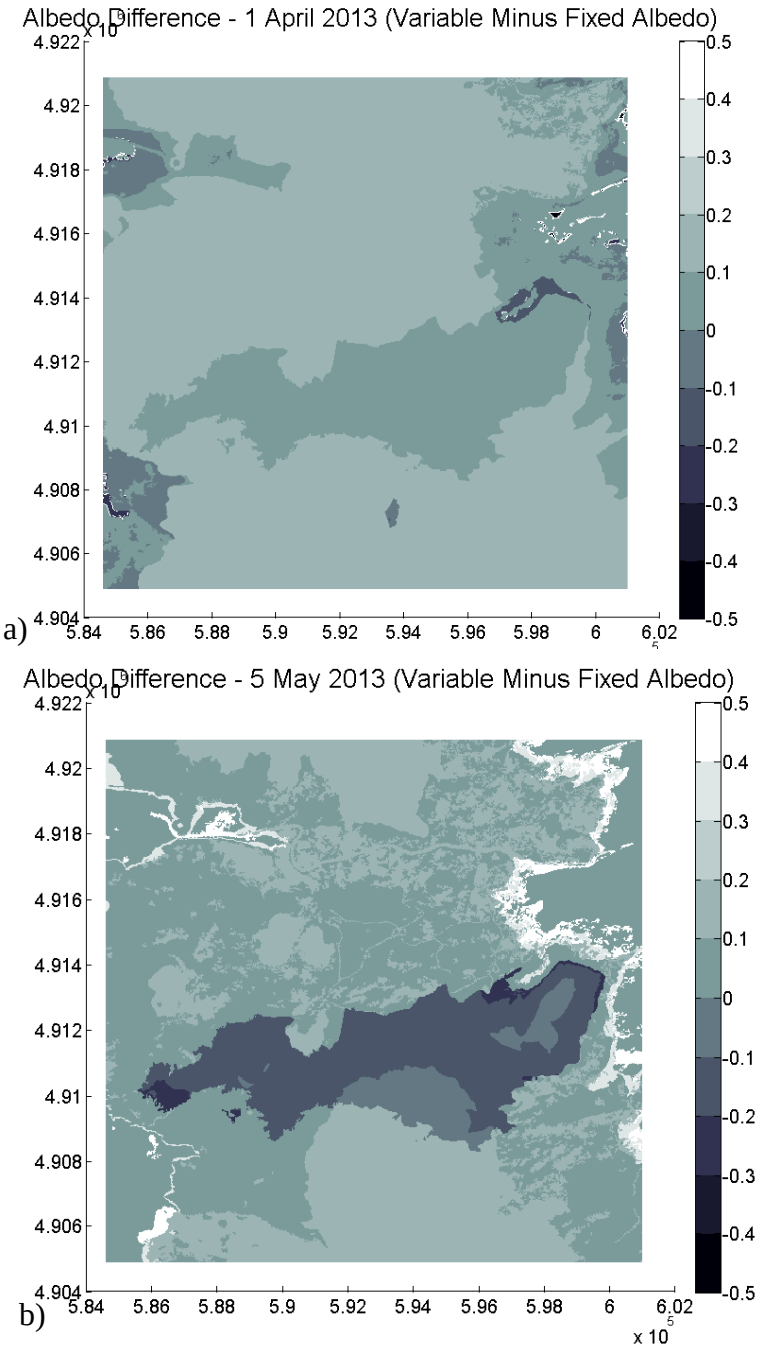

Figure 4.11.a. Spatially-distributed differences maps show the modeled output using the variable albedo decay parameterization minus the modeled output using the fixed albedo decay parameterization is shown) for a) April 1 albedo, and b) May 5 albedo.

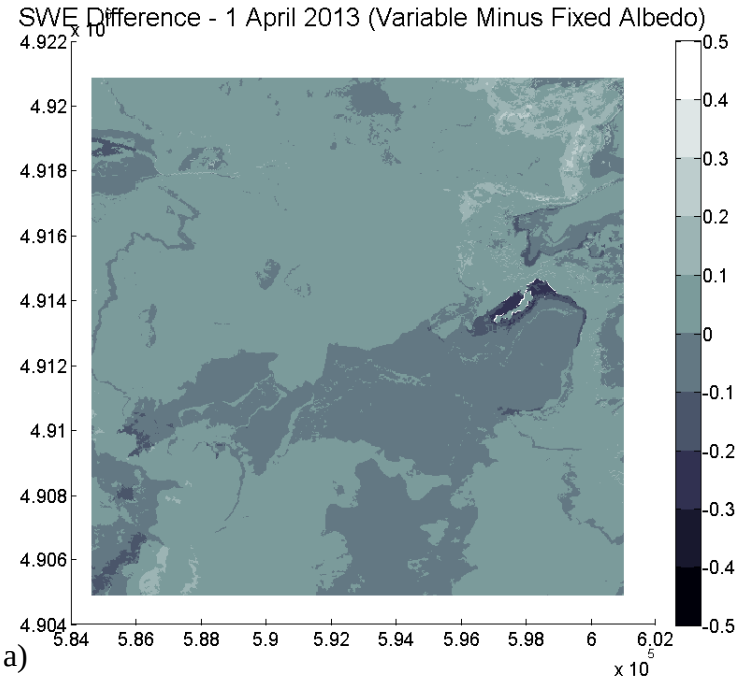

a)

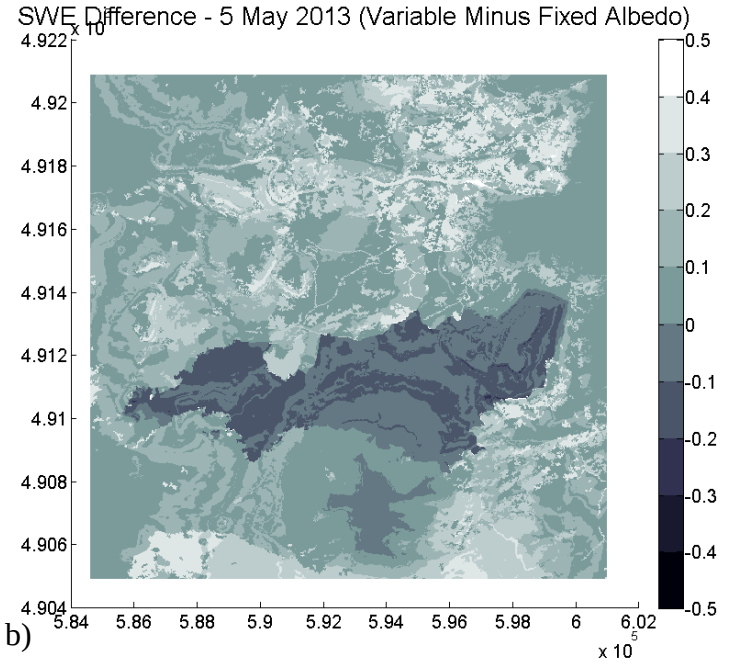

b)

Figure 4.11.b. Spatially-distributed differences maps show the modeled output using the variable albedo decay parameterization minus the modeled output using the fixed albedo decay parameterization is shown) for a) April 1 SWE, and b) May 5 SWE.

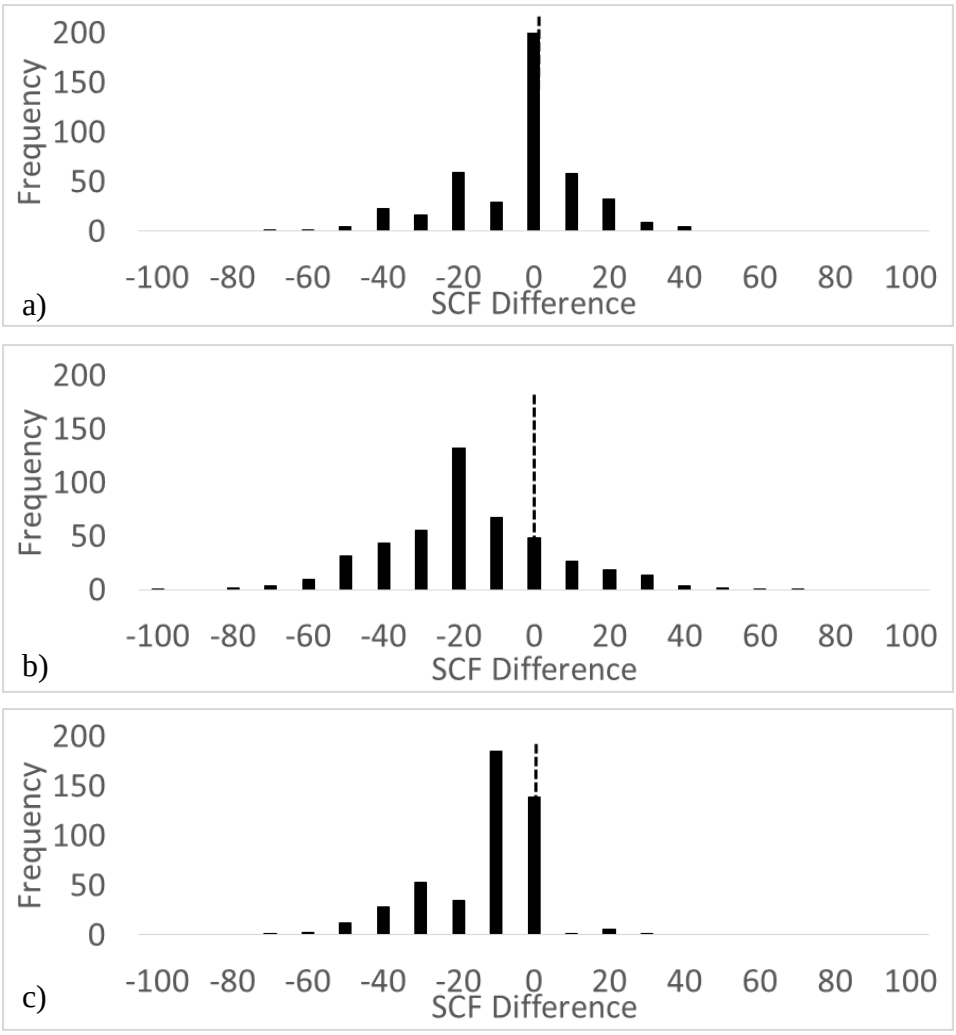

Figure 4.12.a. Probability distribution functions of difference in mean monthly snow cover frequency (2007-2011) and mean monthly snow cover frequency from 2012 for a) April, b) May, and c) June across the extent of the Shadow Lake Fire.

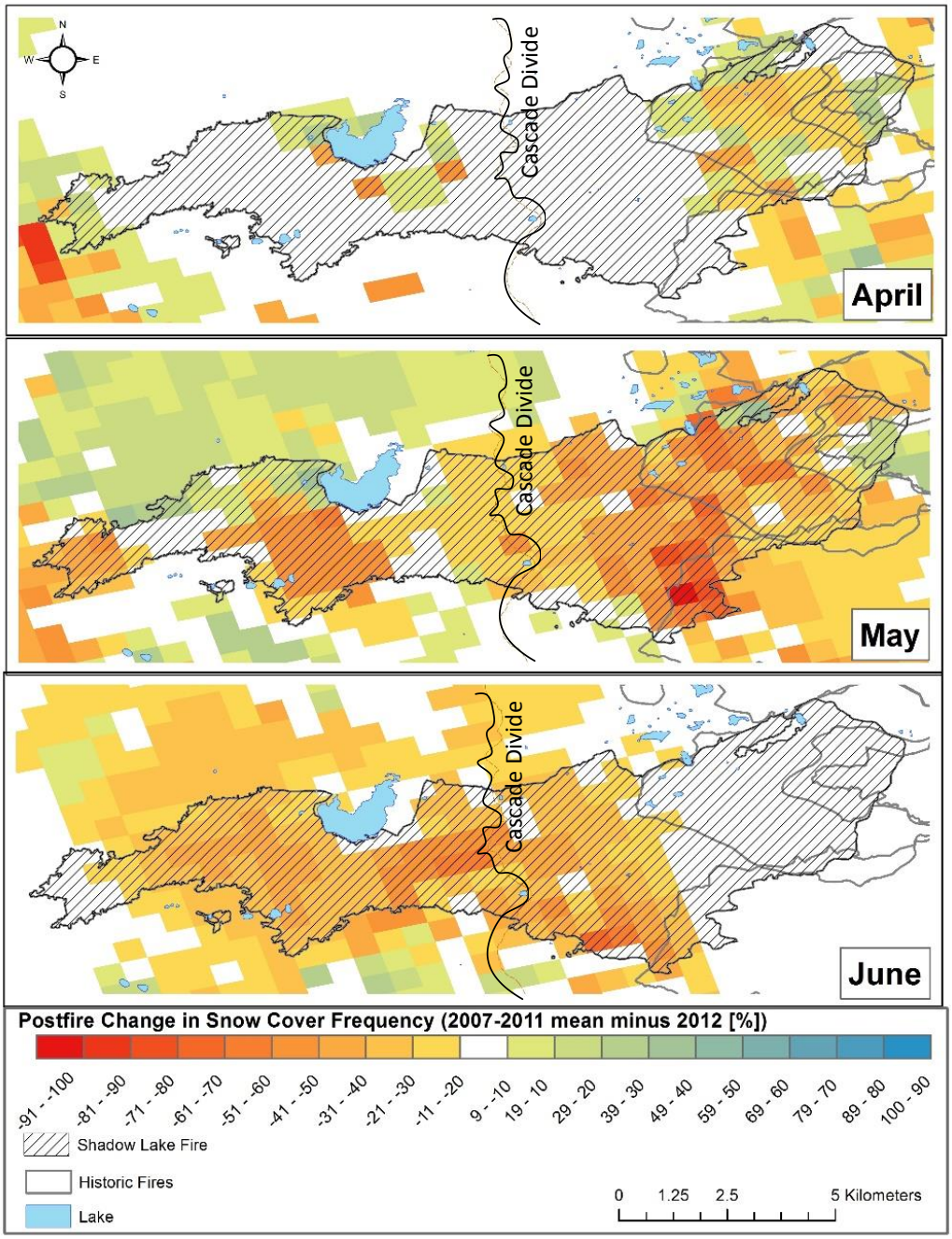

Figure 4.12.b. Difference in mean monthly snow cover frequency (2007-2011) and mean monthly snow cover frequency from 2012, across the extent of the Shadow Lake Fire.

4.10 Tables

Table 4.1. Snow albedo decay parameterizations used in snow accumulation and melt models, all values are expressed for daily time step.

SNOW MODEL	Fixed / Variable	Non-Melt / Melt	Non-Forest / Unburned Forest	Maximum albedo, $\propto_{s,max}$	Minimum albedo, $\propto_{s,min}$	Recession coefficient, κ	Snow Albedo Decay Equations
SNTHERM	F			0.78			$\propto_s = 0.78$
SnowModel Default	F	NM M		0.8 0.8	0.6 0.45		Non-melt or melt fixed albedo coefficient determined by temperature threshold
SnowModel Alternate *Sproles et al., [2013]*	V	NM M	NF	0.85 0.85	0.5 0.5	0.008 0.18	$\propto_{s,(t+1)} = (\propto_{s,(t)} - \kappa)$ $\propto_{s,(t+1)} = \alpha_{s,min} + (\propto_{s,(t)} - \alpha_{s,min})^{-\kappa}$
		NM M	UF	0.6 0.6	0.2 0.2	0.008 0.18	
CLASS	V	NM M	NF	0.84	0.7 0.5	0.01 0.24	$\propto_{s,(t+1)} = \alpha_{s,min} + (\propto_{s,(t)} - \alpha_{s,min})^{-\kappa}$
DHSVM	V	NM M		0.85		$N^{0.58}$ $N^{0.46}$	$\propto_s = \alpha_{snow,max}(0.94)^{\kappa}$ $\propto_s = \alpha_{snow,max}(0.82)^{\kappa}$
VIC	V	NM M		0.85		$N^{0.58}$ $N^{0.46}$	$\propto_s = \alpha_{snow,max}(0.94)^{\kappa}$ $\propto_s = \alpha_{snow,max}(0.7)^{\kappa}$
BATS	V	NM M	V NiR V NiR	0.85 0.65 0.75 0.15			$\left(\alpha_{snow}^{d}\right)^{n+1} = \left(\alpha_{snow}^{d}\right)^{n} + f_{age}\left(\alpha_{snow}^{d} - \alpha_{snow,\min}^{d}\right)$ $f_{age} = -\kappa_{\alpha}\Delta t / \left(1 + \kappa_{\alpha}\Delta t\right)$ $\kappa_{\alpha} = \kappa_{\alpha,0}\left(r_1 + r_2 + r_3\right)$
SNOWPACK Multi-variate albedo decay	V	NM M		0.95 0.7			$\propto_{s,(t+1)} = \propto_{s,(t)} + \ln(1+x)$ x = βVW+ γTA+ δTSS+ ήRSWR+ κTA TSS + λTA RSWR
iSNOBAL	V		V NiR				$\alpha_{snow} = \alpha_{snow,max} - \kappa_v r$
SUMMA	V						Includes fixed/variable/physical options selectable by user.

Table 4.2. Peak SWE date and volume derived from snow course transects, and date of snow disappearance (DSD) derived from the snow pingers at the micrometeorological station locations.

SITE	YEAR	Peak SWE	DSD	Peak SWE (cm)
UF	WY2012	02 Apr	20 June	90
	WY2013	01 Mar	03 June	77
	WY2014	30 Mar	31 May	59
BF	WY2012	15 Apr	29 May	101
	WY2013	01 Mar	05 May	61
	WY2014	03 Mar	20 May	35

Table 4.3. Exponential decay coefficients for burned and unburned forests during net positive and net negative snowpack energy balance periods (statistical significance indicated by symbols: ‘ 0.1 or less, * 0.05 or less).

SITE		**UNBURNED**		**BURNED**	
Net Energy Balance	**Year**	**Exponential Decay Equation**	**R^2**	**Exponential Decay Equation**	**R^2**
NEG	2012	$y = 0.662e^{-0.014x}$	0.03	$y = 0.7282e^{-0.016x}$	0.11
	2013	$y = 0.8678e^{-0.018x}$	0.32’	$y = 0.7101e^{-0.006x}$	0.04’
	2014	$y = 0.7323e^{-0.006x}$	0.04	$y = 0.6779e^{-0.014x}$	0.38*
	all	**$y = 0.7514e^{-0.01x}$**	**0.05**	**$y = 0.7551e^{-0.018x}$**	**0.45***
POS	2012	$y = 0.6599e^{-0.042x}$	0.46*	$y = 0.3464e^{-0.102x}$	0.96*
	2013	$y = 0.7121e^{-0.026x}$	0.47*	$y = 0.7319e^{-0.055x}$	0.82*
	2014	$y = 0.6814e^{-0.009x}$	0.06’	$y = 0.6303e^{-0.07x}$	0.14*
	all	**$y = 0.6791e^{-0.029x}$**	**0.33***	**$y = 0.5844e^{-0.038x}$**	**0.25***

5 Final Thoughts: Key Findings, Future Directions, Management Implications, and Conclusions

5.1 Summary of Key Findings

This dissertation presents a comprehensive evaluation of forest fire effects to snowpack energy balance and the volume and duration of snow-water resources using; a characterization of immediate forest fire effects to snow albedo, snow accumulation, and snowmelt; an evaluation of forest fire effects to the sensible and latent heat fluxes using both eddy covariance and bulk-transfer methods; and a parameterization incorporated into a physically-based spatially distributed energy and mass balance snow model to evaluate immediate and enduring forest fire effects to snow albedo, snow accumulation, and snow melt across the extent of the burned area.

Chapter 2 provided a detailed characterization of the key mechanisms driving forest fire effects to snow-water resources immediately following fire. This research documented forest structure, incoming and outgoing solar radiation, snow albedo, snow accumulation, and snow ablation using field-based snow monitoring, snow surface debris sampling, and snow albedo measurements in a burned and unburned forest. Remote sensing data of snow cover, forest cover, and fire extent were used to evaluate the extent of forest fire effects to snow-water resources across the western United States.

Charred forests increase snow melt and significantly decrease snow albedo immediate following fire disturbance. Significant amounts of black carbon and charred debris shed from the standing charred trees accumulated on the snowpack and darkened its surface. Snow albedo was 40% lower in the burned forest than in the

unburned forest during ablation, while approximately 60% more solar radiation reached the snow surface, driving a 200% increase in net shortwave radiation. Snow accumulation was greater in the burned forest the first winter following fire, however the snowpack disappeared over three weeks earlier and had twice the ablation rate than in the unburned forest. Spatial analysis showed that 80% of all forest fires occurred in the seasonal snow zone, and were 4.4 times larger than fires outside the seasonal snow zone. Over 50% of forest fires in the seasonal snow zone occurred in the Pacific Northwest.

Chapter 3 provided the first evaluation of turbulent fluxes over snow in a burned forest during the second year following fire, and in an adjacent unburned forest. This research used both eddy covariance and bulk-transfer methods to evaluate the sensible and latent heat fluxes over snow. An evaluation of forest fire disturbance effects to turbulent fluxes over snow using both direct and direct sampling methods determines the relative contributions of the turbulent fluxes relative to the radiative fluxes in the burned and unburned forest sites.

Charred forests approximately double the sensible and latent fluxes over snow in the burned forest compared to the nearby unburned forest during snow ablation. These turbulent fluxes are predominately of opposite sign and therefore together tend to contribute very little to the overall snowpack energy balance, although there are warm humid periods during snowmelt where both fluxes become positive and can provide a substantial contribution to snowpack energy balance. Sublimation from the

snow surface was responsible for approximately 2% of the loss of snowpack produced during snowmelt in the burned forest site during clear-sky snowmelt conditions. Due to the increased turbulence in the burned forest, the bulk aerodynamic method better resolved the turbulent energy fluxes in the burned forest than in the unburned forest. Although these simplified bulk aerodynamic methods do not resolve the turbulent fluxes under non-neutral conditions, because these fluxes are typically of opposite sign the errors associated with the fluxes also tend to cancel and therefore improve confidence in net turbulent energy exchange estimation using more simplified bulk methods.

Chapter 4 developed a new parameterization of the post-fire radiative forcing on snow, based on a detailed characterization of snow albedo and forest metrics three years following fire. The combined effect of accelerated snow albedo reduction over time since new snowfall, and increased incoming shortwave radiation as a result of a more open canopy were parameterized using a variable post-fire snow albedo decay function and measured LAI forest metrics. The parameterization was incorporated into a physically-based spatially distributed energy and mass balance snow model to evaluate the immediate and enduring forest fire effects to snow surface albedo, snowpack energy balance, and snowpack duration across the extent of the burned forest. In-situ measurements and remote sensing data were used to validate model results.

Due to the post-fire radiative forcing on snow (the coupled effect of reduced snowpack surface albedo and increased incoming shortwave radiation following forest fire), snow albedo decay accelerates and increases net snowpack energy balance (Figure 1.1). This increased snowpack energy balance drives earlier and more rapid snow melt across the extent of the burned area for at least three years following fire. Incorporating this empirically-based variable snow albedo decay parameterization ensures that the snow model accurately represents key driving mechanisms of snow accumulation and melt which are altered following forest fire disturbance. Using a variable albedo parameterization better predicts snow water equivalent in burned forests, and improves confidence in our results. By more accurately representing the key drivers to the snowpack energy balance, we are more accurately representing snow accumulation and snow ablation processes in the burned forest, that "we are getting the right answer for the right reason" [*Kirchner*, 2006].

5.2 Future Research Directions

Current uncertainties remain in our understanding of the temporal and spatial variability in post-fire radiative forcing on snow and motivate future research opportunities. Time-since-fire and inter-annual variability drive resulting temporal variability in the magnitude and duration of the post-fire radiative forcing on snow. While, antecedent forest conditions and burn severity drive resulting spatial variability in the magnitude and duration of the post-fire radiative forcing.

Although this research focused on the primary contributions to the snowpack energy balance, some components were not fully resolved including the ground flux and most importantly the longwave radiative flux. Due to existing lack of data, variable cloud cover and the forest canopy contribution, net longwave radiation at the snowpack surface is not still well quantified in burned and unburned forests.

5.3 Management Implications

Snowfall patterns, climate, topography, forest characteristics, and disturbance regime will all influence the magnitude and spatiotemporal variability of forest fire effects to snow-water resources. This research may be most applicable immediately following fire when combined disturbance effects are greatest. Depending on the extent of high-severity fire within a forested watershed, it may be critical to predict the initial hydrological consequence of forest fire disturbance. The combination of earlier peak runoff and increased peak runoff due to reduction in evapotranspiration may have consequences from montane to downstream riparian and estuary ecosystems. However, post-fire increase in peak runoff may be overwhelmed by a contrasting reduction in peak runoff due to more frequent mid-winter melt events. Initially these conditions may not be ideal for water managers, but by anticipating the advancement in the timing of peak runoff from burned forests and because of the dam capacity in much of the western US, the overall implications to downstream users can be mitigated.

Although the initial hydrologic response from forest fire in the snow zone may cause earlier and more rapid snowmelt, the enduring effects following fire may eventually retain snowpack longer in the spring (Figure 5.1). After just three years, large strips of bark are falling from standing dead trees in the Shadow Lake Fire area. These standing dead trees which were alive prior to the burn lose the charred bark at the cambium layer. When the bark strips off, these trees turn silver and no longer

contribute to darkening of the snow surface albedo. Although, the standing dead trees which were dead, primarily due to bark beetle kill, are charred through the cambium layer and remain charred throughout the bole for many years following fire disturbance. Once this charred material is all on the ground, over some unknown period of time, the snow albedo and land surface albedo will resemble open areas with more pristine snow (Figure 5.2). Eventually snow surface albedo will increase and may have a lower radiative forcing on snow than even an unburned forest where litter deposition lowers snow surface albedo and longwave radiation contributes to snow melt. Even after this hypothetical transition, the duration of forest fire effects to snow water resources may be most dependent on forest regrowth. In the maritime snow zone of the Pacific Northwest forest regrowth may occur relatively rapidly, however in colder and drier intercontinental subalpine areas forest fire effects to snow-water resources may endure for decades.

Our study has shown that high-severity fire causes big changes in the forest structure and associated post-fire forest effects to snowpack accumulation and ablation. Experiments have shown forest patchiness and lower density forests can increase the snow retention in maritime snow climates [*Lundquist et al.*, 2013]. The heterogeneity of wildfire severity across a landscape could resemble experimental results. Especially after the post-fire radiative forcing has declined over time, snow may be eventually be retained longer in burned areas than in unburned forests (Figure 5.2).

In high elevation porous volcanic systems where snowmelt predominately filters through the soil into underground aquifers such as the Oregon High Cascades, the offset of spring melt may not have such broad ecosystem implications as in more runoff dominated systems as is most of the montane western US, where this initial offset to spring melt may have wide ranging consequences to hydrologic, ecosystem and atmospheric-climate systems.

5.4 Conclusions

Forest fires are increasing across the seasonal snow zone, as snowpacks simultaneously are declining across the western US. These compounding disturbance effects to the radiative and turbulent fluxes over snow and resulting implications to snow-water resources are of serious importance in both current and future climates. Particularly in the Pacific Northwest, where a large proportion of at-risk snowpack resides, and where over half of forest fires in the seasonal snow zone have occurred in the western US since 2000. Earlier snowmelt, due to compounding disturbances of climate change and forest fire disturbance, has implications across the ecosystem to forests, fish, and people.

5.5 References

Lundquist, J. D., S. E. Dickerson-Lange, J. A. Lutz, and N. C. Cristea (2013), Lower forest density enhances snow retention in regions with warmer winters: A global framework developed from plot-scale observations and modeling, *Water Resources Research*, *49*(10), 6356-6370.

5.6 Figures

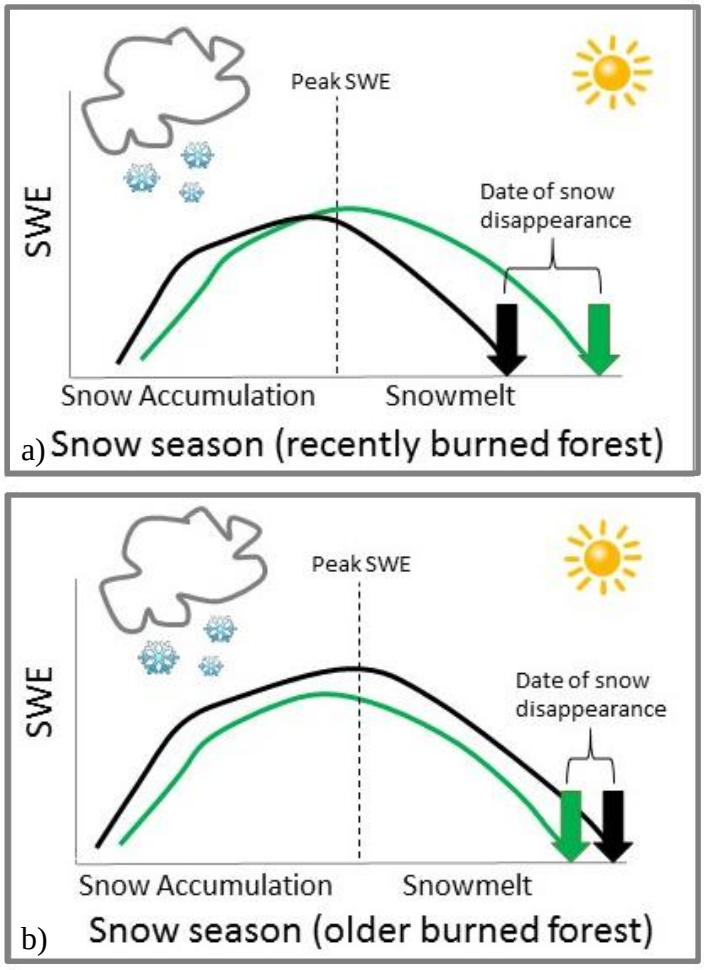

Figure 5.1. Changes in the patterns of snow accumulation and snowmelt for a) a recently burned forest such as results presented in this dissertation, and for b) conceptual results in an older burned forest.

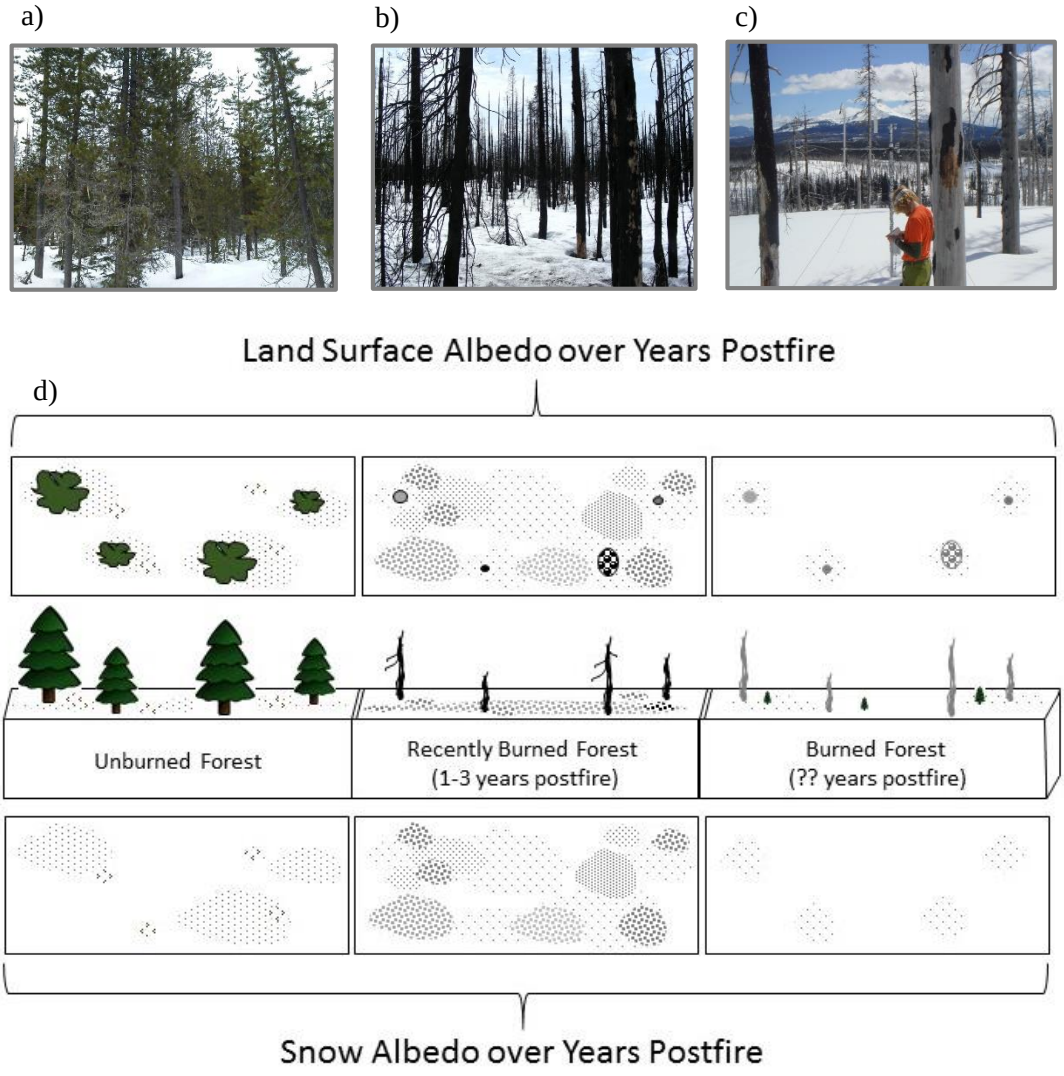

Figure 5.2. Photos of, a) the unburned forest site, b) the recently burned forest first winter following fire (Shadow Lake Fire burned in 2011), and c) an older burned forest 11-years post-fire (B& B Fire burned in 2003) in the western Oregon Cascade Mountains. d) Conceptual changes in land surface albedo and snow surface albedo over years post-fire, for an unburned forest, a recently burned forest (1-3 years post-fire), and an older burned forest (unknown number of years post-fire).

6 Appendix: Classifying the Spatial Distribution of Snow Water Equivalent to Develop a Representative Snow Monitoring Network in a Forested Mountain Watershed

Classifying the Spatial Distribution of Snow Water Equivalent to Develop a Representative Snow Monitoring Network in a Forested Mountain Watershed

Kelly E. Gleason, Anne W. Nolin, and Travis R. Roth

Hydrology and Earth System Sciences
Submitted June 2015

6.1 Abstract

Dominant physiographic drivers of snow water equivalent (SWE) were used to classify snow water equivalent (SWE) in a montane forested watershed in the western Oregon Cascades. A binary regression tree (BRT) non-parametric statistical model was used to explain spatially distributed SWE data derived from an improved SnowModel. Spatially distributed physiographic predictor variables of terrain, vegetation, and location data were used to develop an optimal BRT model of 20 snow classes across the watershed ($R^2 = 0.95$, P-value < 0.01, RMSE = 0.11). Elevation and land cover/vegetation characteristics were the most significant drivers of SWE in the watershed, and were used to develop a geospatial model from the optimal BRT model. We used the geospatial model to spatially distribute the 20 snow classes across the watershed in order to select site locations for a representative snow monitoring network which spans the variability in snow classes to best inform research on snow-vegetation-climate interactions. Snow monitoring locations were selected randomly within the BRT derived snow classes to represent combinations of forested and open land cover types at low-, mid-, and high- elevations to capture the range of variability in snowpack conditions dominate in the McKenzie River Basin. After four years of snow monitoring in the Basin, the ForEST network provides a valuable and detailed dataset of snow accumulation, snow ablation, and snowpack energy balance in forests and open areas from the rain-snow transition zone to high

elevations above the area of greatest volume of SWE in the western Oregon Cascades.

6.2 Introduction

Mountain snowpack is declining as a result of the warming climate [*Mote et al.*, 2005], shifting the timing of snowmelt, and subsequently the late spring or early summer peak in streamflow across the western United States [*Knowles et al.*, 2006; *Stewart et al.*, 2005]. The volume and seasonality of water produced from these snow-dominated watersheds varies spatially and temporally as a function of precipitation and temperature [*Barnett et al.*, 2005; *Regonda et al.*, 2005], as well as local physiographic effects of topography and vegetation dynamics [*Ffolliott et al.*, 1989].

Montane snow-dominated river basins are topographically complex, and in the Pacific Northwest, basins are a successional patchwork of variable forest cover driven by forest harvest and fire disturbance. Elevation, slope, aspect and exposure influence snowpack dynamics across a watershed through alterations of precipitation amount and phase (snow vs. rain), wind speed, temperature, and humidity. Physiographic controls on snow persistence vary as functions of snow accumulation and snow ablation, from the plot to regional spatial scales, and from daily to seasonal scales [*Biederman et al.*, 2014; *Elder et al.*, 1998; *Fassnacht et al.*, 2003; *Harpold et al.*, 2014; *Molotch and Bales*, 2005; *Molotch et al.*, 2004]. In forested regions, snow accumulation and ablation processes are strongly influenced by vegetation structure [*Davis et al.*, 1997; *Faria et al.*, 2000; *Hardy et al.*, 1997; *Jost et al.*, 2007; *Link and Marks*, 1999; *Musselman et al.*, 2008; *Sicart et al.*, 2004]. Both vegetation and

topography influence the distribution of solar radiation [*Davis et al.*, 1997; *Dozier*, 1980; *Musselman et al.*, 2012], snow-surface albedo [*Melloh et al.*, 2002; *Molotch et al.*, 2004], net longwave radiation [*Lundquist et al.*, 2013; *Sicart et al.*, 2004], wind speed [*Winstral and Marks*, 2002] and turbulent fluxes [*Burns et al.*, 2014; *Garvelmann et al.*, 2014; *Marks et al.*, 2008].

Snow water equivalent is a critical hydrologic resource in the rugged montane western US that has been actively monitored for decades by the Natural Resources Conservation Service (NRCS). The NRCS manages almost 858 Snowpack Telemetry (SNOTEL) stations across the western US, which provide real-time SWE, precipitation, and basic micro-meteorological data. These snow and micrometeorological monitoring stations provide essential data for operational hydrological forecasts to determine seasonal water availability for downstream communities, irrigation, reservoir operations, anadromous fish, and other users. Many of these stations have been running for decades, and provide critical data for researchers to evaluate changing climate, hydrology, and ecosystems. The SNOTEL monitoring network stations in the Oregon Cascades are located in a narrow elevation range and may not capture the inherent variability in the spatial distribution of snow [*Nolin*, 2012]. These records are important, but are point-based records and limited in their spatial extent [*Molotch and Bales*, 2006].

Particularly in data-scarce regions, or in cloudy regions where remote sensing techniques fail, modeling is a useful and practical technique to capture snowpack

characteristics across the areal extent of a watershed. In rugged and forested mountainous watersheds of the Pacific Northwest where forest canopies frequently obscure satellite field-of-view, modeling has been shown to be an effective way to predict future climate scenarios and inform water managers of annual water availability [*Sproles et al.*, 2013]. Understanding the physical relationships between physiographic characteristics and snow accumulation and ablation processes at the point scale is therefore a critical step in quantifying the spatial distribution of SWE across montane watersheds.

Physiographic characteristics have been used to predict point-based snowpack conditions at hillslope scales using binary regression tree (BRT) classification models [*Anderton et al.*, 2004; *Balk and Elder*, 2000; *Elder et al.*, 1998; *Erxleben et al.*, 2002; *Molotch et al.*, 2005; *Winstral et al.*, 2002]. Few larger scale BRT approaches have also been conducted using remotely sensed snow covered area and interpolation methods [*Molotch and Bales*, 2006]. However, no study to date has used landscape characteristics in conjunction with modeled and validated spatially distributed SWE data to understand physiographic drivers of snow accumulation at broad scales (> 1000 km^2).

Additionally, most of the research on the physiographic relationships to snow processes has been done in cold-dry continental snowpacks where few mid-winter melt events occur and wind easily redistributes it across a watershed [*Balk and Elder*, 2000; *Erxleben et al.*, 2002; *Molotch et al.*, 2005; *Winstral et al.*, 2002]. Much less is

known about how physiographic conditions influence snowpack dynamics at the watershed scale in maritime systems characteristic of the Pacific Northwest. This paper evaluates the effectiveness of the existing snow monitoring network in the McKenzie River Basin within the context of a projected future warming climate, and presents an objective and representative methodology for site selection of a snow monitoring network that captures the variability in snow accumulation.

Objectives of this research were to,

1. Determine the key physiographic drivers of spatial variability in snow accumulation in a montane forested watershed in the western Oregon Cascades;
2. Classify snow classes in the watershed based on key physiographic drivers using a non-parametric statistical model
3. Spatially distribute these snow classes across the watershed using a geospatial model;
4. Select representative site locations for a snow monitoring network which spans the variability in snow classes to investigate snow-vegetation-climate interactions.

6.3 Research Methods

Study Site

In the heart of the western Oregon Cascades, the McKenzie River Basin is a major tributary of the greater Willamette River Basin (Figure 6.1). The McKenzie River Basin (MRB) drains an area of 3,041 km^2, with elevation ranging from 150m at the confluence of the McKenzie and Willamette Rivers to 3150m at the summit of South Sister nestled in the crest of the Oregon Cascades. The McKenzie River Basin is a densely forested mountainous watershed that is a managed for timber production throughout much of the seasonal snow zone. It provides 25% of the late season volumetric baseflow in the Willamette River Basin, due to the porous High Cascades young volcanic geology where much of the snowmelt percolates directly into groundwater systems [*Tague and Grant*, 2004].

Data Sources

Gridded data were obtained for physiographic variables shown to influence snow dynamics in the literature including elevation, slope, aspect, incoming solar radiation, wind, and three vegetation variables from the following sources for the extent of the MRB. Digital Elevation Models (DEM) were obtained from the National Elevation Dataset at a 10m resolution. Slope, aspect, and insolation rates were calculated from the DEM using the Spatial Analyst and Solar Radiation toolboxes in ArcGIS 10.1 (ESRI, Redlands, CA). Upwind contributing area data, which captures the variability in snow deposition as a result of wind redistribution for each cell

throughout the watershed [*Winstral et al.*, 2002] was calculated following [*Molotch et al.*, 2005]. The United States Geological Survey (USGS), LANDFIRE Data Distribution Site provided the National Land Cover 2001 Data (NLCD), and Existing Vegetation – Percent Canopy Cover (EVC) data at a 30m spatial resolution. Normalized Difference Vegetation Index (NDVI) data give a measure of photosynthetic biomass within an image and were obtained from the Moderate Resolution Imaging SpectroRadiometer (MODIS) MOD13Q1 – Vegetation Indices, 16-day Land Product for the earliest date possible in April 2009 at a 250 m spatial resolution. Watershed boundaries were defined using the National Hydrography Dataset (USGS) obtained from, http://nhd.usgs.gov/data.html. Land ownership was determined using data provided from the Oregon Department of Forestry, and obtained from, http://www.oregon.gov/odf/pages/gis/gisdata.aspx.

Modeled, gridded, SWE data across the MRB extent (Figure 6.3) were provided by *Sproles et al.,* [2013]. These data were developed using a physically-based spatially-distributed snow mass and energy balance model, SnowModel [*Liston and Elder*, 2006], which uses input micrometeorological and topographic data to distribute snow across the landscape accounting for climatic, topographic, and vegetation variability. The model was modified by *Sproles et al.,* [2013] to better capture the rain-snow partition phase change and account for a snow albedo decay function for forested landscapes. This model was calibrated and validating using data from the four NRCS -SNOTEL sites in the MRB during the sampling period 1989-

2009, as well as gauged stream records in the watershed. The model ran at 100m spatial resolution and daily temporal resolution data. Modeled SWE data across the MRB from April 1, 2009 was used to evaluate distribution of peak snow accumulation in an average year snowpack. Modeled SWE data across the MRB for April 1, 2049, was used to evaluate the distribution of peak snow accumulation in a future average year snowpack. These projected data were based on the Intergovernmental Panel on Climate Change A1B temperature scenario ensemble which projects a moderate increase in global mean surface air temperature of 1.8° C by the end of the 21st century [*Pachauri and Reisinger*, 2007]. Only the air temperature parameter was modified in the model for the year 2049 model projections. Modeled SWE data across the MRB from April 1, 2012 was used to independently validate the distribution of peak snow accumulation in an average year snowpack.

Analysis

All spatial data were processed to match the projection and spatial resolution of the modeled SWE data to NAD83 UTM Zone 10, and a 100 m cell size, and then extracted to the extent of the MRB. All image processing of spatial data was conducted in ESRI - ArcGIS 9.3. Descriptive statistics were conducted on the spatial distribution of the snowpack throughout the watershed to determine preliminary relationships with physiographic features. Elevation zones were created for each

100m change in elevation. Descriptive analysis of the mean, range, standard deviation and total SWE distributed in relation to these elevation zones was conducted.

The "average snowpack" or area of greatest SWE volume across the MRB was defined as cells with SWE values within one standard deviation of the overall mean SWE. The locations of SNOTEL sites in the MRB was evaluated in relation to the average snowpack to evaluate how well our current monitoring network captures the bulk of the snowpack for 2009. To evaluate the representativeness of future monitoring networks, this bulk of the snowpack was also reclassified using model-output SWE data projected for 2049.

A BRT model was developed to characterize SWE volume and variability across the MRB using independent physiographic variables. The BRT model is a non-linear hierarchical statistical model that characterizes the mean and variance of a dependent variable using a suite of independent explanatory variables. Input data were obtained by extracting SWE and physiographic variable data for each cell where snow was present on April 1, 2009. An optimal tree was produced to minimize the standard error of the model, which was then pruned down to the simplest tree possible within one standard error of the optimal tree. The resultant tree identified 20 terminal nodes that characterized the full extent of variability in SWE through combinations of independent drivers (Table 6.1). This BRT model was validated for the McKenzie dataset using an alternate set of 10,000 randomly selected cells and analyzed using Classified and Regression Trees (CART) software (Salford Systems, San Diego, CA).

Using a Geographic Information Systems (GIS) model we then spatially distributed these 20 terminal BRT derived snow classes across the MRB. This GIS geospatial model processed physiographic data to determine locations that meet the criteria for each of the BRT classes; reclassified those new raster datasets; and created a mosaic layer of the BRT landscape classes within the MRB. All land area below 600 m in elevation was excluded from the final mosaic raster used for analysis to prevent over-prediction of SCA. Snow water equivalent (SWE) was calculated across the watershed for each BRT snow class using the mean and variance of SWE values characterized by the BRT model and areal extent of each BRT snow class. A point-based validation was carried out through a comparison of the BRT-predicted SWE to the four NRCS – SNOTEL sites in the MRB.

Finally, an evaluation of land available and accessible during winter was conducted to ensure the final snow monitoring network was feasible. Using a GIS-based binary selection model all non-public lands, and areas located within 500 m of a major road was excluded from the final randomized site selection. This final area which met the selection criteria were then made into a random raster from which final site locations were selected.

6.4 Results

SnowModel derived SWE throughout the MRB was normally distributed across the range of elevations (Figure 6.2). The four SNOTEL sites were located within one standard deviation of mean basin-wide SWE (area of greatest SWE volume) in the MRB on 01 April 2009 (Figure 6.3). Projected SWE data for 01 April 2049 showed that the snow covered area, as well as area with the greatest SWE volume will increase in elevation, out of the range of the current SNOTEL snow monitoring network (Figure 6.3). The area of greatest SWE volume from modeled data for 01 April 2009 ranged from 843 – 1845 m in elevation from 0.41-0.87 m of SWE. The area of greatest SWE volume from modeled 01 April 2049 ranged from 986 – 1866 m in elevation and from 0.2 - 0.8 m of SWE.

The BRT model identified elevation, land cover, % canopy cover, slope, NDVI and latitude as significant explanatory drivers of SWE distribution (listed in the order of significance). The explanatory drivers characterized modeled SWE output within the MRB by its mean and variance into 20 distinct classes as defined by its physiographic parameters ($R^2 = 0.95$, P-value < 0.01, RMSE = 0.11) (Table 1). Elevation explained the most variance of modeled SWE, followed by vegetation type as the second most explanatory variable (Figure 6.4). NLCD land cover types were grouped by the BRT model into land cover classes that distinctly fell into forested and open/clearcut vegetation classes. Slope and aspect were not significantly important in explaining 01 April 2009 SWE. Although latitude above or below 44.0537° were

separated into two classes within the elevation range from 1426 – 1545 m, these classes was lumped in the final analysis because we believed the topography of the Three Sisters Mountains in the southern portion to be skewing the statistical distinction of latitude in this analysis.

The BRT-derived SWE volume estimates for the McKenzie River Basin had a similar distribution across the elevational gradient as the SnowModel data (Figure 6.5). The BRT-derived estimate of 1.07 km^3total SWE volume stored in the April 1, 2009 snowpack within the MRB was 7.7% greater than the SnowModel-derived estimate of 0.99 km^3. The BRT-model results demonstrated good aerial agreement with Snow-modeled SWE data across the MRB. Increasing elevation enhances snowpack accumulation resulting in a greater volume of SWE per unit area at the highest elevations although these areas only cover a small aerial extent of the MRB. The BRT model performed best across the area of greatest SWE volume within one standard deviation of mean SWE, and at the highest elevations. At the lowest elevations in the transient snow zone (600-844 m - BRT classes 1-2), the BRT-model over-predicted mean SWE by approximately 25% with a volumetric estimate of 0.048 km3, as compared to 0.036 km3 of SWE as estimated by SnowModel. Across the bulk of the snowpack (843-1845 m – also BRT classes 3-16), the BRT-model estimated 0.895 km^3 of SWE, 7.7% greater than the SnowModel-derived estimate of 0.833 km^3 SWE. At the highest elevations of the MRB (above 1845 m – BRT classes

17-20), the BRT-model estimated 0.128 km^3 of SWE, 0.4% less than the SnowModel derived estimate of 0.129 km^3.

The GIS spatial exclusion and random selection model provided just 16 of the 20 classes as being on available land and within 100-500m of a road, a necessary criterion for winter access. The highest elevations in the MRB are far from road networks and difficult to monitor due to steep and avalanche prone slopes. From these 16 eligible BRT classes, random site locations were selected from low, medium, and high elevation and paired by forested and open BRT classes. The resultant Forest Elevation Snow Transect (ForEST) monitoring network was thus objectively selected to sample across the full range of variability SWE (Figure 6.4) and provide quality data to evaluate forest-vegetation-climate interactions in the watershed. The network is comprised of 10 meteorological stations and snow courses, and was deployed at the start of the 2011-2012 winter.

The ForEST network is valuable in that the site locations are independent of the traditional biases that tend to occur in site location determination. We did not rely on arbitrarily defined criteria of location based selection processes that can mask important snow forest processes. The paired forest-open canopy cover selection process alone is not unusual and has already led to important understanding of key sub-canopy snow processes [*Golding and Swanson,* 1986; *Storck et al.,* 2002]. Variability in both the snow surface energy budget and snow-vegetation interactions during snow accumulation and ablation across the elevational gradient was captured

in the data retrieved in this snow-monitoring network during the four years since it was deployed (Figure 6.6).

6.5 Discussion

In the face of the changing climate and associated hydrologic uncertainty, it is important that monitoring networks not only capture normal snowpack conditions, but the range of temporal and spatial variability in SWE across the landscape. The SNOTEL monitoring sites within the MRB capture peak SWE conditions well, but little of the spatial variability relative to topography and forest cover. The current snow monitoring network was designed based a historical climate that we may not experience in the future, and therefore adding additional stations that capture the range of variability is imperative.

Coupling the spatially distributed modeled SWE with the BRT statistical classification model, insightfully characterized the area of greatest SWE volume (within one standard deviation of mean SWE) and variability of SWE relative to landscape physiography across the watershed. This objective method is a useful tool in determining representative locations for intelligent snowpack monitoring. The method of site selection does incorporate uncertainty as a result of compounding physically based, statistical, and spatial models; however it meets assumptions of non-parametric data analysis, is performed with relative ease, and if data are available for the research basin of interest it can be well validated.

Elevation was identified as the most important driver of snow accumulation processes in the western Oregon Cascades. Based on known climatological lapse rates which drive precipitation and temperature changes along elevation gradients, this

result was expected. Forest cover related variables were identified as the second most significant driving factor in explaining snow accumulation: It has been hypothesized that forests play an extraordinary role in snow accumulation dynamics in the Pacific Northwest, however most research has been conducted at fine scales [*Storck et al.*, 2002] or in the Inner-Mountain West regions [*Ellis et al.*, 2013]. This study emphasizes the broad-scale control vegetation and particularly land cover change relative to timber harvest has on snowpack accumulation in the western Oregon Cascades. The need to accurately quantify forest structure effect on snow accumulation and ablation rates across elevation gradients is increasingly important to modeling efforts that help guide regional water managers decision making in a changing climate.

The ForEST network contributes to the existing network to explicitly investigate forest-vegetation interactions across the range of elevations and forest types in the watershed. The range of elevations serves as a proxy for temperature and provides insight into potential snow-vegetation interactions under warming climatic conditions. After four years of consecutive snow monitoring efforts, we have collected a valuable and detailed dataset of snow accumulation, snow ablation, and snowpack energy balance that spans the variability in forest and open land covers in low-, mid-, and high- elevation snowpack conditions.

6.6 Conclusions

This BRT landscape based model characterized peak SWE conditions in an average year and provided spatially-distributed information on the quantity and location of the bulk of snow stored water. The BRT snow classification across the landscape was an objective approach to design a monitoring network which captured variability of snowpack conditions within the selection criteria. This method guided the distribution of a sampling network that spans the data space of peak SWE accumulated in the MRB (Figure 6.9). Using an integrated approach of physically and statistically based models to characterize the physiographic relationships of how the landscape interacts with the snowpack and predict the location of snow stored water guided an objective and representative sampling network.

The use of validated model outputs as a predictor of the spatial variability on an outcome is a not new. *Randin et al.*, [2014] employed SnowModel to predict SCA in the determination of alpine plant distribution and ecosystem health. By quantifying the spatial variability of principle components researchers can focus study goals to sensitive areas which may not be identified through traditional site selection means. The novelty of this research stems from the coupling of a traditional BRT classification process with a validated spatially distributed model to drive a site selection process by its principle parameters across a physiographically and topographically diverse space.

As the scientific community turns to more complex, rescaled and nested parameterized models to predict ecosystem responses to perturbation, there is still a place for simple approaches to inform scientific research priorities. Although there is uncertainty propagated in nesting multiple models which justifies caution in implementing these estimates in management decisions. Particularly in the densely forested mountain regions of the western Cascades where there are few alternatives to estimating spatially distributed SWE information, this model provides a working hypothesis.

6.7 References

Anderton, S. P., S. M. White, and B. Alvera (2004), Evaluation of spatial variability in snow water equivalent for a high mountain catchment, *Hydrological Processes*, *18*(3), 435-453.

Balk, B., and K. Elder (2000), Combining binary decision tree and geostatistical methods to estimate snow distribution in a mountain watershed, *Water Resources Research*, *36*(1), 13-26.

Barnett, T. P., J. C. Adam, and D. P. Lettenmaier (2005), Potential impacts of a warming climate on water availability in snow-dominated regions, *Nature*, *438*(7066), 303-309.

Biederman, J. A., P. D. Brooks, A. A. Harpold, D. J. Gochis, E. Gutmann, D. E. Reed, E. Pendall, and B. E. Ewers (2014), Multiscale observations of snow accumulation and peak snowpack following widespread, insect-induced lodgepole pine mortality, *Ecohydrology*, *7*(1), 150-162.

Burns, S. P., N. P. Molotch, M. W. Williams, J. F. Knowles, B. Seok, R. K. Monson, A. A. Turnipseed, and P. D. Blanken (2014), Snow temperature changes within a seasonal snowpack and their relationship to turbulent fluxes of sensible and latent heat, *Journal of Hydrometeorology*, *15*(1), 117-142.

Davis, R. E., J. P. Hardy, W. Ni, J. Woodcock, J. C. McKenzie, R. Jordan, and X. Li (1997), Variation of snow cover ablation in the boreal forest: A sensitivity study on the effects of conifer canopy, *Journal of Geophysical Research. D. Atmospheres*, *102*, 29.

Dozier, J. (1980), A Clear-Sky Spectral Solar Radiation Model, *Water Resources Research*, *16*(4), 709-718.

Elder, K., W. Rosenthal, and R. E. Davis (1998), Estimating the spatial distribution of snow water equivalence in a montane watershed, *Hydrological Processes*, *12*(10-11), 1793-1808.

Ellis, C. R., J. W. Pomeroy, and T. E. Link (2013), Modeling increases in snowmelt yield and desynchronization resulting from forest gap-thinning treatments in a northern mountain headwater basin, *Water Resources Research*, *49*(2), 936-949.

References (Continued)

Erxleben, J., K. Elder, and R. Davis (2002), Comparison of spatial interpolation methods for estimating snow distribution in the Colorado Rocky Mountains, *Hydrological Processes*, *16*(18), 3627-3649.

Faria, D. A., J. W. Pomeroy, and R. L. H. Essery (2000), Effect of covariance between ablation and snow water equivalent on depletion of snow-covered area in a forest, *Hydrological Processes*, *14*(15), 2683-2695.

Fassnacht, S. R., K. A. Dressler, and R. C. Bales (2003), Snow water equivalent interpolation for the Colorado River Basin from snow telemetry (SNOTEL) data, *Water Resources Research*, *39*(8).

Ffolliott, P. F., G. J. Gottfried, and M. B. B. Jr (1989), Water yield from forest snowpack management: research findings in Arizona and New Mexico, *Water Resources Research*, *25*(9), 1999-2007.

Garvelmann, J., S. Pohl, and M. Weiler (2014), Variability of Observed Energy Fluxes during Rain-on-Snow and Clear Sky Snowmelt in a Midlatitude Mountain Environment, *Journal of Hydrometeorology*, *15*(3), 1220-1237.

Golding, D. L., and R. H. Swanson (1986), SNOW DISTRIBUTION PATTERNS IN CLEARINGS AND ADJACENT FOREST, *Water Resources Research*, *22*(13), 1931-1940.

Hardy, J. P., R. E. Davis, R. Jordan, X. Li, C. Woodcock, W. Ni, and J. C. McKenzie (1997), Snow ablation modeling at the stand scale in a boreal jack pine forest, *J. Geophys. Res.-Atmos.*, *102*(D24), 29397-29405.

Harpold, A. A., J. A. Biederman, K. Condon, M. Merino, Y. Korgaonkar, T. Nan, L. L. Sloat, M. Ross, and P. D. Brooks (2014), Changes in snow accumulation and ablation following the Las Conchas Forest Fire, New Mexico, USA, *Ecohydrology*, *7*(2), 440-452.

Jost, G., M. Weiler, D. R. Gluns, and Y. Alila (2007), The influence of forest and topography on snow accumulation and melt at the watershed-scale, *Journal of Hydrology*, *347*(1-2), 101-115.

Knowles, N., M. D. Dettinger, and D. R. Cayan (2006), Trends in snowfall versus rainfall in the Western United States, *Journal of Climate*, *19*(18), 4545-4559.

References (Continued)

Link, T., and D. Marks (1999), Distributed simulation of snowcover mass- and energy-balance in the boreal forest, *Hydrological Processes*, *13*(14-15), 2439-+.

Liston, G. E., and K. Elder (2006), A distributed snow-evolution modeling system (SnowModel), *Journal of Hydrometeorology*, *7*(6), 1259-1276.

Lundquist, J. D., S. E. Dickerson-Lange, J. A. Lutz, and N. C. Cristea (2013), Lower forest density enhances snow retention in regions with warmer winters: A global framework developed from plot-scale observations and modeling, *Water Resources Research*, *49*(10), 6356-6370.

Marks, D., M. Reba, J. Pomeroy, T. Link, A. Winstral, G. Flerchinger, and K. Elder (2008), Comparing Simulated and Measured Sensible and Latent Heat Fluxes over Snow under a Pine Canopy to Improve an Energy Balance Snowmelt Model, *Journal of Hydrometeorology*, *9*(6), 1506-1522.

Melloh, R. A., J. P. Hardy, R. N. Bailey, and T. J. Hall (2002), An efficient snow albedo model for the open and sub canopy, *Hydrological Processes*, *16*(18), 3571-3584.

Molotch, N. P., and R. C. Bales (2005), Scaling snow observations from the point to the grid element: Implications for observation network design, *Water Resources Research*, *41*(11).

Molotch, N. P., and R. C. Bales (2006), Comparison of ground-based and airborne snow surface albedo parameterizations in an alpine watershed: Impact on snowpack mass balance, *Water Resources Research*, *42*(5).

Molotch, N. P., and R. C. Bales (2006), SNOTEL representativeness in the Rio Grande headwaters on the basis of physiographics and remotely sensed snow cover persistence, *Hydrological Processes*, *20*(4), 723-739.

Molotch, N. P., T. H. Painter, R. C. Bales, and J. Dozier (2004), Incorporating remotely-sensed snow albedo into a spatially-distributed snowmelt model, *Geophysical Research Letters*, *31*(3).

References (Continued)

Molotch, N. P., M. T. Colee, R. C. Bales, and J. Dozier (2005), Estimating the spatial distribution of snow water equivalent in an alpine basin using binary regression tree models: the impact of digital elevation data and independent variable selection, *Hydrological Processes*, *19*(7), 1459-1479.

Mote, P. W., A. F. Hamlet, M. P. Clark, and D. P. Lettenmaier (2005), Declining mountain snowpack in western north America, *Bulletin of the American Meteorological Society*, *86*(1), 39-+.

Musselman, K. N., N. P. Molotch, and P. D. Brooks (2008), Effects of vegetation on snow accumulation and ablation in a mid-latitude sub-alpine forest, *Hydrological Processes*, *22*(15), 2767-2776.

Musselman, K. N., N. P. Molotch, S. A. Margulis, P. B. Kirchner, and R. C. Bales (2012), Influence of canopy structure and direct beam solar irradiance on snowmelt rates in a mixed conifer forest, *Agricultural and Forest Meteorology*, *161*, 46-56.

Nolin, A. W. (2012), Perspectives on Climate Change, Mountain Hydrology, and Water Resources in the Oregon Cascades, USA, *Mountain Research and Development*, *32*(S1), S35-S46.

Pachauri, R., and A. Reisinger (2007), IPCC fourth assessment report, *IPCC, Geneva*.
Randin, C. F., J. P. Dedieu, M. Zappa, L. Long, and S. Dullinger (2014), Validation of and comparison between a semidistributed rainfall–runoff hydrological model (PREVAH) and a spatially distributed snow-evolution model (SnowModel) for snow cover prediction in mountain ecosystems, *Ecohydrology*.

Regonda, S. K., B. Rajagopalan, M. Clark, and J. Pitlick (2005), Seasonal cycle shifts in hydroclimatology over the western United States, *Journal of Climate*, *18*(2), 372-384.

Sicart, J. E., J. W. Pomeroy, R. L. H. Essery, J. Hardy, T. Link, and D. Marks (2004), A sensitivity study of daytime net radiation during snowmelt to forest canopy and atmospheric conditions, *Journal of Hydrometeorology*, *5*(5), 774-784.

Sproles, E. A., A. W. Nolin, K. Rittger, and T. H. Painter (2013), Climate change impacts on maritime mountain snowpack in the Oregon Cascades, *Hydrology and Earth System Sciences*, *17*(7), 2581-2597.

References (Continued)

Stewart, I. T., D. R. Cayan, and M. D. Dettinger (2005), Changes toward earlier streamflow timing across western North America, *Journal of Climate*, *18*(8), 1136-1155.

Storck, P., D. P. Lettenmaier, and S. M. Bolton (2002), Measurement of snow interception and canopy effects on snow accumulation and melt in a mountainous maritime climate, Oregon, United States, *Water Resources Research*, *38*(11).

Tague, C., and G. E. Grant (2004), A geological framework for interpreting the low-flow regimes of Cascade streams, Willamette River Basin, Oregon, *Water Resources Research*, *40*(4).

Winstral, A., and D. Marks (2002), Simulating wind fields and snow redistribution using terrain-based parameters to model snow accumulation and melt over a semi-arid mountain catchment, *Hydrological Processes*, *16*(18), 3585-3603.

Winstral, A., K. Elder, and R. E. Davis (2002), Spatial snow modeling of wind-redistributed snow using terrain-based parameters, *Journal of Hydrometeorology*, *3*(5), 524-538.

6.8 Figures

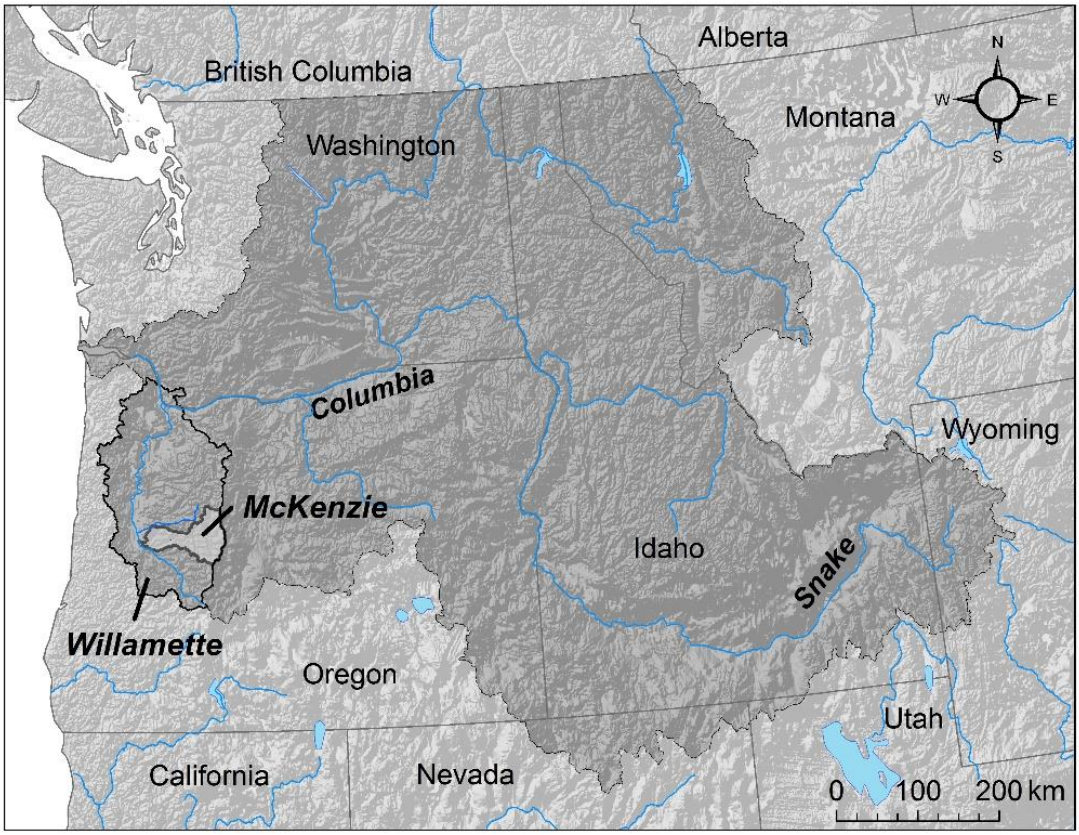

Figure 6.1. McKenzie River Basin is nested in the Willamette River Basin within the greater Columbia River Basin.

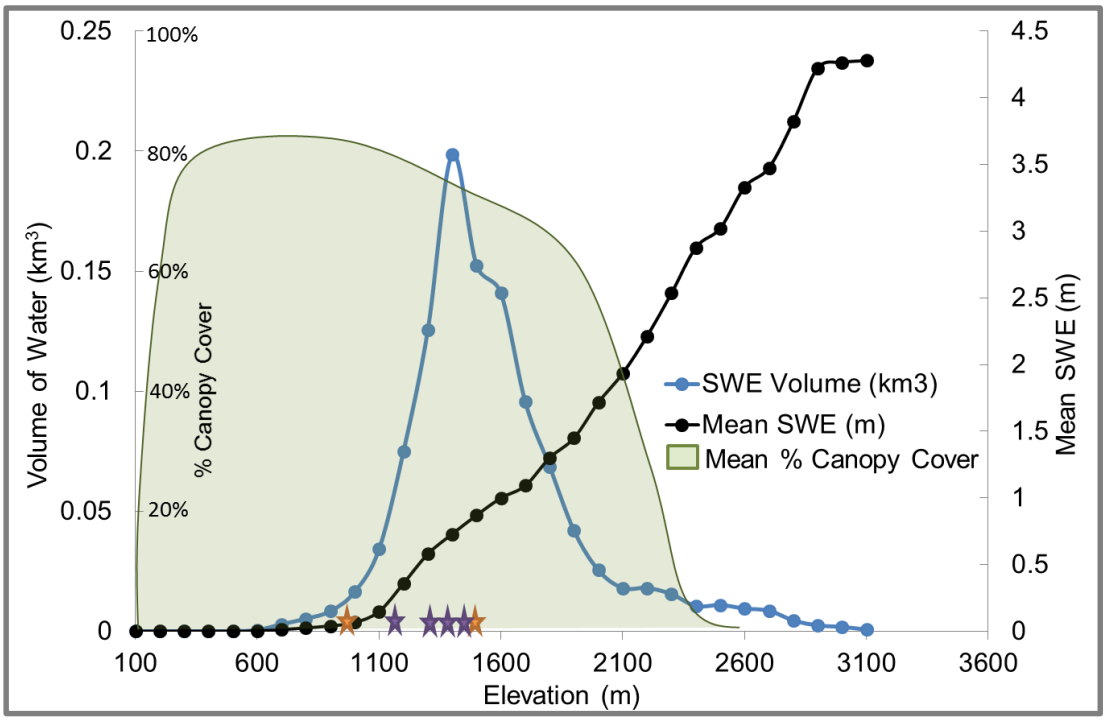

Figure 6.2. Elevation distribution of SnowModel data in the McKenzie River Basin. Bulk of the SWE persists in a narrow elevation range which is well-monitored by six SNOTEL stations (elevations of the four historical stations are shown as purple stars, and of the two new stations as of 2012 are shown as orange stars).

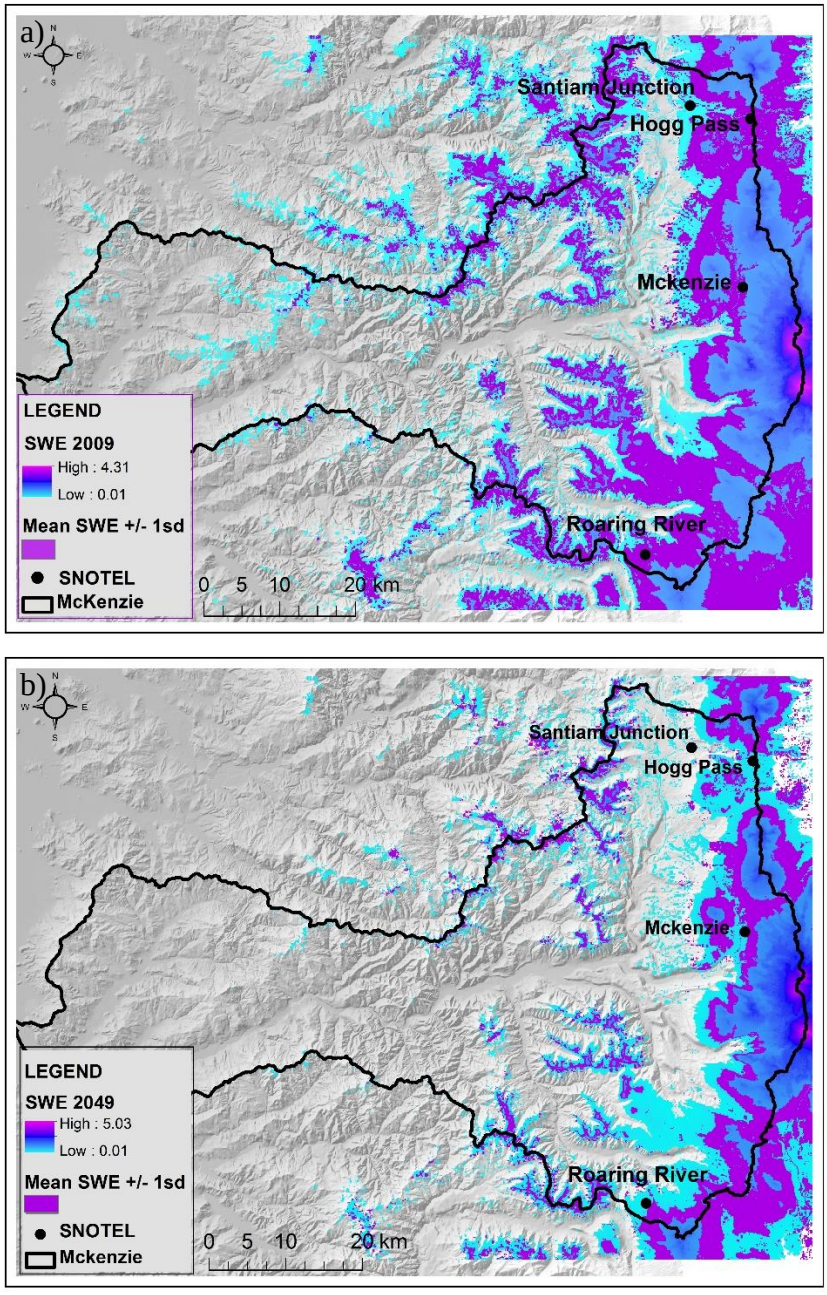

Figure 6.3. Total snow covered area extent in blue and the area of greatest SWE volume in purple (+/- 1standard deviation around mean SWE) for a) April 1, 2009 (average snow year) and b) April 1, 2049 (future average snow year).

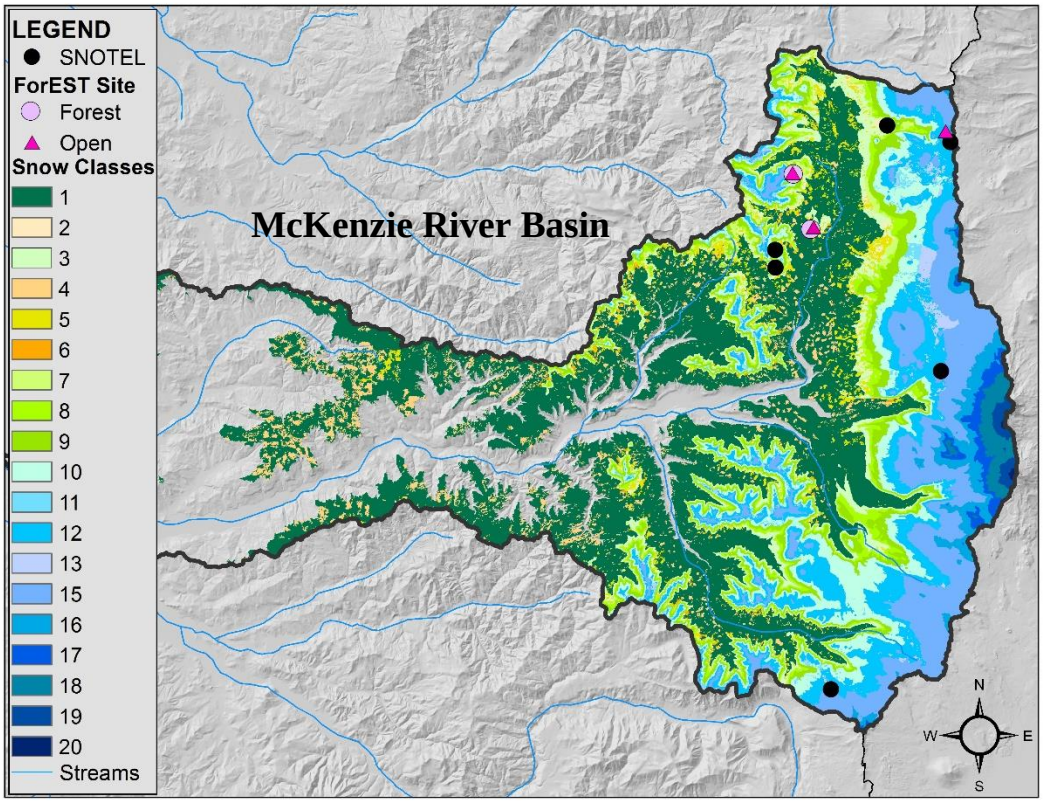

Figure 6.4. Binary regression tree classification McKenzie River Basin. Final snow monitoring sites were distributed in the Basin are not evenly distributed but selected to span the range of variability in snow-vegetation-climate interactions.

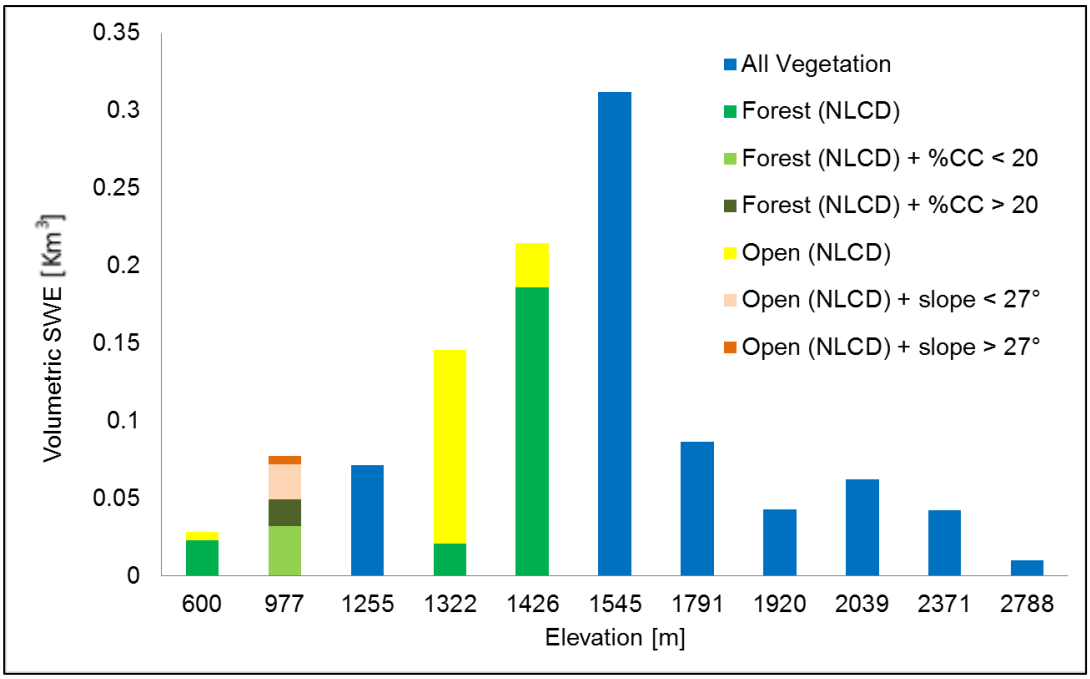

Figure 6.5. Predicted volumetric SWE [km^3] across the McKenzie River Basin for each BRT class stacked along the elevational gradient. In the low-, and mid-elevations, the forest vs. open distinction is statistically important in distinguishing snow classes. However in the high-elevations, above treeline, only elevation drives snow accumulation.

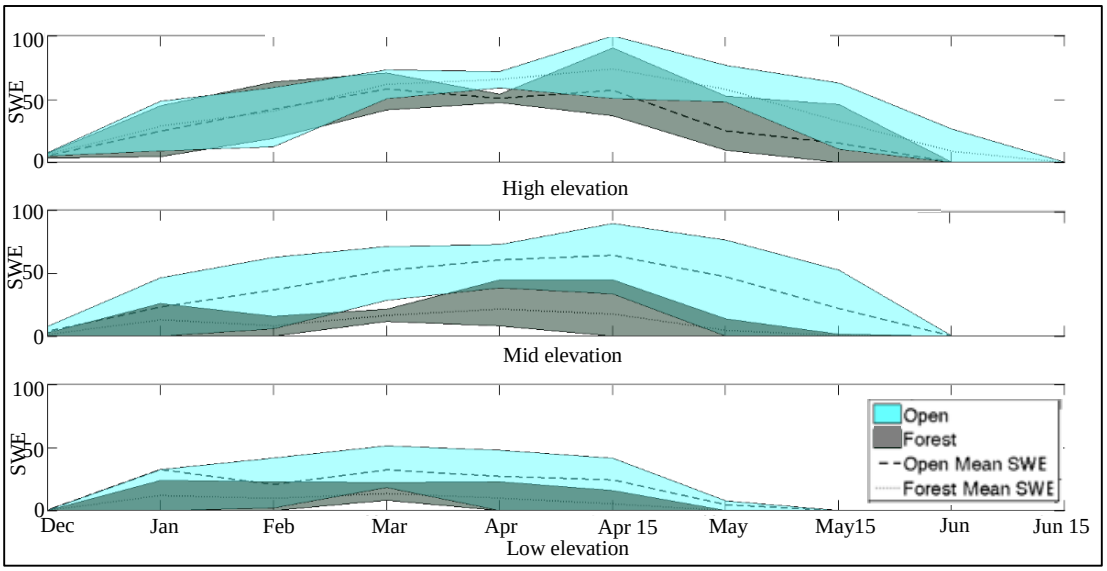

Figure 6.6. SWE [m] measurements from three years of snow course data. Light blue represents the range of average open canopy cover SWE measurements and grey represents the range of average forest cover SWE measurements.

6.9 Tables

Table 6.1. The binary regression tree characterized SWE within the McKenzie River Basin into 20 distinct landscape classes defined by the following physiographic parameters: elevation, land cover (forested vs. open/clearcut), latitude, NDVI, slope, and percent forest canopy cover. The colors represent the landscape classes used for the ForEST network; green represents the class with forest stations, yellow represents classes with open stations, and light blue represents new stations installed to capture forest/vegetation interactions at the upper edge of the subalpine forests.

Snow Class	Elevation	Veg Class	Other	Snow Class	Elevation	Veg Class	Other
1	< 1121	Forest		11	> 1332 < 1426	Open	
2	> 1121 < 1199	Forest	%CC <-20	12	> 1426 < 1545	Forest	
3	> 1121 <1199	Forest	%CC >20	13	> 1426 < 1545	Open	
4	< 977	Open		14	> 1545 < 1791		Y> 4878574
5	> 977 < 1199	Open	Slope < 27	15	> 1545 < 1791		Y< 4878574
6	> 977 <-1199	Open	Slope >27	16	> 1791 < 1919		
7	> 1199 < 1255		NDVI < 2063	17	> 1919 < 2039		
8	> 1199 < 1255		NDVI >2063	18	> 2039 < 2371		
9	> 1255 < 1332			19	> 2371 < 2788		
10	> 1332 < 1426	Forest		20	> 2788		